



REPUBLIC OF IRAQ

**MINISTRY OF HIGHER EDUCATION AND SCIENTIFIC
RESEARCH**

**AL-FURAT AL-AWSAT TECHNICAL UNIVERSITY
ENGINEERING TECHNICAL COLLEGE- NAJAF**

**WIRELESS AND IMAGING
APPLICATIONS ANTENNA BASED ON
METASURFACE MODIFIED DESIGNS**

A THESIS
SUBMITTED TO THE COMMUNICATION TECHNIQUES
ENGINEERING DEPARTMENT IN PARTIAL
FULFILLMENT OF THE REQUIREMENTS FOR THE
TECHNICAL MASTER DEGREE IN THE TECHNICAL
ENGINEERING COLLEGE OF NAJAF/AL FURAT AL
AWSAT TECHNICAL UNIVERSITY

BY

Qahtan Mutar Gatea

(B. Sc. in Communication Techniques Engineering)

Supervised by

Prof.Dr
Abdulkadhum Jaafar Alyasiri

Asst.Prof.Dr
Faris Mohammed Ali

September 2020



جمهورية العراق
وزارة التعليم العالي والبحث العلمي
جامعة الفرات الاوسط التقنية
الكلية التقنية الهندسية-نجف

هوائي لتطبيقات لاسلكية ومصورة قائم على التصاميم المعدلة لسطح الخارقة

رسالة مقدمة الى
قسم هندسة تقنيات الاتصالات
كجزء من متطلبات نيل درجة ماجستير تقني في هندسة الاتصالات

تقدم بها
قحطان مطر كاطع
بكالوريوس في هندسة تقنيات الاتصالات

أشراف

ا.م.د.

فارس محمد علي

ا.د.

عبد الكاظم جعفر الياسري

تشرين الثاني / 2020

انوار السمرقند
 من نور المشكاة فيما صحح الاصل
 في جواهر النجاة كما هو كوكب دري قوام
 من حركاتها في نور شرفية ولا خفية
 في نور السمرقند نور على نورها في
 من اشراقها في نور السمرقند نور على نورها في

انوار السمرقند
 من نور المشكاة
 في جواهر النجاة

Dedication

To the greatest person that Allah has ever created, Prophet

Mohammad peace is on him.

To the best person that Allah has ever created after His Prophet,

Imam Ali peace be upon him.

To those who have all the credit on me, to those who were the
cause of my existence, to my beloved **parent**.

To my **brothers**, my **wife** and my **friends**...

To all who supported and encouraged me to achieve my success.

Acknowledgement

Before everything, I would like to express my gratitude to Allah Almighty for His kindness and mercy and for giving me the opportunity to complete my study.

I would like to appreciate the extraordinary efforts and advice of **Prof. Dr Abdulkadhum Jaffer Alyasiri** and **Asst. Prof. Dr Faris Mohammed** Ali who had the greatest impact in fulfilling the requirement of the present study.

Finally, I would like to express my thanks to my family for their patience and for supporting me during the study period.

Supervisor Certification

We certify that this thesis titled "**Wireless and Imaging Applications Antenna Based on Metasurface Modified Designs**" which is being submitted by **Qahtan Mutar Gatea** was prepared under our supervision at the Communication Techniques Engineering Department, Engineering Technical College-Najaf, AL-Furat Al-Awsat Technical University, as partial fulfilment of the requirements for the degree of Master in Communication Techniques Engineering.

Signature: **Prof.Dr. Abdulkadhum .Jaafar.Alyasiri**

(Supervisor)

Date: / / 2020

Signature: **Asst.Pro.Dr. Faris . Mohammed. Ali**

(Co-Supervisor)

Date: / / 2020

In view of the available recommendation, I forward this thesis for debate by the examining committee.

Signature:

Name: **Dr. Salem Muhsin Wadi.**

(Head of Communication Tech. Eng. Dept.)

Date: / / 2020

Committee Report

We certify that we have read this thesis titled " **wireless and imaging applications antenna based on metasurface modified design**" which is being submitted by Qahtan Mutar Gatea and as Examining Committee, examined the student in its contents. In our opinion, the thesis is adequate for the award of Master degree in Communication Techniques Engineering.

Signature:

Name:

Prof. Dr. Abdulkadhun .J.Alyasiri

(Supervisor)

Date: / / 2020

Signature:

Name:

Asst. Prof. Dr. Faris .M. Ali

(Supervisor)

Date: / / 2020

Signature:

Name:

Prof. Dr.

(Member)

Date: / / 2020

Signature:

Name:

Asst. Prof.

(Member)

Date: / / 2020

Signature:

Name:

Prof. Dr.

(Chairman)

Date: / / 2020

Approval of the Engineering Technical College- Najaf

Signature:

Name:

Prof. Dr.

(Chairman)

Date: / / 2020

Abstract

Metasurfaces are artificial materials that added to the front of the microstrip antenna by using Fabry Perot technique to convert the spherical waves of the antenna to a plane wave in order to minimize the radiation beam and this result in an increase the antenna gain, While the antenna bandwidth expansion is achieved by adding an additional resonant frequency by each unit cell to the microstrip antenna, thus extending its operating range.

Due to its good features on the gain and bandwidth aspect, microstrip antennas designed with metasurface layer dependency make it a candidate option for use with both imaging and wireless applications.

By carrying out an extensive study of each element inside the antenna design and attaining the best result by using the parametric Sweep property in CST in the four designs. A brief description of the four designs and materials used for the substrate's construction. The first design is a $4 * 4$ metasurface layer with an X slot within each unit cell mounted on a TLF-35A substrate that achieves a bandwidth of 3GHz and a gain of 10.7 dB. The slot within the cell, the slot shape and the feeding line all contributed to improving the efficiency of the antenna.

Obtaining the gradient distribution design results after observing the uniform distribution of unit cells, where the metasurface layer mounted on the FR-4 substrate to obtain 2.4 GHz as bandwidth and 9.75 dB gain, where the gradient distribution represents the second design. The gradient distribution of cell sizes contributed well to antenna beam concentration in a narrow range and thus increased gain. The third design depends on different cell sizes mount on a RO4003C substrate, which achieved 2.92 GHz as bandwidth and 8.78 dB gain, as the different sizes contributed to adding a set of resonant frequencies to original

bandwidth. The last design relies on a wide range of slots in the hash shape to improve performance, which achieved 2.18 GHz as bandwidth and 7.43 dB gain. The best results achieved in the four antennas were in the first antenna, which achieved the highest Bandwidth and gain in the amount of 3GHz a bandwidth and 10.7 dB as gain.

Contents

Title	Page
Acknowledgement	I
Supervisor Certification	II
Committee Report	III
Abstract	IV
Contents	VI
List of Symbols	IX
List of Abbreviations	XI
List of Tables	XII
List of Figures	XIII
Chapter One: Introduction	
1.1 Introduction	1
1.2 Metamaterial	1
1.3 Metasurface	3
1.4 Motivation	6
1.5 Problem of Statement	6
1.6 Contribution of The Thesis	7
1.7 Thesis Layout	7
Chapter Two: Literature Review	
2.1 Introduction	8
2.2 Literature Survey	8
Chapter Three: Theory and Proposed Antennas	
3.1 Introduction	24
3.2 Negative Refractive Index	24
3.3 High-Gain Antennas	28
3.4 Fabry Pérot Technique	28
3.5 Feeding Techniques	29
3.5.1 Microstrip Line Feed	30
3.5.2 Coaxial-Line Feed	30
3.5.3 Aperture-coupled Feed	31
3.5.4 Proximity-Coupled Feed	32
3.5.5 Waveguide Feed	32
3.6 Extraction of Metasurface Parameters	33
3.6.1 Method Definition	33
3.6.2 Mathematical Formulation	34
3.6.3 Simulation and Extraction of Results	36
3.7 Antenna Parameters	37
3.7.1 Directivity	37
3.7.2 Gain	37
3.7.3 Efficiency	38

3.7.4 Bandwidth	38
3.8 The Proposed Model(I):Metasurface with X Slot in The Center of Unit Cell	39
3.9 The Proposed Model(II):Metasurface with (Uniform Distribution and Gradient Distribution)	40
3.9.1 Slot antenna	41
3.9.2 Metasurface Based The Antenna Design	42
3.9.2.1 Metasurface with Equal Length Unit Cell(Uniform Distribution)	42
3.9.2.2 Metasurface with Unequal Length Unit Cell(Gradient Distribution)	44
3.10 The Prposed Model(III):Metasurface with Different Cell Form	45
3.11 The Prposed Model (IIV):Metasurface with Hash Unit Cell	49
Chapter four: Results and Discussion	
4.1 Introduction	53
4.2 Characteristics of Metasurface with X Slot in The Center of Unit Cell	53
4.2.1Extracting Permeability ,Permittivity and Refractive index from S-parameter	53
4.2.2 Reflection Coefficient,Gain,Directivity ,Current Distribution	55
4.2.2.1 Parametric Study	55
4.4.2.1.1 Impact of Gap Between Cell	55
4.4.2.1.2 Impact of Cell Number	57
4.4.2.1.3 Impact of Cell Size	58
4.4.2.1.4 Influences of Air Cavity Height	59
4.4.2.1.5 Effect of Feed Line Width	60
4.4.2.1.6 Effect of Feed Line Length	62
4.4.2.1.7 Effect of Slot Length Inside Cell	63
4.2.2.2 Reflection Coefficient ,Gain ,Directivity	64
4.3 Characteristics of Metasurface with (Uniform Distribution and Gradient Distribution)	72
4.3.1Extracting Permeability,Permittivity and Refractive Index from S-Parameter	72
4.3.2 Reflection Coefficient,Gain,Directivity,Current Distribution	73
4.3.2.1 Parametric Study for Gradient Unit Cell Metasurface	75
4.4 Characteristics of Metasurface with Different Cell Forms	82
4.4.1 Extracting Permeability, Permittivity and	82

Refractive Index from S-Parameter	
4.4.2 Reflection Coefficient ,Gain , Directivity ,Current Distribution	83
4.5 Characteristics of Metasurface With Hash Unit Cell (III)	91
4.5.1 Extracting Permeability, Permittivity and Refractive Index from S-Parameter	91
4.5.2 Reflection Coefficient , Gain, Directivity ,Current Distribution	92
4.5.2.1 Parametric Study for Hash Unit Cell metasurface	94
Chapter Five: Conclusion and Future Work	
5.1 Introduction	105
5.2 Conclusions	105
5.3 Recommendations for Future Work	107
List of Publications	108
References	109

List of Symbols

TLF-35A	A Type of substrate used in designing antennas that has relative permittivity " $\epsilon = 3.5$ ", and loss tangent of 0.002.
FR4	A type of substrate used in designing antennas that has relative permittivity " $\epsilon = 4.3$ ", and loss tangent of 0.0025.
RO4003C	A type of substrate used in designing antennas that has relative permittivity " $\epsilon = 3.55$ ", and loss tangent of 0.0025.
ϵ_r	Relative Permittivity
δ	Tangent Loss
B	Unit Cell Size
θ	Theta
ϕ	Phi
λ_0	Free Space Wavelength
λ_g	Guided Wavelength
n	Refractive Index
μ_r	Relative Permeability
μ_0	The Permeability of Free Space
ϵ_0	The Permittivity of Free Space
ω	The Angular Frequencies
ω_{pe}	Electric Plasma Frequencies
ω_{pm}	Magnetic Plasma Frequencies
R	Purely Real
I	Purely Imaginary
θ_i	Incident Angle
θ_r	Reflected Angle
θ_t	Transmitted Angles
S_{11}	Reflection Coefficient
S_{12}	Transmission Coefficients
Z	The Impedance
k_0	Wavenumber
d	The Maximum Length of The Unit Element
m	Is The branch Due to The Periodicity of The Sinusoidal Function
E	Electric Field Components
H	Magnetic Field Components
R_{01}	Reflection Coefficient
D	The Directivity

U	Radiation Intensity
U_0	Radiation Intensity of Isotropic Source
G	Gain
P_{rad}	Represents Total Power Radiation
P_{in}	Represents Total Input Power
e_0	Total Efficiency
e_r	Reflection(Mismatch) Efficiency
e_c	Conduction Efficiency
e_d	Dielectric Efficiency
Γ	Reflection Coefficient
N	The Side Length of Patch
M	The Side Width of Patch
A	Gap Between Cells
X	Substrate Length
Y	Substrate Width
S	Feed Line Length
W	Feed Line Width
L_z	Length of Slot
W_z	Width of Slot
hair ₁	Air Gap 1
hair ₂	Air Gap 2
C_x	Slot Length Inside Cell
mn	Slot Width Inside Cell
T_1	Substrate Thickness for Slot
T_2	Substrate Thickness for Metasurface
M_1, N_1	Big Cell Width ,Length
M_2, N_2	Medium Cell Width,Length
M_3, N_3	Small Cell Width ,Length
A_1	Gap Between Cell
A_2	Gap Between Cell
A_3	Gap Between Cell
G	Line Inside Cell
B	Line Inside Cell
C	Line Inside Cell
D	Line Inside Cell
E	Line Inside Cell
F	Line Inside Cell
T	Line Inside Cell

List of Abbreviations

Symbol	Description
EM	Electromagnetic
MTM	Metamaterial
MS	Metasurface
SRR	Split Ring Resonator
C	Complementary
2D	Two Dimensions
3D	Three Dimensions
SAR	Synthetic Aperture Rader
UHF	Ultra High Frequency
RFID	Radio Frequency Identification
FP	Fabry P�erot
CP	Circular Polarization
GPS	Global Positing System
AMC	Artificial Magnetic Conductor
SIR	Stepped Impedance Resonator
MFSA	Microstrip Fed Slot Antenna
DMS	Directive Metasurface
FSMS	Fractal Shaped Metasurface
IO	Iteration order
IF	Iteration Factor
IA	Iteration Angle
LHM	Left-Hand Medium
RHM	Right-Hand Medium
SNR	Signal To Noise Ratio
PRS	Partially Reflection Surface
PM-PE	Perfect Magnetic – Perfect Electric
BC	Boundary Condition

List of Tables

Chapter Three: Theory and Proposed Antennas		
Table 3.1	List of symbol	35
Table 3.2	The dimensions of the antenna parameters	40
Table 3.3	A summary of the slot antenna dimensions	42
Table 3.4	A summary of the gradient metasurface dimensions	45
Table 3.5	Final antenna dimensions	48
Table 3.6	Final antenna dimensions of hash unit cell	51
Table 3.7	A comparison of theoretically calculated cell size and the size used in simulation	52
Chapter Four: Results and Discussion		
Table 4.1	Results of the proposed antenna	70
Table 4.2	Performance Comparison	70
Table 4.3	Results of the gradient metasurface antenna	79
Table 4.4	A comparison between the proposed antenna with other works	80
Table 4.5	Proposed antenna result for (only slot antenna, Slot antenna with MS metasurface) and (slot antenna+metasurface layer)	88
Table 4.6	Comparing with other antennas	88
Table 4.7	Antenna performance parameters	99
Table 4.8	Antenna performance parameters	100
Table 4.9	Comparison between the Four proposed metasurface antennas	102
Table 4.10	Application for each antenna	104

List of Figures

Chapter one: Introduction		
Fig.1.1	(a)Illustrations of the metafilm surfaces (b) A metascreen	5
Fig.1.2	Various categories of materials and how a metafilm as a kind of metamaterials	5
Chapter three : Theory and proposed antenna		
Fig.3.1	Material classification. The angular frequencies ω_{pe} and ω_{pm} represent the electric and magnetic plasma frequencies, respectively. R, purely real. I, purely imaginary	26
Fig.3.2	(a) Media with right-handed properties (b) Media with Left-handed properties	26
Fig 3.3	Double focusing effect in a “flat lens,” which is a LH slab of thickness d and refractive index nL sandwiched between two RH media of refractive index nR with $nL = -nR$.	27
Fig.3.4	Schematic diagram of the partial reflection surface	29
Fig.3.5	Microstrip feed line	30
Fig.3.6	Coaxial-line feed	31
Fig.3.7	Aperture-coupled feed	31
Fig.3.8	Proximity-coupled feed	32
Fig.3.9	Waveguide feed	32
Fig.3.10	Unit cell between two waveguide port	36
Fig.3.11	Proposed antenna structure: a- slot antenna with metasurface MS (side view) and b-Metasurface MS layer c- slot and feed-line .	39
Fig.3.12	Structure of the slot antenna.	41
Fig.3.13	The proposed antenna with uniform size distribution metasurface:(a) top view (b) side view.	43
Fig.3.14	A metasurface engineered with discrete elements that provide spatial phase distribution that offset the sphere-like front of the wave into a planar one	44
Fig.3.15	(a) The proposed antenna with gradient size distribution (b) metasurface 2D.	45
Fig.3.16	(a) Feed line and slot (b) Top view of metasurface (c) Side view of antenna (d) 3D view of prposed antenna.	48
Fig.3.17	shows (a) Top view of metasurface (b) hash unit cell (c) Feed line and slot (d) 3D view of prposed	50

	antenna.	
Chapter four : Results and Discussions		
Fig.4.1	(a) The single unit cell of MS in CST,(b), Relative permeability of MS. (c), Relative permittivity of the MS. (d), Refractive index of the MS.	54
Fig.4.2	Study (a) S11 and (b) Gain on gaps between unit cell start from 1.3mm to 1.9mm	56
Fig.4.3	Study effect of the number of the unit cells of the metasurface layer when A=1.7mm on (a) S11 and (b) Gain on	57
Fig.4.4	Study the effect of the cell size on (a) S11 and (b) Gain from 9mm to 11mm	58
Fig.4.5	Study the effect of air cavity height on (a) S11 and (b) Gain from 2.4mm to 3.6mm	60
Fig.4.6	Study the effect of feed line width on (a) S11 and (b) Gain from 0.5 mm to 1.1mm.	61
Fig.4.7	Study the effect of feed line length on (a) S11 and (b) Gain from 38.5 mm to 41.5mm.	63
Fig.4.8	Study the effect of slot inside unit cells on (a) S11 and (b) Gain from 4mm to 7mm.	64
Fig.4.9	S11 of (Conventional slot antenna , Metasurface antenna).	66
Fig.4.10	Gain of (Conventional slot antenna , Metasurface antenna).	66
Fig.4.11	3D Pattern for (a) Gain (b) Directivity at resonant frequency	67
Fig.4.12	Current Distribution at (a) 4.33GHz (b) 5.5 GHz (c) 6.5 GHz	68
Fig.4.13	Radiation pattern (a) Y-Z view (b) X-Y view (c) X-Z view	69
Fig.4.14	(a) The single unit cell of MS in CST,(b), Relative permeability of MS. (c), Relative permittivity of the MS. (d), Refractive index of the MS.	72
Fig.4.15	(a) S11 of slot antenna (b) Gain of slot antenna	74
Fig.4.16	(a) S11 of uniform distribution of metasurface (b) Gain of uniform distribution of metasurface	74
Fig.4.17	(a) S11 of gradient distribution of metasurface (b) Gain of gradient distribution of metasurface	74
Fig.4.18	The simulated return loss S11 of the proposed antenna with various Ls when W= 3 mm, and hair = 4.8 mm	77
Fig.4.19	The simulated return loss S11 of the proposed antenna	78

	with various h_{air} when $W=3$ mm, and $L_s = 14$ mm	
Fig.4.20	(a) S11 of Gradient distribution of metasurface (b) Gain of distribution of metasurface	79
Fig.4.21	3D Pattern for (a) Gain (b) Directivity	80
Fig.4.22	Current Distribution at 6.5 GHz	80
Fig.4.23	Radiation pattern (a) Y-Z view (b) X-Y view (c) X-Z view	81
Fig.4.24	(a) The single unit cell of MS in CST,(b), Relative permeability of MS. (c), Relative permittivity of the MS. (d), Refractive index of the MS.	82
Fig.4.25	S11 of (only slot , slot antenna+metasurface)	84
Fig.4.26	Gain of (only slot , slot antenna+metasurface)	84
Fig.4.27	The simulated return loss S11 of the proposed antenna with various h_{air} from 2.5mm to 4mm.	85
Fig.4.28	The simulated gain of the proposed antenna with various h_{air} from 2.5mm to 4mm.	86
Fig.4.29	3D Pattern for (a) Gain (b) Directivity	87
Fig.4.30	Current Distribution at 6.3GHz	89
Fig.4.31	Radiation pattern (a) X-Y view (b) Y-Z view (c) X-Z view	91
Fig.4.32	(a) The single unit cell of MS in CST,(b), Relative permeability of MS. (c), Relative permittivity of the MS. (d), Refractive index of the MS.	91
Fig.4.33	S11 of (only slot , slot antenna+metasurface)	93
Fig.4.34	Gain of (only slot , slot antenna+metasurface)	93
Fig.4.35	The simulated return loss S11 of the proposed antenna with various slot length from 6mm to 11mm.	94
Fig.4.36	The simulated return loss S11 of the proposed antenna with various h_{air} from 0.6 mm to 1.6mm.	96
Fig.4.37	(a) Feed line length various from 21.5mm to 26.5mm (b) Feed line width various from 0.4mm to 0.8	97
Fig.4.38	(a) S11 of Metasurface antenna (b) Gain of Metasurface antenna	98
Fig.4.39	3D Pattern for (a) Gain (b) Directivity	99
Fig.4.40	Current Distribution at 6.75GHz	100
Fig.4.41	Radiation pattern (a) X-Y view (b) Y-Z view (c) X-Z view	101

Chapter One

Introduction

CHAPTER ONE

INTRODUCTION

1.1- Introduction

An antenna is defined by Webster's Dictionary as a usually metallic device (as a rod or wire) for radiating or receiving electromagnetic waves. The IEEE Standard Definitions of Terms for Antennas defines the antenna or aerial as "a means for radiating or receiving electromagnetic waves." In other words, the antenna is the transitional the structure between free-space and a guiding device. [1] .

In addition to receiving or transmitting electromagnetic waves, antenna is typically required in advanced wireless systems to maximize or boost the antenna's radiation energy in some directions, and to suppress radiation in others. Thus antenna, in addition to the probing device, acts as the directional device. It may then take different types to satisfy a particular requirement at hand, and it may be an aperture, a piece of conducting wire, a patch, element assembly (array), a reflector, a lens, etc. The most important components of the wireless communication system is the antenna. A good antenna structure contributes to relax system requirements and boost overall system performance[1].

1.2 Metamaterials

Metamaterials are artificial materials that have unconventional properties satisfying particular requirements [2]. They are currently in a focus of intense research, particularly in connection with electromagnetics. Grand research programs have launched in recent years and institutional networks have been developed with the goal of

researching, designing and developing metamaterials and their applications [2].

Metamaterial is an entity that derives its material properties electromagnetic from its arrangement rather than having inherited them directly from the materials of which it is composed. This term has been used when the resulting material has characteristics which are not found in nature. For a variety of optical / microwave applications, metamaterials are promising, such as new types of modulators, beam steerers, super lenses, band-pass filters, and antenna radomes, and microwave couplers[3].

Metamaterials are practical,artificial electromagnetic materials multi-functional engineered to meet the specified requirements.The meta prefix means after, beyond, and also of a higher kind. These unorthodox responses are predominately produced by repeating patterns,at scales which are smaller than wavelengths of the phenomena that influence on it [2,3].

The modern metamaterials are first hypothesized and then experimentally perceived as the medium that at the same time has negative permeability and permittivity at a given frequency [4,5]. As it well known, system response is defined by system material properties which are permeability and permittivity. The metamaterial is three dimensional, therefore classified as artificial electromagnetic materials that can be used to manipulate electromagnetic fields if the materials' permeability and permittivity are properly engineered[6]. Metamaterials are mainly developed as the periodic ensemble of conducting elements such as metallic rods and rings or up to spherical particles that

collectively act as the electromagnetic medium with efficient permeability and permittivity [5, 7].

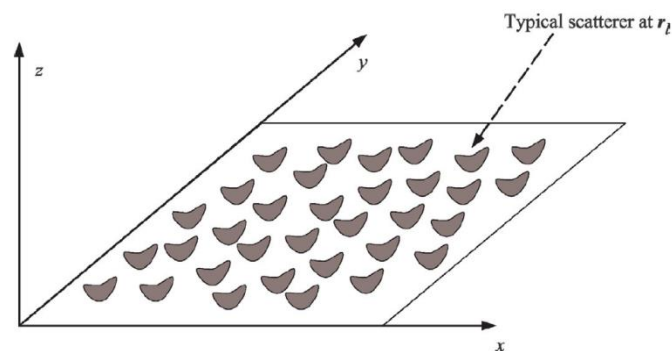
The fundamental concept of metamaterial MTM is defined as a group of electrically small resonators which contribute to the product of electromagnetic media. These resonators have a variety of combinations from the spheres to simple wires, which can construct various shapes and be scalable in its geometries. So, as an example on resonators is split-ring resonators (SRR). It consists mainly of a broken ring of controllable dimensions to establish a custom response to an electromagnetic field [5]. The Metamaterials are in all spectrum bands starting from the radio [8], passing through microwave [5], and millimeter wave [9], to each of terahertz wave [10], and to near optical [11]. These artificial materials, not found in nature, raise a wave of great interest, especially in the engineering and scientific communities. Thus, there are many applications for electromagnetic research, including cloaking [12], advanced lenses [13], energy harvesting [14], and the most important part is metamaterial-based antennas [15]. One of the most important obstacles that has emerged in some applications when using metamaterial MTM is a large size [6,7], as it has a three-dimensional 3D structure that has led to the search for a new generation of materials that fulfills the purpose and overcomes all obstacles that emerged from the metamaterial [7]. The next generation is metasurfaces.

1.3 Metasurfaces

The new version that comes as an upgrade to the old three-dimensional metamaterials version is metasurface, where the metasurface surface consists of very tiny electrically scatters called metafilm [16]. The two-dimensional metasurface MS is composed of periodic structures with

sub-wavelength scattering elements using these elements in a manner that leads to the reconstruction of the incident waves on its surface to the desired transmission and reflection level. Two important aspects of the structure of metasurfaces are the thickness and the periodicity, which are much smaller than the surrounding media wavelength. Metasurfaces have the advantages of having less physical space than 3D-metamaterial structures and are less-lossy structures due to the reduction of volume metamaterials. Additional advantages are that they are light, easy to fabricate, flexible, and reliable[17,18,19].

As mentioned earlier, metasurface represents 2D periodic structures that are known as very thin when compared with 3D metamaterial [7]. With that general meaning, MS falls into two separate categories. Starting with the metafilm as the first form, described as an array of fully isolated scattering elements from each other which are called metafilms following cermet topology. The term metafilm for these surfaces was coined in [7]. Fig1.1.(a) displays the metafilm configuration. The metascreen representing the other category, the arrangement structure which follows by this type is the fishnet topology where the elements of metascreen are periodically spaced apertures on a surface. So the metascreen is allocated to the homogenous slab with isolated aperture, as shown in Fig1.1.(b) [7].



(a)

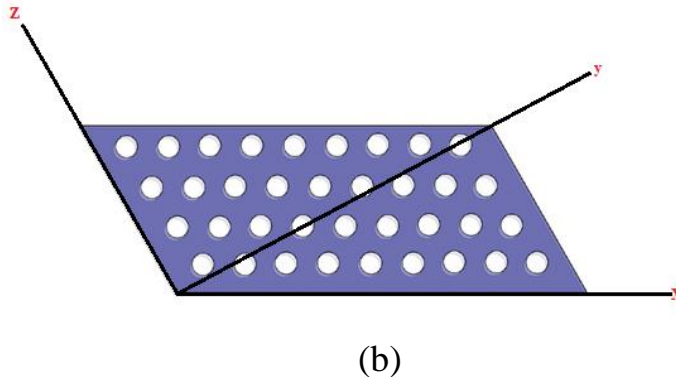


Fig.1.1: (a) Illustrations of the metafilm surfaces (b) A metascreen [7]

The general classification of materials is given in Fig1.2 below. There are two sections of the materials, one is normal and the other artificial[19]. In this thesis, the designs is based on metafilm which is considered part of the metasurface as it is the modified version of metamaterial.

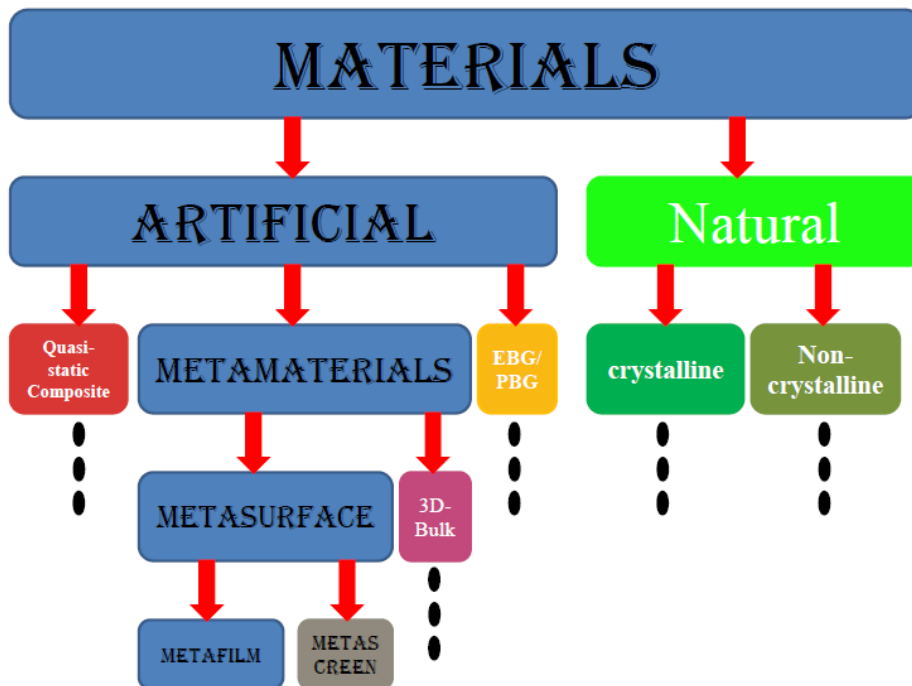


Fig.1.2: Various categories of materials and how a metafilm as a kind of metamaterials [19].

Due to all these features of metasurfaces, there are wide ranges of applications for these surfaces. Along with the features mentioned earlier, the metasurface particles are scalable, which gives the freedom to use them in the desired frequency band [19].

Over the past years, there has been growing interest in the societies and engineering communities for developing metasurface applications due to their versatility. Metasurfaces have wide potential applications: such as absorbers, Metasurface holography, harvesters, metasurfaces for tuning, sensing, antennas are one of the most important applications where metasurface is used. It can be utilized in receiving mode and transmitting mode [20,21,22,23].

1.4 Motivation

One of the most important points that has motivated researcher to work with the metasurface is that it is a new technology and something new for the Iraqi scientific community. Besides, the advantages that this technology has in greatly improve antenna performance.

1.5 Problem of Statement

Microstrip antennas suffer from limitations in both the gain and the bandwidth sides, so wireless and imaging applications need more efficient antennas to do their work, as the imaging applications need a wide bandwidth in order to increase scanning accuracy and high gain in order to increase the coverage distance ,while for wireless applications, the bandwidth needs to increase the flow of data within an application or use more than one application.

1.6 Contribution of The thesis

1- After reviewing a wide range of references and observe the limitations faced by the microstrip antennas in the gain and bandwidth side.

2- Four antennas were designed, two for wireless applications and two for imaging applications, as the designed group covered a frequency range from 4 GHz to 9 GHz. The results achieved in the first antenna are considered the best by 10.7 dB as gaining and 3 GHz bandwidth.

3- After obtaining good results in both the gain and the bandwidth sides, the limitations faced by the imaging applications were overcome, which are the narrow bandwidth of the microstrip antennas, thus improving the scanning accuracy as well as increasing the coverage distance. While for the wireless applications, they were suffering from the narrow bandwidth achieved by the microstrip antenna, which was treated in the designs mentioned in the thesis

1.7 Thesis Layout

Chapter Two: deal with literature review on many of the antennas that relate to our work.

Chapter Three: covers the theory and design of the proposed metasurface layer-based antennas.

Chapter Four: This chapter includes a discussion of all simulated results for proposed antennas.

Chapter Five: In this chapter includes the conclusions of proposed metasurface antennas and the recommendations.

Chapter Two

Literature Review

CHAPTER TWO

LITERATURE REVIEW

2.1 Introduction

In this chapter of the thesis, discuss the works related to our research, as well as reviewing the previous works, are particularly focused in this section with microstrip antenna approved on the metasurface and clarify certain details. For example the frequency band in which the antenna operates, Substrates types used to add metasurface layer on them, the cell shape and distribution technique, the feeding method and the most important point to be highlighted is the purpose of using a metasurface with an antenna. All of these for every antenna derived from a specific reference will be discussed in detail.

Through looking at the previous references in metasurfaces, it was found that metasurface layers are used in the antennas in several uses, such as converting linear polarization into circular polarization, manipulating beam steering, reducing the antenna size, and finally increasing the gain and bandwidth, where this thesis seeks to realize an increase in gain and bandwidth in addition to minimization antenna size, Based on the four classifications and not the year of publication of the article, references would be mentioned.

2.2 Literature Survey

In [2015] ,P. Vijitsulakkana [24], a slanting metasurface unit cells are mounted above the microstrip patch antenna with an air gap between the patch and the metasurface sheet. Its height is estimated at around 30 mm. Where antenna operates at the ultra-high frequency (UHF) is used in the

radio frequency identification reader RFID. The metasurface MS is mainly used to achieve two goals in the efficiency of the antenna, which are to increase the gain well and also to support circular polarization without manipulating the feeding method via the diagonal line found in cell design. The metasurface layer is mounted on the a FR-4 substrate of 1.6mm thickness. The designed antenna leads to getting impedance bandwidth (854 MHz - 928 MHz), axial ratio bandwidth (895 MHz-953 MHz) and peak gain 5.1 dBi.

In 2017, Son Xuat Ta [25], the designed of this antenna is to achieve circular polarization which depends on cutting the patch corners instead of cutting the cell corners. Where the antenna patch is positioned over the cells of the metasurface, which are periodically distributed. The antenna lacks the use of Fabry-Pérot (FP) technology. The layer of the metasurface is placed over a substrate with a thickness of 3.2mm. Metasurface based antenna has circularly polarized (CP) radiation which use for a Global Positioning System GPS receivers. This structure results in an achieved bandwidth from (1.562 GHz –1.733 GHz), axial ratio bandwidth (1.570 GHz–1.592 GHz) at 1.58 GHz and gain about 2.75 dBi.

In 2017, Yongjun Huang [26], compact, a wideband, and Low-profile circular polarization CP an antenna which based on truncating the edge of the square patches metasurface layer, in order to achieve circular polarization. The metasurface layer is composed of a group of unit cells with uniform distribution on a substrate. The resonance frequency on which the antenna operates is 5.6 GHz. Fabry-Pérot (FP) technique is missing in the design because there is no air gap among metasurface layer and a ground plane. The simulation results lead to getting impedance bandwidth from (4.7 GHz-6.5 GHz), axial ratio bandwidth of 20% and

peak gain is 6 dBi. Converting antenna polarization is the main benefit of this antenna.

In 2018, José Lucas da Silva Paiva[27], the effects of adding the metasurface layer on the performance of rectangular microstrip antenna has been studied and the conversion process from linear to circular polarization is accomplished without going into complicated processes in the form of the feeding method. The metasurface layer is added to rectangular microstrip antenna using the fabry-pérot FP technique where the metasurface layer mounted on RO4350 substrate with an array of the unit cell which has a shape that depends on the formula of the edges for a clear purpose, which is polarization. The original rectangular microstrip antenna operates at 2.45 GHz and preserve the same frequency when the metasurface layer adds. The overall dimension of the antenna is 96.5mm×96.5mm. This structure achieves impedance bandwidth 60MHz, axial ration 72.3 MHz with peak gain is 5.69 dB.

In 2014 , Idellyse Martinez[28], an extremely-thin, reconfigurable metasurface absorber composed of an artificial magnetic conductor AMC type of mushroom is proposed. The reflection phase can be shifted by capacitively loading the unit cells, enabling the metasurface to steer the incoming wave to the desired direction, acting as the phase gradient absorber. To determine the necessary phase shift needed to direct the main beam, a formula based on the antenna array theory is utilized. Compared to a perfect electric conductor PEC ground plane, the configuration of antenna can steers the main beam from the specular direction to $\varphi=0^\circ$ and $\theta= 15^\circ$. It was also further shown that the main beam width can indeed be increased by integrating resistors into the loaded design.

In 2017, Peng Xie [29], Fabry-Perot cavity antenna is extremely important to the communication system and is widely used. Conventional Fabry-Perot cavity FPC antennas, however, suffers from narrow working patterns, restricted range of beam steering and even complicated configurations. Here, they design a modern, reconfigurable metasurface for extending the FPC antenna's working modes and thus improving the beam steering angles from (-54° to 54°). The reconfigurable metasurface MS layer composes of 6×6 unit cells which occupy a $90 \text{ mm} \times 90 \text{ mm}$ region. Well-designed of bias circuits can manipulate the metasurface reflection phase via tuning the inserted PIN diode states, as antenna operates at centre frequency 5GHz. Thus simulation leads to getting bandwidth 4.92- 5.08 GHz with good gain.

In 2016, Wei Liu [30], because of wide operating bandwidth, the broadband antenna has a very important role to play in increasing the resolution of synthetic aperture radar SAR, leading to an improvement in finer resolution scanning, better reflection data and penetration from multiple scatters. So the metasurface based on stepped impedance resonators SIR often used to carry out this task with an H-shaped SIR unit cell to achieve a miniaturized low-profile and broadband antenna. The metasurface layer was placed on the substrate of Rogers RO4003C, which has $\epsilon = 3.55$, $\tan \delta = 0.0027$. The SIR metasurface antenna results in getting footprint of ($11.8 \text{ mm} \times 11.0 \text{ mm} \times 1.524 \text{ mm}$) $0.40\lambda_0 \times 0.37\lambda_0 \times 0.05\lambda_0$ at the operating frequency of 10.1 GHz with bandwidth from (9.43 10.77 GHz) and gain value 7.8 dB.

In 2017, Wei E. [31], Metasurface with single-layer and dual-layer is proposed to achieve miniaturized wideband and low-profile antenna. The metasurface for single and dual-layer composed from one and two arrays of the square patch with uniform size for both single and dual-layer,

respectively. The single layer composes from 4x4 metallic unit cell distribution on the surface of the layer, while the dual-layer is composed of two-layer upper and lower where the upper layer consists of 4 x 4 and low layer of 8 x 8 metallic unit cells which insert in the same antenna. Antenna miniaturization has been realized with raising the effective refractive index, which is obtained from a narrowed gaps that exist in single-layer metasurface and improve capacitive couplings in dual-layer metasurface. The process of adding metasurface layer to slot antenna is done without an air gap. Both design miniaturized antennas achieve gain with a value greater than 6.5 dBi through the bandwidth of 30% and decrease radiating aperture of $(0.46\lambda_0 \times 0.46\lambda_0)$ with the thickness of $0.06\lambda_0$ where (λ_0 is the wavelength for free-space at 5.5 GHz). Moreover, metasurface with dual-layer presenting additional freedom to raise an effective refractive index with realizable gap widths as compared with a single layer of the metasurface.

In 2018, Ximing Li[32], to miniaturize a micropatch antenna, metasurface is presented to accomplish this mission using a palisade-shaped structure. Miniaturization of the footprint is achieved with the aid of the metasurface, where double resonant modes are obtained at the same time. However, from the dispersion curve study of metasurface unit cells element in order to optimize a structure, a proposed antenna realizes a condensed structure with a maximum size of $0.38\lambda_0^2$, a low profile of $0.08\lambda_0$ where (λ_0 is a free space wavelength at frequency 5.0 GHz) showing 19.6 % values as impedance bandwidth for $S_{11} < -10\text{dB}$ which has the average gain of 6.76 dBi through the bandwidth.

In 2011, Sarawuth Chaimool[33], the modern design used for microstrip fed slot antenna MFSA has been developed to improve gain, minimize back radiation and bandwidth. Unlike most unidirectional

MFSAs, the metasurface as the upper layer is utilized to decrease back-lobe radiation and improve a gain without the metal reflection. Metasurface layer consists of an array of the narrow square unit cell with an empty center, the metasurface layer is mounted on FR-4 substrate with an approximately air gap of 7.5 mm. The measuring radiation patterns demonstrate that the structure indicates that a good co-cross polarization ratio, and high radiation efficiency can be present. Due to the negative metasurface MS reflection phase, the total antenna thickness is 9.9 mm at the center frequency 2.45 GHz. The design antenna has reached a bandwidth of 2.14 to 2.70 GHz for the metasurface slot antenna with good gain.

In 2015, Ke Chen[34], Metasurface is represented as a 2D version of the artificial electromagnetic metamaterial MTM which provides the effective method to control and manipulate the propagation of EM waves. Here, the transparent metasurface is present for compensating an out of phase radiation which dispersion from the microstrip patch antenna to enhance its radiation bandwidth and gain. Depending on the equivalence principle of the Huygens' surface, metasurface consist of both capacitive and inductive resonant elements, producing high transmission with changing phase characteristics. Metasurface layer is placed on a patch of microstrip antenna which can transform spherical like phase profile generated from a patch into an in-phase planar one. The antenna design operating at a frequency around 5.7 GHz, as a potential application for the proposed antenna in wireless communication such as Wi-Fi.

In 2015, B. Majumde[35], this article proposes a compact, wideband antenna and a simple novel metasurface directive DMS. To excite metasurface-layer, two with exactly the same dimensions of the edge fed slots are used. Metasurface MS layer composed of the periodic

arrangement of rectangular loop-based unit cells. Metasurface layer mounts on slot antenna without an air gap between them, feeding method is done by coaxial cable. The antenna produces the bandwidth from (5.89 GHz - 6.6 GHz) and good gain. Simulated efficiency is greater than 87%. Cross polarization value is so small under 20 dB.

In 2016, Y. M. Pan[36], wideband, a low profile and high gain metasurface MS-based filtering antenna with great selectivity is realized in this research. The planar metasurface MS is made up of non-uniform copper patch cells where it is fed from the bottom by two independent microstrip-coupled slots. The separation of the two slots together with a shortcut through is used to provide a good filtering efficiency in the lower stop band, while the MS is elaborately built to get a sharp roll-off percentage for the filtering function at the upper band edge. The metasurface also at the same time operate as the high efficient radiator, improving antenna gain and impedance bandwidth of feeding slots. The design antenna simulation giving bandwidth range from (4.26 to 5.75 GHz) with perfect gain.

In 2017, Neha Rajak[37], this research discusses a two-layer metasurface antenna, which the metasurface is the top most part, and the patch antenna is the lower part. The metasurface increases patch antenna gain and bandwidth. It consists of a radiating elements array that are organized in a 5 x 6 form. The complementary split-ring resonator CSRR is utilized as a radiating element. The MS is represented as Double Negative material where permittivity and permeability are negative, as the result ,refractive index will also be negative. The wave emitted from a patch antenna is influenced by an array of the unit cell radiating element on the metasurface. It is placed above a patch antenna as a result of the equivalent relative permeability and permittivity of metasurface layer

occur change in performance of a patch antenna. The proposed antenna is operating at 5.7 GHz with a gain of 5.8 dBi and bandwidth enhancement from (150 to 260 MHz). The proposed antenna can be utilized in Wi-Fi application.

In[2017], Ming Cai[38], compact and broadband coplanar waveguide CPW depending on metasurface was design. The main aim of this antenna is imaging application which is represented by synthetic aperture radar SAR. It works in C-band exactly in 5.5 GHz. The metasurface composes of 16 periodic metallic patches unit cells which are distributed in a uniform pattern on a substrate which presents as radiators. The fed structure of the coplanar waveguide introduces two tasks:(a) it represented as a ground plane for MS unit cells, and (b) it triggers the aperture coupling slot design exactly under the middle of metasurface patch array. The hourglass-shaped slot is chosen after testing many types of slots. The antenna realizes bandwidth range from (5.14 GHz to 5.82 GHz), with average gain value is 7.2 dBi.

In[2017], Chairunnisa[39], a rectangular patch based on metasurface in its structure. The MS composes of 2 x 2 metallic patches unit cell with many amendments in their dimension to realize the desired resonant frequency of 2.3GHz. The metasurface is placed in the back of the antenna on FR4 Epoxy substrate, where the rectangle patch is placed on the top of an antenna to demonstrate the merit of bandwidth improvement, the antenna based on metasurface operate at the same resonant frequency of conventional rectangular patch. The antenna improvement value is 530MHz when the antenna's band changes from 100MHz to 630MHz. Although there is good increase in bandwidth but gain is very little.

In [2018] Niamat Hussain [40], the antenna for WiMAX applications is presented, planar low-profile microstrip antenna places such sandwiched among metasurface and a finite ground plane. The rectangular patch is used as the radiating element and feeding is done by microstrip line, the lower ends of the rectangular patch are truncated. While the metasurface is composed of 4×4 uniform distribution of unit cells which mount on Rogers RO4003 substrate. The process of adding a metasurface layer for the original antenna is done without an air gap between them. The measurement of antenna results in the impedance bandwidth of (20%) which start from (3.14 to 3.88 GHz) for $|S_{11}| < -10$ dB. A result for the successful implementation of adding metasurface layer for patch radiator, where the antenna present high gain, additional to high radiation efficiency which reaches from 95%.

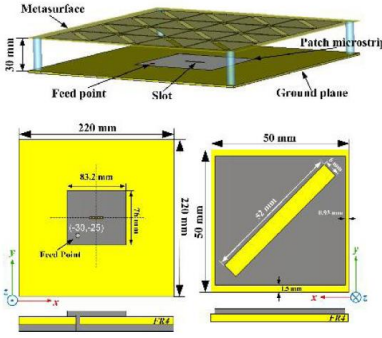
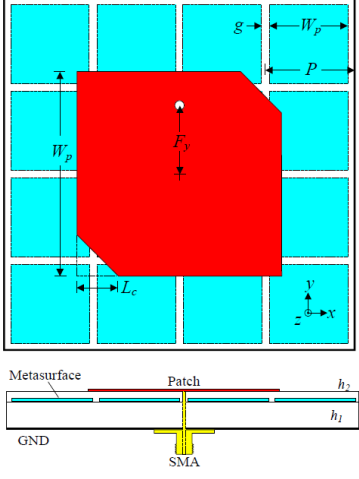
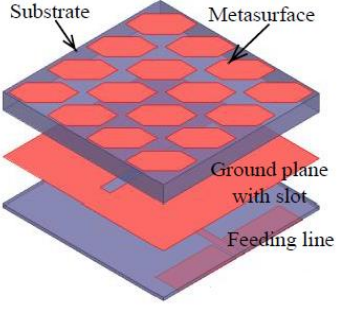
In [2019], Paulkani Iyampalam [41], the design and study of the fractal shaped metasurface FSMS antenna for applications in public safety is discussed in this research. The antenna consists of two layers, lower layer and upper layer. The lower layer has the monopole antenna inspired by fractals and metasurface MS has the upper layer. Metasurface consists of a fractal unit cell in the form of Sierpinski Knopp, arranged in a 4 x 6 configuration to achieve miniaturization. The projected FSMS antenna has been manufactured using dielectric FR4 material. Results indicate that the FSMS antenna shows a 200 MHz bandwidth and a gain around 1.56 dBi at 4.89 GHz. The results in obtained through measurement and simulation are in good consent. Consequently, the suggested antenna with a low profile of $0.43\lambda_0 \times 0.43\lambda_0$ is well suited for applications of public safety.

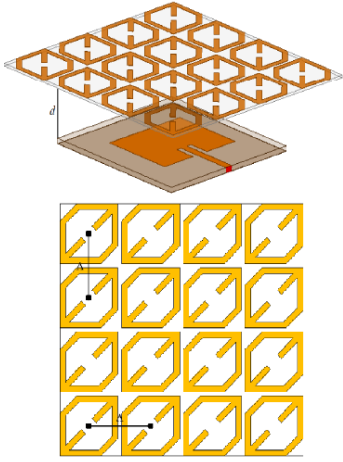
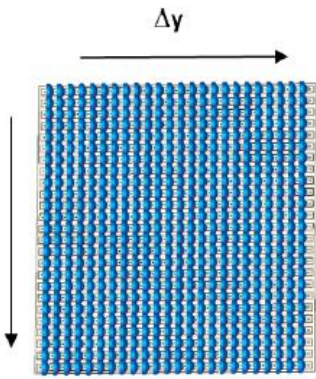
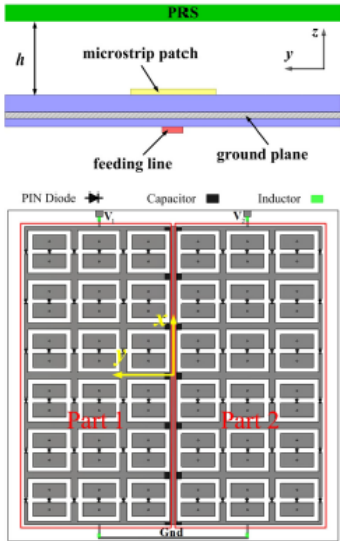
In [2019], Guo Liu [42], A novel wideband slot antenna with Koch fractal metasurface structure is presented in study. Using Koch metasurface as a

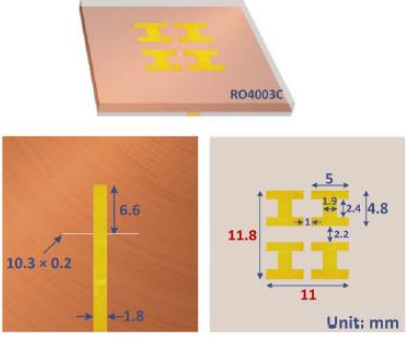
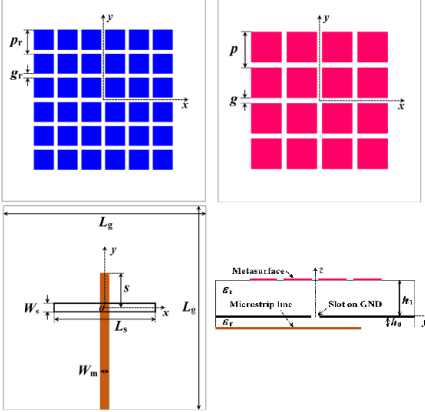
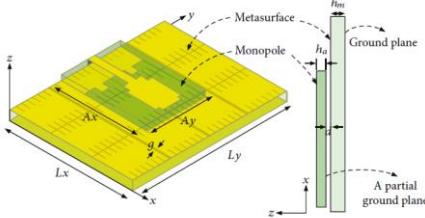
slot edge, the proposed antenna obtains excellent performance in bandwidth. For maximum bandwidth, each iteration order (IO) is optimized for both the iteration factor (IF) and the iteration angle (IA).

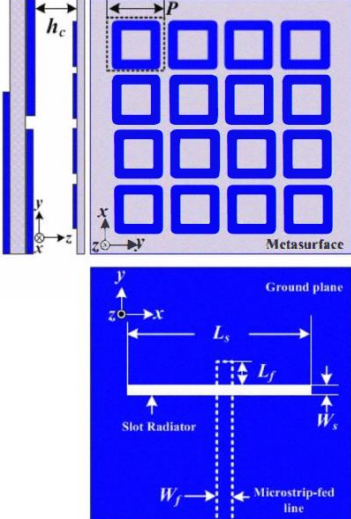
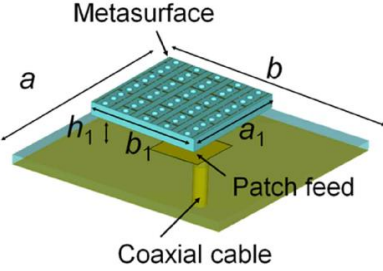
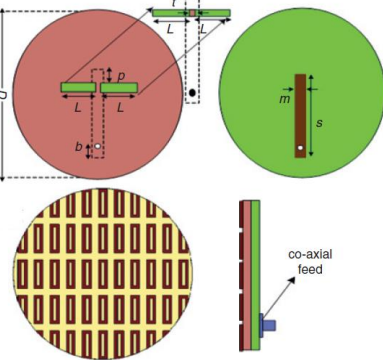
The work mainly relied on increasing the antenna characteristics in the two sides of the bandwidth and the gain by manipulating in the shape of the cell, such as using slots in the middle of cells to stimulate additional resonance frequencies or gradations in the size of cells for the concentrating the radiation beam in the small area and increasing the gain, in addition to using different cell sizes to add resonance frequencies of different ranges to the original frequency, and the last design dependence on the hash format, which contains a large number of slots in details.

The approved shapes in the designs were mentioned briefly and comparison with the previous references such as a reference [31] , [33] and [38] some. Observing that these references rely on work in one method only, which is the uniform distribution of cells. It should be noted that this case was used as a reference for comparison in the second design and to highlight the added differences in the gradient design through a comparison between them.

No	Ref	Substrate	Gain and Bandwidth	Fabry P�erot	Metasurface antenna and cell shape
1	[24]	FR4	74 MHz 5.1 dB	Existing	
2	[25]	FR4	171 MHz 2.75 dB	No	
3	[26]	-	1.8 GHz 6 dB	No	

No	Ref	Substrate	Gain and Bandwidth	Fabry P�erot	Metasurface Antenna and Cell Shape
4	[27]	RO4350	60 MHz 5.69 dB	Existing	
5	[28]	FR-4	-	No	
6	[29]	FR4	160 MHz	Existing	

No	Ref	Substrate	Gain and Bandwidth	Fabry Péro	Metasurface Antenna and Cell Shape
7	[30]	Rogers RO4003C	1.34 GHz 7.8 dB	No	 <p>The image shows a photograph of a metasurface antenna on a Rogers RO4003C substrate. Below the photograph are two diagrams. The left diagram shows a single vertical microstrip line with dimensions: width 10.3×0.2 mm, height 6.6 mm, and a gap of 1.8 mm. The right diagram shows a grid of microstrip lines with dimensions: grid width 11 mm, grid height 11.8 mm, and individual cell dimensions of 5 mm by 4.8 mm. A unit of mm is specified.</p>
8	[31]	Rogers RO4003C	1.71GHz 8 dB	No	 <p>The image contains four schematic diagrams. The top-left diagram shows a grid of blue squares with period p_x and p_y. The top-right diagram shows a grid of red squares with period p_x and p_y. The bottom-left diagram shows a cross-section of a microstrip line with width W_m, gap W_g, and length L_g. The bottom-right diagram shows a cross-section of the metasurface structure with a microstrip line, a slot on the ground plane, and a partial ground plane. Labels include ϵ_r, h_m, h_a, and h_s.</p>
9	[32]	Rogers RO3003	990 MHz 6.76 dBi	Exist ing	 <p>The image shows a 3D schematic of a metasurface antenna structure. The metasurface is a grid of yellow squares on a substrate. A monopole antenna is shown above the metasurface. The ground plane is a partial ground plane. Labels include L_x, L_y, A_x, A_y, h_m, h_a, and h_s.</p>

No	Ref	Substrate	Gain and bandwidth	Fabry P�erot	Metasurface antenna and cell shape
10	[33]	FR4	560MHz 9 dB	Existing	
11	[34]	FR4	-	Existing	
12	[35]	-	710 MHz 9.4 dB	No	

No	Ref	Substrate	Gain and bandwidth	Fabry P�erot	Metasurface antenna and cell shape
13	[36]	FR4	1.49 GHz 8.2 dBi	NO	
14	[37]	Rogers RO4350B	110 MHz 5.8 dB	No	
15	[38]	RO4350B	68 MHz 7.2 dB	No	

N o	Ref	Substra te	Gain and bandwidth	Fabry Pérot	Metasurface antenna and
16	[39]	FR4 Epoxy	530 MHz 1 dBi	No	
17	[40]	Rogers RO400 3	740MHz 8.6 dBi	NO	
18	[41]	FR4	200 MHz 1.56 dBi	No	
19	[42]	Taconi c RF	5.38 dBi	No	

Chapter Three

Theory and The

Proposed Antennas

CHAPTER THREE

THEORY AND PROPOSED ANTENNAS

3.1 Introduction

In this chapter, in addition to listing other aspects of the metasurface, address the basis on which the metasurface is centered, which is metamaterial. After that, emphasise the importance of high-gain antennas, and the most effective technique used to boost antenna performance. Then, in addition to clarifying the process by which make sure the design is metasurface, describe a set of methods used to feed the antenna. And the last thing that is discussed in the thesis is the designs that based on metasurface with full details about the dimensions and types of materials used in substrate.

3.2 Negative Refractive Index

The widespread concept of electromagnetic metamaterial (MTM) is an artificial and effectively homogeneous electromagnetic structure including unusual properties that do not occur in nature. One of the most critical conditions that must be provided to the effect that the structure is homogeneous, the average unit cell size B must be smaller than wavelength λ_g [43]. Where B represents the cell size.

Therefore, the average cell size utilized in any structure must be $B < \lambda_g/4$ which mean less than a quarter of a wavelength. In order to ensure refractive dominance over scattering-diffraction phenomena when electromagnetic wave EM propagates into a metamaterial medium, the average cell size used in any structure will be indicated as an effective-

homogeneity condition when it achieved $B < \lambda_g/4$ [43]. Where λ_g represent guided wavelength.

This limit corresponds to a rule of thumb effectiveness condition. Microwave engineers often use the limit $B = \lambda_g/4$, where B is the size of the component considered, to distinguish lumped components ($B < \lambda_g/4$) from quasi-lumped components ($\lambda_g/4 < B < \lambda_g/2$) and distributed components ($B > \lambda_g/2$). In the lumped case, the phase variation of the signal from the input to the output of the component is negligible, and the component may therefore be considered as a localized (sizeless) element. In contrast, in the distributed case, phase variation along the component cannot be ignored, and the component must consequently be considered as a transmission line section. MTMs are thus distributed structures constituted of lumped elements [43].

The constitutive parameters are the permeability μ additional to permittivity ϵ , which are linked to a refractive index n by [43] :

$$n = \pm \sqrt{\epsilon_r \mu_r} \quad (3.1)$$

Where μ_r and ϵ_r the relative permeability and permittivity which linked to a free space permeability ϵ_0 and permittivity μ_0 by [43]:

$$\mu_0 = \frac{\mu}{\mu_r} = 4\pi * 10^{-7} \quad (3.2)$$

$$\epsilon_0 = \epsilon / \epsilon_r = 8.854 * 10^{-12} \quad (3.3)$$

As shown in Fig3.1, four potential signs are; (+, -), (+,+), (-,+) and (-,-) in the pair. While the first three signs are well known in traditional materials, the fourth sign (-,-) has negative value for each of permeability and permittivity simultaneously. Compatible with new materials of the left-handed form (LH), Clearly left-handed structures are metamaterials. Depending on the description given above, call artificial material because the human hand made it, effectively homogeneous $B < \lambda_g/4$, unusual properties appear ($\epsilon, \mu < 0$) [2,43].

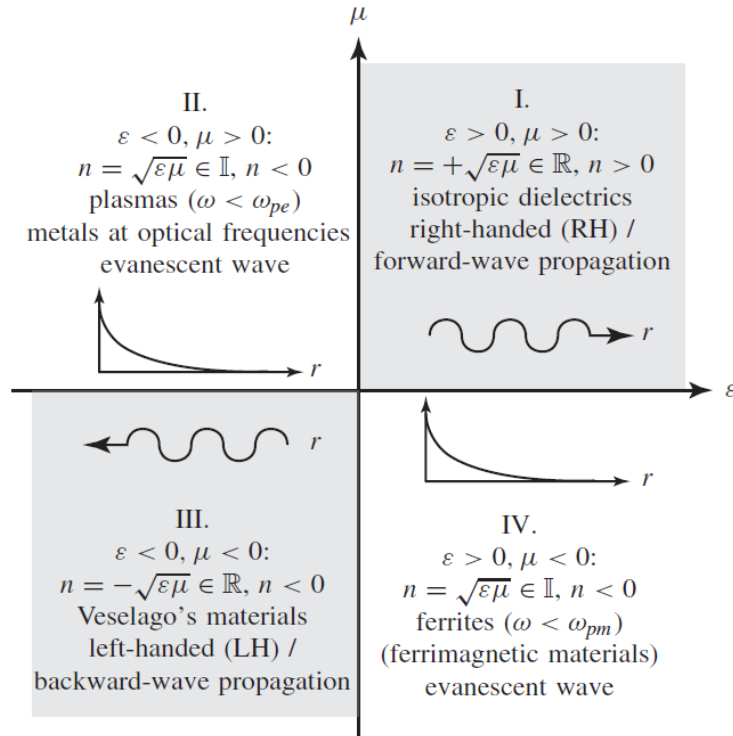


Fig3.1: Material classification [43]. The angular frequencies ω_{pe} and ω_{pm} represent the electric and magnetic plasma frequencies, respectively. R, purely real. I, purely imaginary

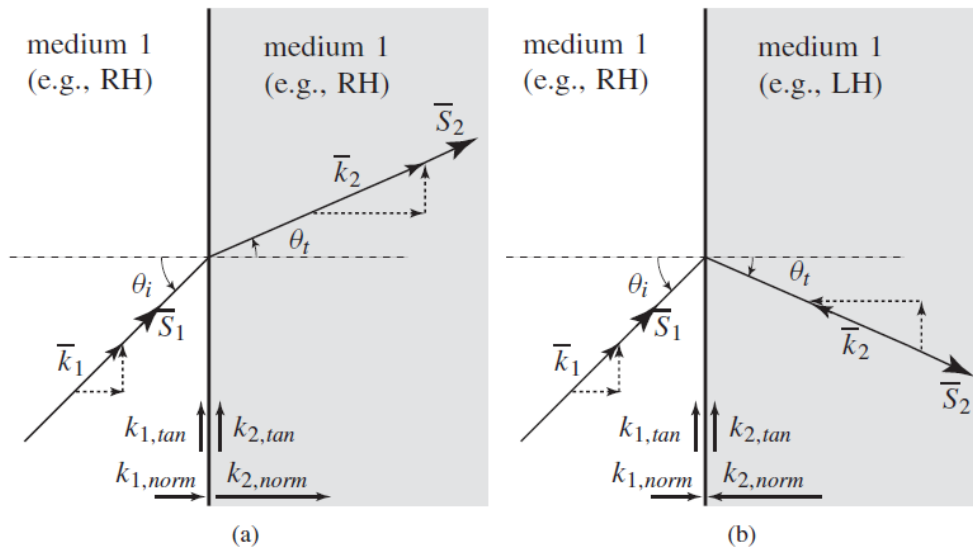


Fig 3.2: (a) Media with right-handed properties (b) Media with Left-handed properties [43].

The main purpose of Fig.3.2 is to illustrate the difference between the negative refractive index of Left hand material and positive refractive index in right hand materials only [43].

For materials with negative permittivity and permeability, one of the most important aspects is the concentration of waves. This feature is shown in Fig.3.3 below [43]. This characteristic plays a major role in converting the metasurface layer into a lens that focuses the electromagnetic waves traveling from the original antenna into plane waves and thus narrows the radiation beam's width, resulting in a good gain increase.

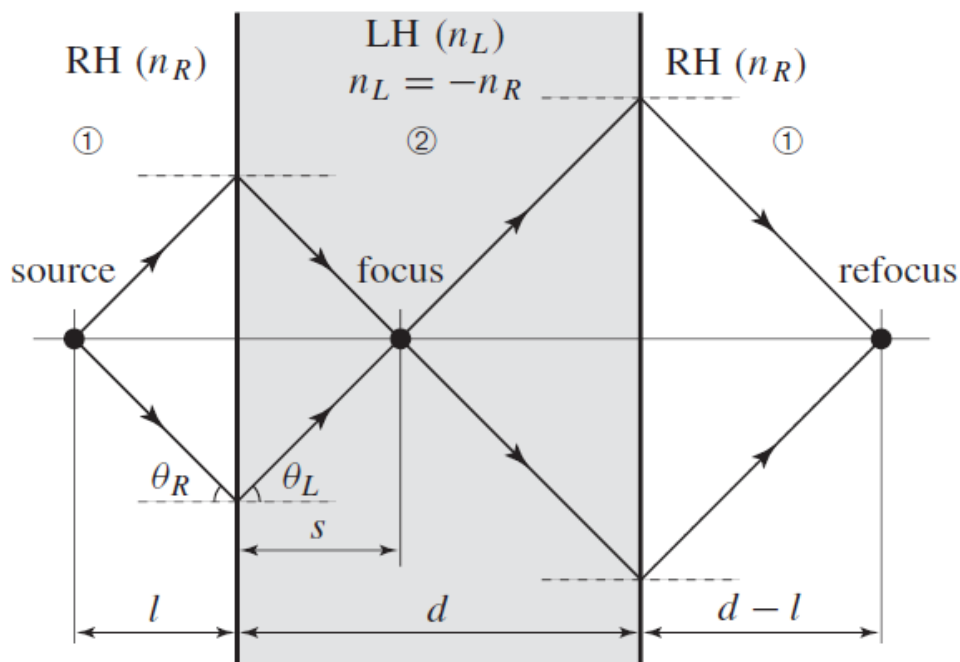


Fig 3.3 Double focusing effect in a “flat lens,” which is a LH slab of thickness d and refractive index n_L sandwiched between two RH media of refractive index n_R with $n_L = -n_R$. [43].

3.3 High-Gain Antennas

Gain is a merit figure which defines an antenna's ability to radiate input energy efficiently through space, modern communication systems have increasing the demands for high gain antennas to improve the overall system the signal to noise ratio (SNR) and gain [44,45]. To achieve an increase in antenna gain, will use new technologies to boost antenna efficiency. Fabry Perot is technology.

3.4 Fabry Pérot Technique

Employing doubly periodic arrays of conducting elements, or apertures in a conducting sheet, have been investigated in recent years [44,45], as they provide high-gain, high efficiency and a simple feeding network. Their name is derived from the classical fabry-perot interferometer which is widely used in optics. The latter is based on multiple reflections of waves between two parallel reflecting surfaces placed in close proximity creating a resonant cavity [45]. Fabry Pérot consist of a metallic or metallo-dielectric periodic array placed at approximately half-wavelength distance over a metallic ground plane and a low-directivity primary source (e.g. dipole). The passive array acts as a Partially Reflective Surface (PRS), creating a fabry-perot type resonant cavity that significantly increases the gain and directivity of the primary source [45].

The concept of FP antennas was first demonstrated by Trentini who studied how several types of PRSs can increase the directivity of a waveguide aperture in the ground plane. He was also the first to employ a ray optics approximation to describe the antenna operation by means of the multiple reflections between the ground plane and the PRS [45].

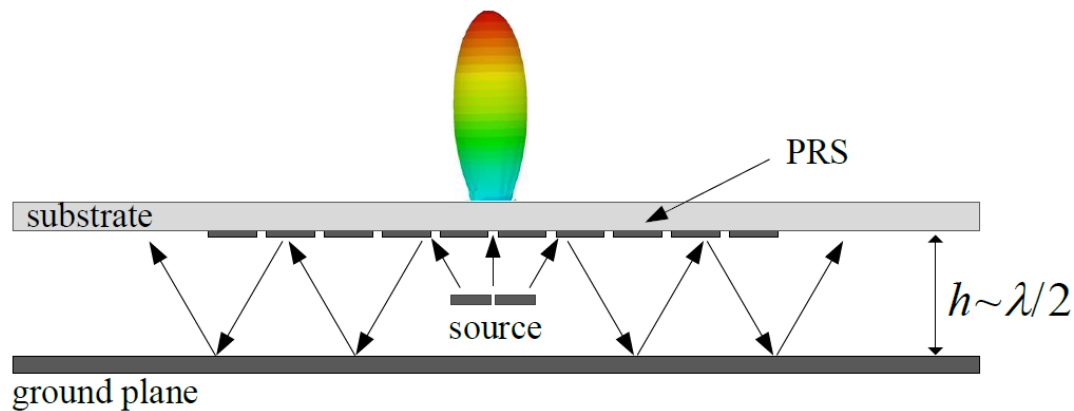


Fig 3.4: Schematic diagram of the partial reflection surface[45].

The operating frequency is defined by the cavity distance which is typically half-wavelength in order to achieve constructive interference of the waves bounced between the PRS and the ground. Later, different configurations were proposed employing one or more dielectric layers with different dielectric constants and thicknesses replacing the PRS layer. Since the operation of these antennas is based on the reflection characteristics of the PRS, high dielectric constant values were chosen to achieve high reflectivity values. PRS represent metasurface layer [45].

3.5 Feeding Techniques

There are many configurations that can be used to feed microstrip antennas. The five most popular are the microstrip line, coaxial probe, aperture coupling, proximity coupling, and Waveguide feed [1].

For the purpose of clarifying the mechanism of each feeding method correctly and the main components that contribute to the basic design of each type. The following paragraph will include a detailed definition of each model with an illustration.

3.5.1 Microstrip Line Feed

The microstrip feed line is also a conducting strip, usually of much smaller width compared to the patch. The microstrip-line feed is easy to fabricate, simple to match by controlling the inset position and rather simple to model. However as the substrate thickness increases, surface waves and spurious feed radiation increase [1,46]. Microstrip configuration is given below in Fig.3.5.

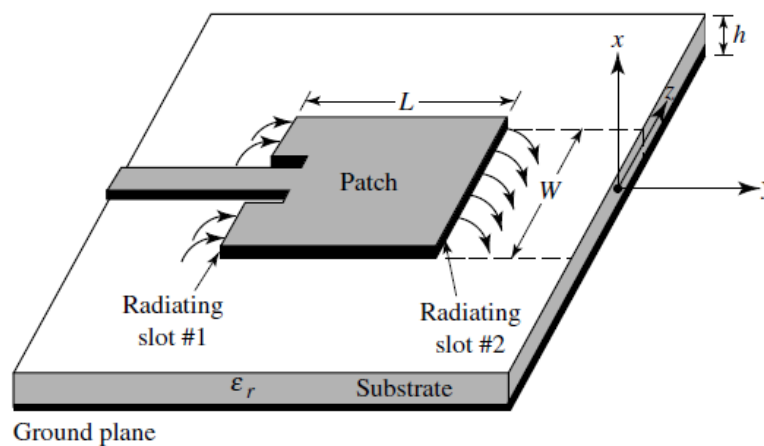


Fig 3.5: Microstrip feed line [1].

3.5.2 Coaxial-Line Feeds

This form of feeding consists of two parts internal and external. The inner conductor of the coaxial cable passes through the substrate to connect to the radiation layer, while another section of the coaxial cable is used to connect the ground plane. It has features such as matching and simple to manufacture [1,46]. Coaxial-line is shown in the Fig.3.6 below.

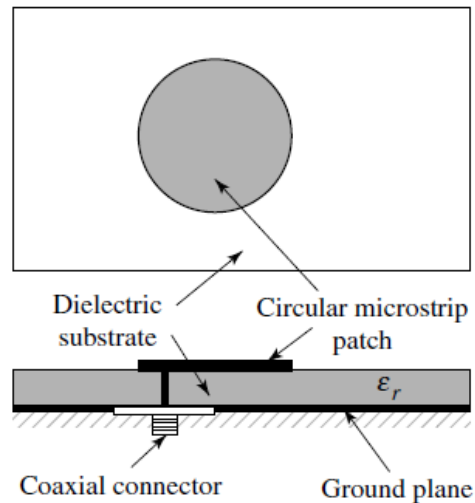


Fig3.6 :Coaxial-line feed [1].

3.5.3 Aperture-Coupled Feed

Figure.3.7 shows the aperture coupling which is considered to be the most difficult in terms of manufacturing between the other forms, in addition to its narrow bandwidth. It is composed of two substrates separating the ground level. At the bottom of the substrate is the microstrip feed line, the energy being coupled to a patch through the slot that etches on a ground plane disconnecting two substrates [1,46].

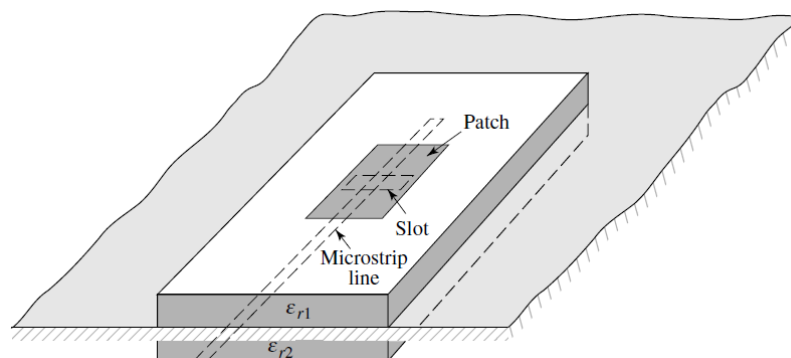


Fig 3.7: Aperture-coupled feed [1].

3.5.4 Proximity-Coupled Feed

The fourth form of the method of feeding [1,46] is shown in Fig.3.8 below:

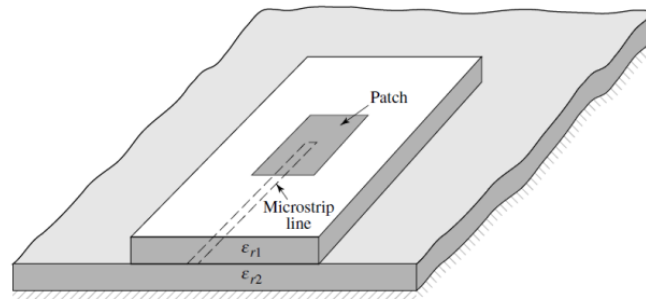


Figure 3.8: Proximity-coupled feed [1].

3.5.5 Waveguide feed

Waveguide port is the most common type of feeding methods. Waveguide feeding impedance is selected as 50Ω for matching purposes [47,48]. In other section of this chapter, address in detail the use of this method of feeding due to the consideration of the basic and significant role in the process of extracting permittivity and permeability values from a single cell. Fig.3.9 below shows waveguide feed.

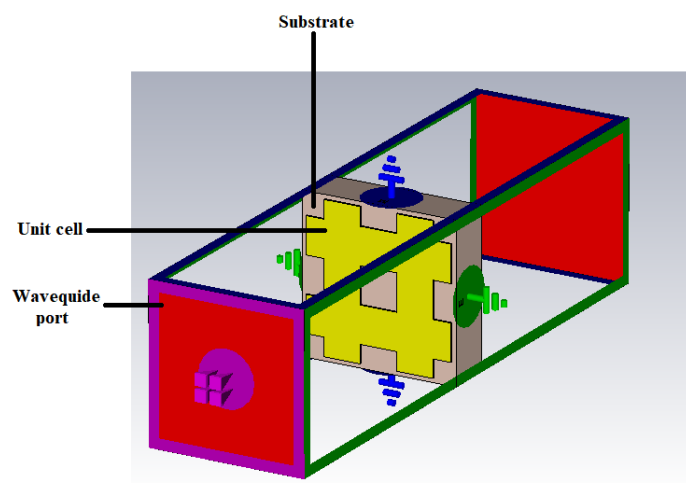


Fig 3.9: Waveguide feed.

3.6 Extraction of Metasurface Parameters

3.6.1 Method Definition

In this section, a step-by-step procedure is devised for extracting the material parameters to facilitate and simplify the design procedure of metasurface structures using commercial software packages. A parameter-retrieval method using the S-parameters is used to calculate the curves for the complex permittivity and permeability of the metasurface based on its unit element. The S parameters are extracted using CST. The permittivity and permeability curves are calculated using a CST package. Two different methods are used in CST to extract the S-parameters: one using perfect electric and perfect magnetic (PE-PM) boundary conditions, and the second using the master-slave boundary conditions[41,49].

Metasurfaces are usually realized by repeating a basic building block in a specific pattern. The basic building block is known as the unit element (UE), and it defines the basic properties of the metasurface. In a simulator, metasurface are modeled and simulated by introducing periodic boundary conditions applied to the boundaries of the unit element; it is assumed that the metasurface is formed by an infinite array of the unit element in the direction of the periodic boundary conditions[49,50,41].

The selection and design of a metasurface depend on the application and available resources. metasurfaces can be accurately designed using full-wave analysis, but it is a time-consuming task. On the other hand, a priori knowledge of the electromagnetic properties of the material will accelerate the design procedure. The electromagnetic properties, such as the complex permeability (μ) and the permittivity (ϵ) can be evaluated either by the analytical Drude-Lorentz model [49,52] or

by the S-parameter-retrieval method [49]. The Drude- Lorentz method is not accurate, especially if the unit element of the metasurface is a complex structure. On the other hand, the S-parameter-retrieval method depends on the S parameters extracted from the actual structure and hence provides more accurate values for the permittivity and permeability. In this work, will rely on this method. The S parameters will be extracted from CST, which is reliable and commercially [49].

3.6.2 Mathematical Formulation

In electromagnetics, the permittivity, permeability, and conductivity define the material's characteristics. The extraction of these values for different frequencies defines the propagation profile of the material at that frequency. In the extraction method used in this work, the refractive index and impedance of the material are used to extract the permittivity and permeability of the material under test [41,49].

To extract these material parameters (ϵ and μ), consider the unit element of a metasurface with lattice vectors in all three dimensions. Appropriate boundary conditions and excitations are assigned to the different surface of the three-dimensional unit element to simulate the periodic metasurface and excitation of this metasurface to extract the S parameters[41,53,49].

$$S_{11} = \frac{R_{01}(1-e^{i2nk_0d})}{1-R_{01}^2e^{i2nk_0d}} \quad (3.4)$$

$$S_{21} = \frac{(1-R_{01}^2)e^{i2nk_0d}}{1-R_{01}^2e^{i2nk_0d}} \quad (3.5)$$

Solve equ (3.4) in (3.5) gives:

$$Z = \pm \sqrt{\frac{(1+S_{11})^2-S_{21}^2}{(1-S_{11})^2-S_{21}^2}} \quad (3.6)$$

$$e^{ink_0d} = \frac{S_{21}}{1 - S_{11} \frac{Z-1}{Z+1}} \quad (3.7)$$

$$n = \frac{1}{k_0d} [\{ [\ln(e^{ink_0d})]'' \} + 2m\pi\} - i[\ln(e^{ink_0d})]'] \quad (3.8)$$

$$R_{01} = \frac{Z-1}{Z+1} \quad (3.9)$$

The permeability (μ) and permittivity (ε) are related to impedance and the refractive index by the following expressions:

$$\varepsilon = \frac{n}{Z} \quad (3.10)$$

$$\mu = nZ \quad (3.11)$$

$$n = \pm \sqrt{\varepsilon_r \mu_r} \quad (3.12)$$

The table below contains all the symbols mentioned in the above equations in detail:

Table 3.1: List of Symbol	
symbol	definition
(-)"	Complex Component
(-)'	Real Component
S_{11}	Reflection Coefficients
S_{21}	Transmission Coefficients
Z	Wave Impedance
n	Refractive Index
k_0	Wave Number
d	The unit Cell Maximum Length
m	The branch Due to The periodicity of The sinusoidal Function
R_{01}	The reflection Coefficient

3.6.3 Simulation and Extraction of Results

For the purpose of ensuring that the engineered metasurface layer includes negative permittivity and permeability properties, as well as the refractive index at the frequency at which the original microstrip antenna operates, thus guaranteeing a beneficial contribution to the original antenna's characteristics of the metasurface layer and achieving the best performance in antenna. This procedure is carried out by installing the unit cells first, which is the main component of the design on a substrate sheet slightly larger than the size of the unit cell patch surrounded by sufficient boundary conditions, such as perfect electricity on the X-axis, perfect magnet on the Y-axis, and two z-axis waveguide ports. In order to finally achieve the extraction for permittivity, permeability and refractive index. The S-parameter algorithm uses reflection and transmitted confection to get wanted curves [49,54]. Fig.3.10 below shows the full details of single unit cell to reach the required curves.

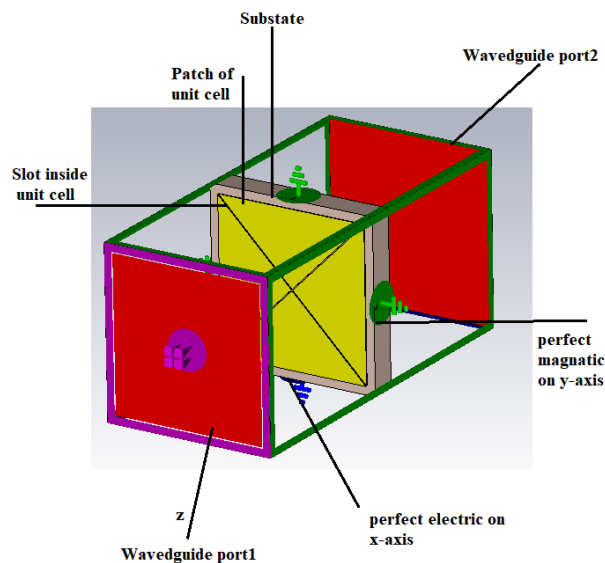


Fig 3.10: Unit cell between two waveguide ports.

3.7 Antenna Parameters

3.7.1 Directivity

The antenna directivity can be defined as the ratio between two values: the first one is the radiation intensity of the antenna in a given direction to the radiation intensity averaged which emitted over all directions. So the average radiation intensity for the antenna is equal to the total power radiated divided by 4π . If the direction is not specified, the direction of maximum radiation intensity is implied. The directivity can be calculated from eq (3.13) [1].

$$D = \frac{U}{U_0} = \frac{4\pi U}{P_{rad}} \quad (3.13)$$

Where: P_{rad} : represents total power radiation; U : represents radiation intensity ; U_0 = radiation intensity of isotropic source. reference [1] provides more information on the topic.

3.7.2 Gain

The gain of every antenna is formulated as the intensity ratio, in a particular direction, to the radiation intensity which would be obtained if the power is accepted by the antenna isotopically radiated. The radiation intensity equivalent to the isotopically radiated power is equal to the total power that the antenna divided by 4π accepts input. The gain can be compute from equ (3.14) [1]:

$$G = \frac{4\pi U}{P_{in}} \quad (3.14)$$

Where: P_{in} : represents total input power ; U : represents radiation intensity. Reference [1] provides more information on the topic.

3.7.3 Efficiency

Associated with an antenna are a number of efficiencies. The total antenna efficiency e_0 is used to take into account losses at the input terminals and within the structure of the antenna. Such losses may be due[1,56]:

1. reflections because of the mismatch between the transmission line and the antenna.
2. I^2R losses (conduction and dielectric).

In general, the overall efficiency can be written as

$$e_0 = e_r e_c e_d \quad (3.15)$$

e_0 = total efficiency (dimensionless).

e_r = reflection(mismatch) efficiency = $(1 - |\Gamma|^2)$ (dimensionless).

e_c = conduction efficiency (dimensionless).

e_d = dielectric efficiency (dimensionless).

$$e_0 = e_r e_{cd} = e_{cd} (1 - |\Gamma|^2) \quad (3.16)$$

Where $e_{cd} = e_c e_d$ = antenna radiation efficiency, which is used to relate the gain and directivity.

3.7.4 Bandwidth

The bandwidth for any antenna is defined as “the range of frequencies within which the performance of the antenna, with respect to some characteristic, conforms to a specified standard.” [1] So, the bandwidth of the antenna is obtained from the curve of reflection coefficient S11 depending on the -10 dB. Which represents a distance starting from the lower frequency and ending with the higher frequency [55].

3.8 The Proposed Model (I): Metasurface with X Slot in The Center of Unit Cell.

The design of a proposed metasurfaces based antenna is displayed in Fig.3.11. The proposed antenna is fed via aperture coupling of the microstrip line with a slot which has boarder ends etched in the centre of the ground plane. A feeding line is mounted on TLF-35A with substrate thickness $T_1 = 0.762$ mm, relative permittivity " $\epsilon = 3.5$ ", and loss tangent of 0.002. The metasurface is based on partial reflection surface composed of dual-layers with fully equal size, every one of them consists of a metallic square patch an array with X slot in the centre of each unit cell. As offered in Fig.3.11.(b), the metasurface contains 4×4 square metallic cells with X slot in the centre of each unit cell with N directional length and N directional width. The unit cells are distributed uniformly along with X and Y direction, with a gap among cells A. The proposed antenna feeding via microstrip line which placed at the centre of the slot is shown in Fig.3.11.(c).

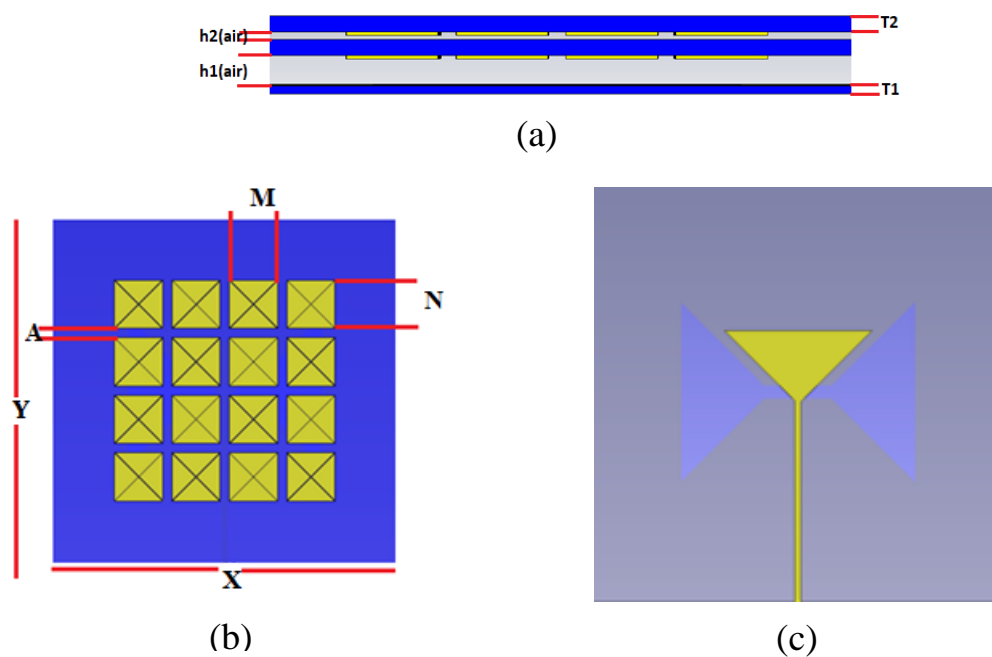


Fig.3.11: Proposed antenna structure: a- slot antenna with metasurface MS (side view) and b-Metasurface MS layer c- slot and feed-line .

The dimensions of antenna parameters are mentioned in Table 3.2.

Table 3.2: The dimensions of the antenna parameters

No	Element Names	Symbol	Value
1	The side length of patch	N	9 mm
2	The side width of patch	M	9 mm
3	Gap between cells	A	1.7 mm
4	Substrate length	X	65 mm
5	Substrate width	Y	65 mm
6	Feed line length	S	40.5 mm
7	Feed line Width	W	1 mm
8	Length of slot	L_z	36 mm
9	Width of slot	W_z	2mm
10	Air gap 1	hair ₁	3.2 mm
11	Air gap 2	hair ₂	0.75 mm
12	Slot length inside cell	C_x	7 mm
13	Slot width inside cell	mn	0.03 mm

3.9 The Proposed Model (II): Metasurface with (Uniform Distribution and Gradient Distribution).

Two different types of antennas are designed based on metasurface, being uniform and gradient distributions of patches unit cells. The aim of using of such a periodic metasurface structure is to enhance some antenna performance parameters such as gain, bandwidth, and return loss (matching). The proposed antenna structures are divided into three parts, a microstrip transmission line feeding, a slot antennae, and a metasurface layer. The energy provided by the microstrip feeding is coupled to the antenna slot where the slot antenna launches electromagnetic waves into space. The metasurface which in turn is electromagnetically coupled to the slot antenna focuses the launched waves in smaller areas. Thus, the antenna radiation beams become narrower and the gain becomes higher. Because the metasurface layers

consist of 2D distributed rectangular metallic unit cells made from copper with a certain number of cells separated by a gap width of (A), the proposed antenna has a large number degree of freedom to improve its functionalities.

3.9.1-Slot Antenna

Figure 3.12 displays the design layout of an proposed antenna, consisting of only a rectangular slot fed by the aperture coupling technique. The length of the slot L_z determines the resonant frequency, according to the half wavelength while the slot width W_z plays a vital role in optimizing the antenna matching. A slot is etched on the top of the substrate and the microstrip transmission line is printed on the bottom of the substrate. The substrate is FR4 with thickness of $T_1=0.762\text{mm}$, loss tangent 0.0025, and dielectric constant $\epsilon = 4.3$. Table 3.3 presents the slot antenna dimensions; all dimensions are in mm.

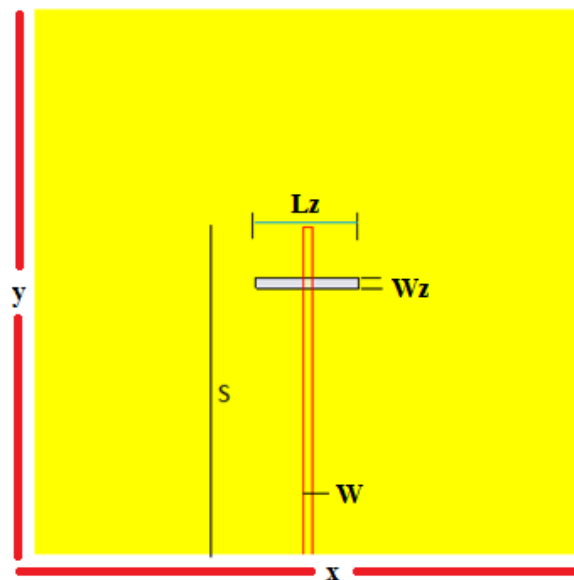


Fig.3.12: Structure of the slot antenna.

Table 3.3: A summary of the slot antenna.

No	Parameter	Symbol	Value
1	Width of substrate	X	108
2	Length of substrate	Y	108
3	Slot width	Wz	3
4	Slot length	Lz	14.5
5	Feed length	S	58
6	Feed width	W	3

The feeding is 50Ω microstrip transmission-line. Indeed, it extends beyond the slot to reach the optimum matching. The distance beyond the slot should be around a quarter wavelength $\lambda/4$ at a frequency of interest to effectively excite the slot. Since the microstrip transmission-line is open-ended, the current reaches its maximum value at the slot. This procedure aids to transfer the energy from microstrip transmission-line to a slot. One of the conventional slot antenna disadvantages is its narrowband response, so using the metasurface assists to widen the bandwidth. Furthermore, there are a lot of ways to increase the bandwidth, but most of them do not enhance the gain. The most attractive property carried out by using the metasurface is the enhancement of the gain as given in the following subsection.

3.9.2 Metasurface Based on The Antenna Design

3.9.2.1. Metasurface with Equal Length Unit Cells (Uniform Distribution)

Present thesis work is primarily concerned with the designing of small footprint antenna for wireless applications. To bear in mind, the proposed design can be scaled up or down to obtain any frequency, so the design is

frequency scalable. In this part, a metasurface layer, consisting of periodic 5×5 metallic patches i.e., unit cells with equal dimensions is added at the top of slot separated by a distance h_{air} . The space between the slot and the metasurface layer is air. The metallic patches are etched over an FR4 substrate with thickness $T_2=1.6\text{mm}$, the loss tangent of 0.0025, and relative permittivity $\epsilon = 4.3$. The arm side length of each unit cell is $M = N = 10\text{mm}$ and the gap between the unit cells is $A = 2\text{mm}$. Height of the air cavity is 4.8mm. These dimensions are obtained after a huge number of simulations to realize the best responses for the proposed antennas. Fig.3.13 shows the proposed antenna with uniform MS layer.

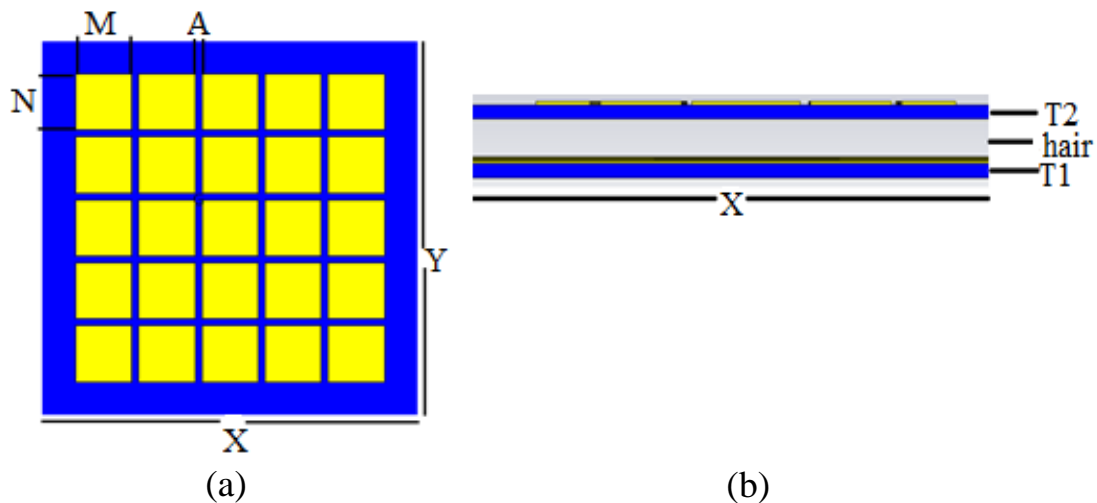


Fig.3.13: The proposed antenna with uniform size distribution metasurface:(a) top view (b) side view.

The metasurface is placed in the near-field region of the slot antenna. The waves have a spherical-like phase behavior, so adding the metasurface in front of the spherical waves converts them to plane waves, being in-phase as shown in Fig.3.14. In other words, these periodic unit cells converge the electromagnetic waves in narrower volumetric space, leading to increase the antenna gain and radiating for long distances.

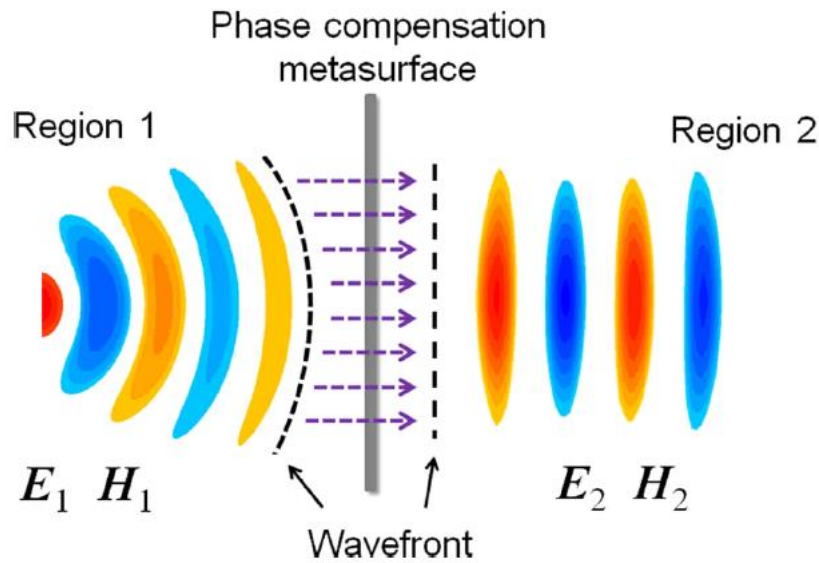


Fig 3.14: A metasurface engineered with discrete elements that provide spatial phase distribution that offset the sphere-like front of the wave into a planar one [34].

3.9.2.2. Metasurface with Unequal Length Unit Cells (Gradient Distribution)

Figure 3.15 shows the structure of metasurface with gradient size distribution of the metasurface. This type of metasurface has the ability to bend the electromagnetic wave into the focal point of the metasurface. Compared to conventional metasurface, the gradient metasurface focuses the electromagnetic power in more narrow volumetric spaces. As a result, the antenna increases the gain, because the unit cells have different dimensions and they are transparent for the electromagnetic waves, waves passing through unit cells experience to different phase shift. Gradient size distribution is symmetrically implemented along the x-axis, but it still the same along the y-axis. This means that the proposed antenna focuses the power in one direction more than the other. Moreover, the gradient distribution can be extended to the y-axis, but it is left as a future work. Table 3.4 presents the dimensions of the new metasurfaces.

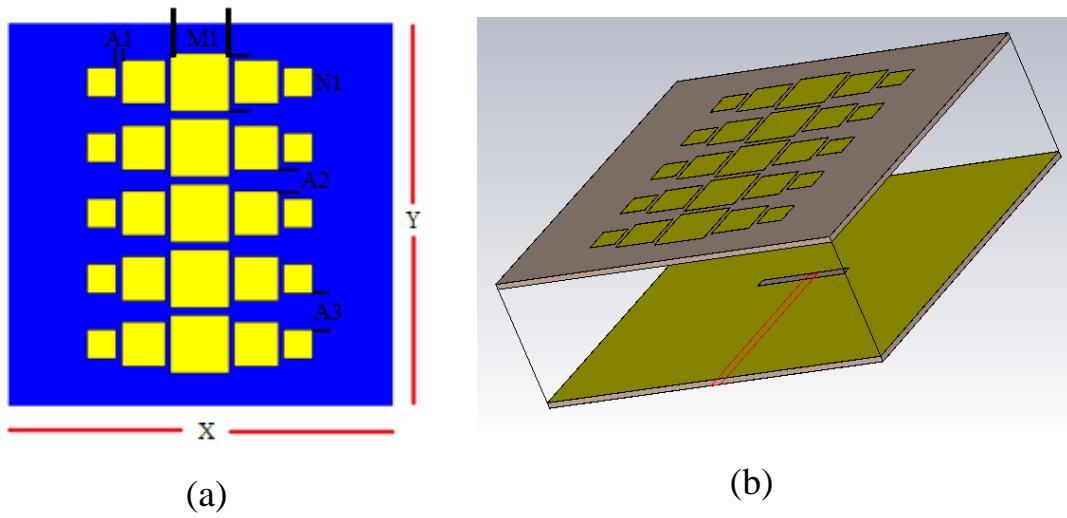


Fig 3.15 (a) The proposed antenna with gradient size distribution (b) metasurface 2D.

Table 3.4: A Summary of The Gradient metasurface dimensions

No	Parameter	symbol	Value mm
1	Big cell width ,length	M1,N1	8
2	Medium cell width,length	M2,N2	6
3	Small cell width ,length	M3,N3	4
4	Gap between cell	A1	1.5
5	Gap between cell	A2	6
6	Gap between cell	A3	10

3.10 The Proposed Model (III): Metasurface with Different Cell Forms

This construction mainly deals with the design of a small footprint antennas. To bear in mind, the proposed design size can be scaled up or down to operate at any desired frequency, making an adjustable structure.

In this section, we will discuss parts of the proposed antenna in detail, starting with the slot antenna as shown in Fig. 3.16.

The slot antenna is cut out from a conductor layer placed over a RO4003C substrate with a dielectric constant 3.55 and a thickness of 1.5mm. The slot has two slot triangles attached to ends of slots, aiming to widen the bandwidth and enhancing the matching. This slot is excited by a microstrip feeding line with 50 ohm characteristics impedance. This line extends about a quarter-wavelength at the desired frequency to excite the slot with a maximum current. The shape of extended line is a triangle as well for the same reason, broadening the bandwidth. Fig.3.16.b shows the metasurface layer used in the proposed structure.

Thus, unit cells have two different sizes. Each four patches within the small size unit cells are equal to one size of the big unit cell. The variation in size results in a wide bandwidth. The distance separating between the slot antenna and the metasurface denoted by hair plays a vital role in determining the overall performance as will be seen later in this research study. Also, the RO4003C substrate is used to design the metasurface layer. The thickness T_2 is 0.81mm and the relative dielectric constant is 3.55. The bigger unit cell has side length equal to $M_1=N_1=5.42\text{mm}$ and the smaller one equal to $M_2=N_2=2.68\text{mm}$, see Fig. 3.16.b. The air cavity, known as Fabry-Parot FP resonating cavity is optimized at 3mm to obtain the highest possible gain.

The radiated power is focused in smaller beams, resulting in high gain structures. The side view and three-dimensional views of the proposed antenna are portrayed in Fig3.16.c and 3.16.d, respectively. Table 3.5 lists the proposed antenna dimensions. The dimensions given in the table are chosen after a huge number of attempts to optimize the antenna work.

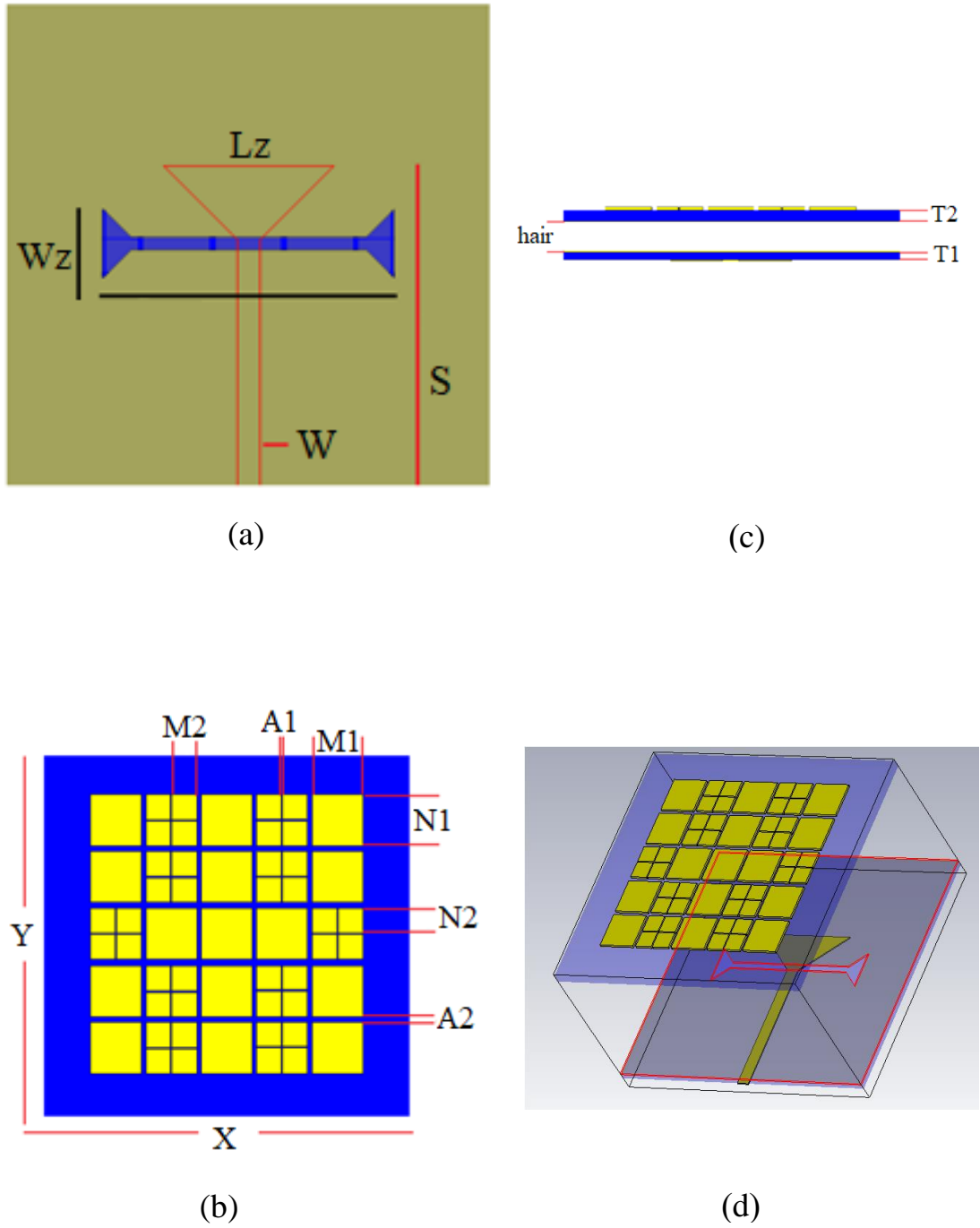


Fig.3.16: (a) Feed line and slot (b) Top view of metasurface
 (c) Side view of antenna (d) 3D view of proposed antenna.

Table 3.5: Final Antenna Dimensions

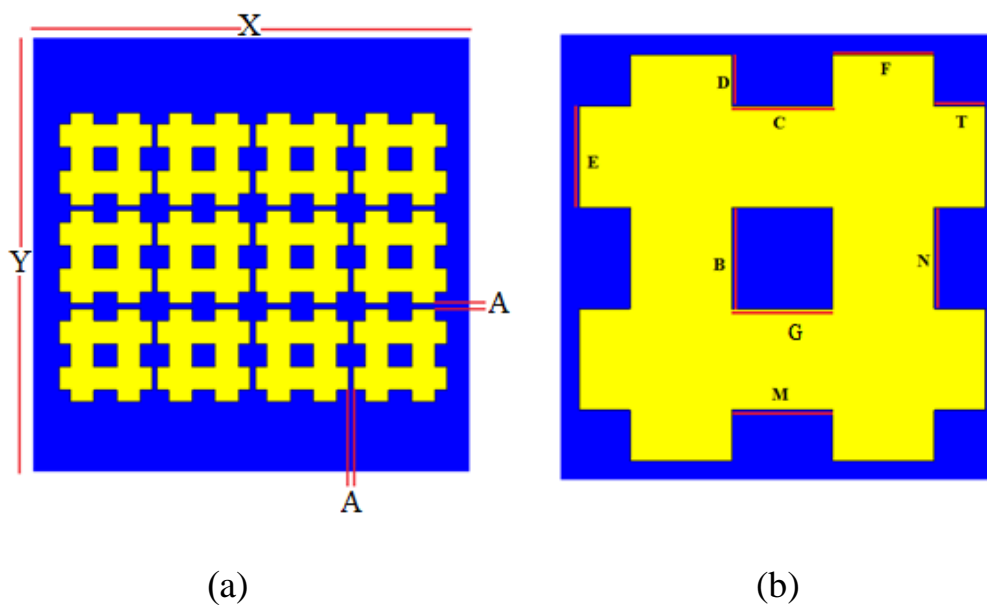
No	Parameters	Symbol	Value
1	The side length of big patch	M_1	5.42 mm
2	The side width of big patch	N_1	5.42 mm
3	The side length of small patch	M_2	2.68 mm
4	The side width of small patch	N_2	2.68 mm
5	Gap between cells	A_1	0.7 mm
6	Gap between cells	A_2	0.16 mm
7	Substrate length	Y	40 mm
8	Substrate width	X	40 mm
9	Length of feed line	S	26.5 mm
10	Width of feed line	W	0.9 mm
11	Slot length	L_z	12 mm
12	Slot width	W_z	0.5 mm
13	Air gap 1	hair	3 mm
14	Substrate of slot antenna	T_1	0.813mm
15	Substrate of metasurface	T_2	0.81mm

The MS layer is added in the near field of the slot antenna, so the waves leaving the slot antenna that have spherical-like phase are converted to plane waves, being in phase. In other words, these periodic unit cells concentrate the EM waves in narrower volumetric space, leading to enhance an antenna gain and radiating for long distances. Furthermore, unit cells also improve an impedance bandwidth by adding many resonance effects into antenna response.

Figure 3.14 includes a complete illustration of the wave transfer process from the conventional antenna to the metasurface layer, which in turn performs the most important process, which is the transformation of the emission form for the purpose of focusing in narrow areas, thus effectively contributing to improving the general performance of the antenna.

3.11 The Proposed Model (IIV): Metasurface with Hash Unit Cell.

The configuration of the proposed antenna composed of metasurface layer with 4 X 4 unit cells takes the form of a hash sign (#) with equal dimensions is added at the top of slot separated by a distance hair. The space between the slot and the metasurface layer is air. The hashes unit cells are etched over a RO4003C substrate with thickness $T_2=2.5\text{mm}$, the loss tangent of 0.0025, and relative permittivity $\epsilon = 3.55$. The hash unit cell dimension mentioned in Table 3.6 with the gap between the unit cells is $A=0.5\text{mm}$ while ground plane placed on substrate $T_2=0.813$. Height of the air cavity is 1 mm. These dimensions are obtained after a huge number of simulations to realize the best responses for the proposed antennas. Fig. 3.17 shows the proposed antenna with metasurface layer based on the hash shape of the unit cell.



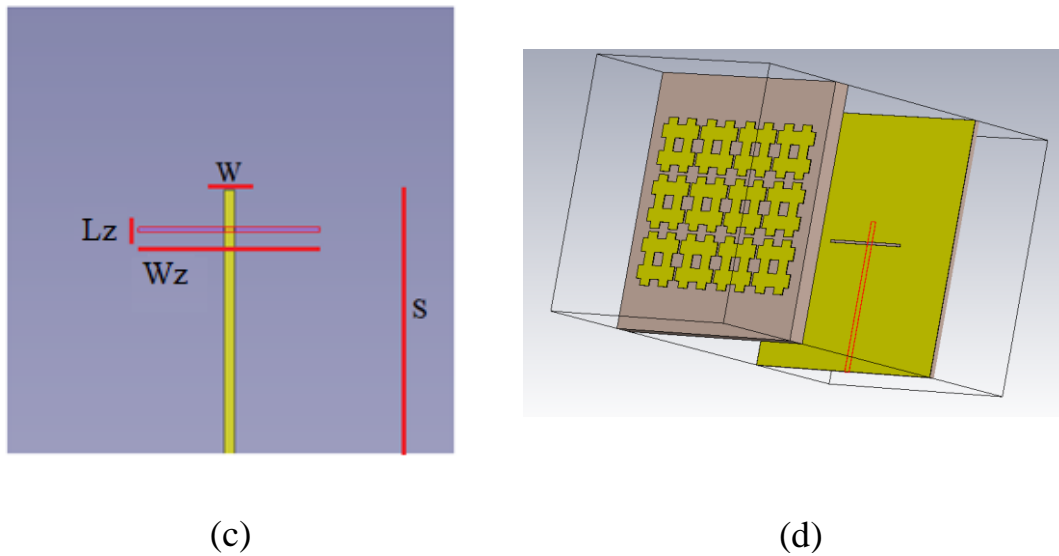


Fig 3.17: shows (a) Top view of metasurface (b) hash unit cell (c) Feed line and slot (d) 3D view of proposed antenna.

The metasurface is placed in the near-field region of the slot antenna. The waves have a spherical-like phase behavior, so adding the metasurface in front of the spherical waves converts them to plane waves, being in-phase. In other words, these periodic unit cells converge the electromagnetic waves in narrower volumetric space, leading to increase the antenna gain and radiating for long distances. Furthermore, unit cells also enhance the impedance bandwidth via adding more resonance effects to the antenna response.

Figure 3.14 includes a complete illustration of the wave transfer process from the conventional antenna to the metasurface layer, which in turn performs the most important process, which is the transformation of the emission form for the purpose of focusing in narrow areas, thus effectively contributing to improving the general performance of the antenna.

No		Symbol	Value
1	Substrate width	X	40 mm
2	Substrate length	Y	40 mm
3	Gap between cells	A	0.5 mm
4	Line inside cell	G	2mm
5	Line inside cell	B	2.1 mm
6	Line inside cell	C	2.1 mm
7	Line inside cell	D	1.05 mm
8	Line inside cell	E	2.1mm
9	Line inside cell	F	2.1 mm
10	Line inside cell	T	1.05 mm
11	Cell length	N	2.1 mm
12	Cell width	M	2.1 mm
13	Feed line length	S	23.5 mm
14	Feed line width	W	0.5mm
15	Line inside cell	K	16 mm
16	Line inside cell	Z	0.4mm

Until check the condition mentioned at the beginning of the third chapter in relation to the size of the cell, which must be the size of the cell smaller than a quarter of the wavelength. A comparison will be made between the theoretical calculation of the cell size and that used in the simulation. This comparison is mentioned in Table 3.7.

17.32 mm is The theoretically obtained value for the first antenna is While the best value obtained from the simulation was at the value 9mm, in which the capacitive effect of the metasurface layer is equal to the inductive effect of the conventional antenna, which leads to the cancellation of one of the other. While the rest value was very close between the theoretical and the value used in the simulation process. All values are listed in the table below.

No	Design Name	Theoretical Cell Size Less Than a quarter Of The wavelength	Cell Size That Used in Simulation
1	First Design :Metasurface With X Slot in Center of unit cell	17.32 mm	9 mm
2	Second Design : part 1 Uniform Distribution Of unit Cell	8.75 mm	8 mm
3	Second Design :part 2 Gradient Distribution Of unit Cell	8.75 mm	8 mm ,6 mm ,4 mm
4	Third Deign : Different cell size	8.75 mm	6mm
5	Fourth Design: Metasurface with Hash Unit Cell	10.75 mm	9.45mm

Chapter Four

Results and

Discussion

CHAPTER FOUR

RESULTS, DISCUSSION AND PARAMETRIC STUDY

4.1 Introduction

In this chapter studying the effect of changing a number of elements on the performance of the antenna, as well as obtaining results after simulating the designs that have been mentioned in Chapter Three, which include both S-parameter, gain, directivity, current distribution and the bandwidth, Radiation pattern, in addition to making a comparison between the original antenna (slot antenna) before adding the metasurface layer and after adding, then comparing it with other references to show the contribution get from these designs.

4.2 Characteristics of metasurface with X slot in the center of unit cell (I).

4.2.1 Extracting Permeability, Permittivity and Refractive Index from S-Parameter

In this part of chapter will discuss the results of the first design, and the discussion focused on the method of extracting the results through which can make sure that the design that was simulated in the CST is a design that depends on the metasurface in its construction. The parameter retrieval mode using the S-parameters is employed to computation a curve for complex permeability and permittivity of metasurface depend on its unit cell element, as mentioned in detail in the third chapter. After isolating only one cell from the design, placing it appropriately on the substrate and feeding it with a pair of the waveguide ports and applying the appropriate boundary condition from an

appropriate electric and magnetic field the results based on CST program appear. The results of method is shown in Fig. 4.1 below.

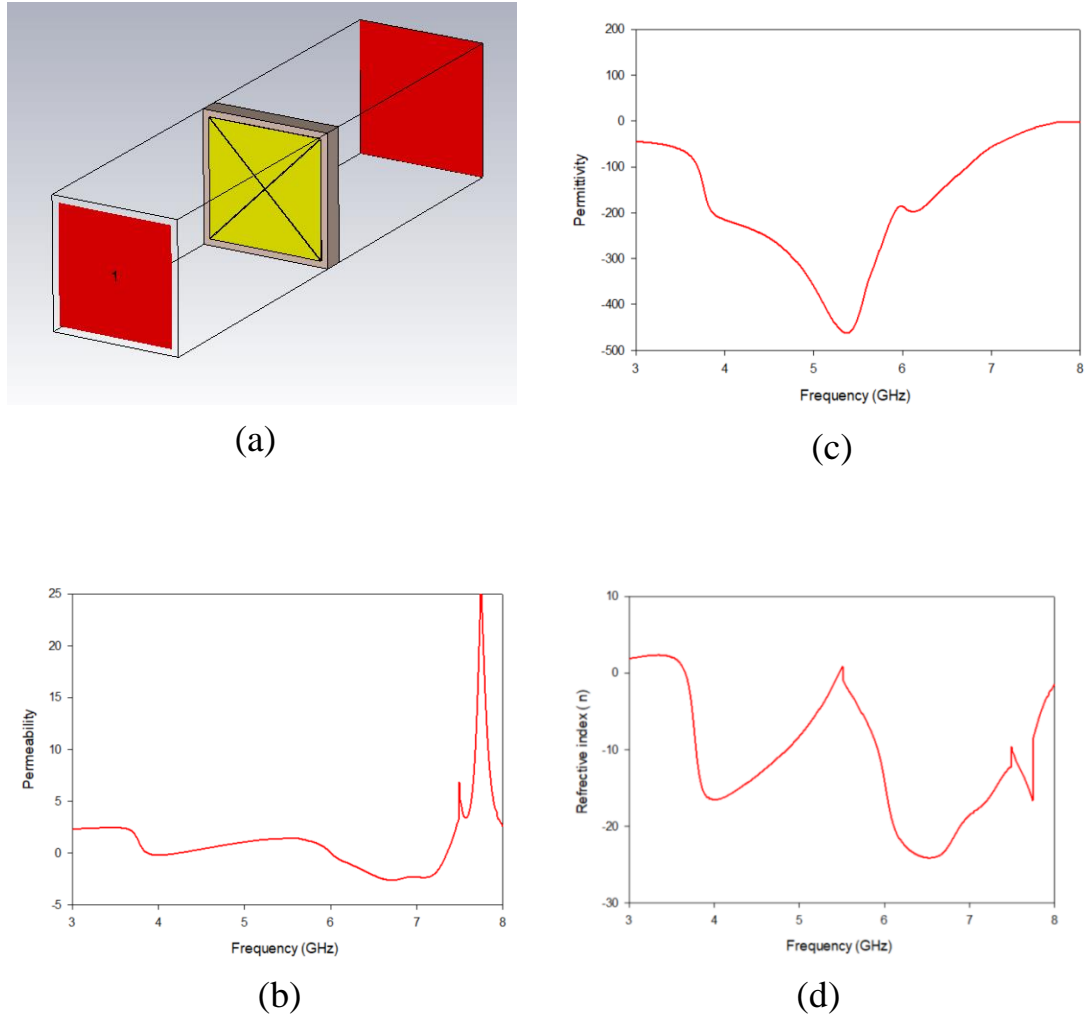


Fig 4.1:(a) The single unit cell of MS in CST,(b), Relative permeability of MS. (c), Relative permittivity of the MS. (d), Refractive index of the MS.

The curves showed negative characteristic for permittivity, permeability and refractive index, which in turn represent the metasurface layer at the wanted frequency, which represents the frequency range from 4.01 GHz to 7.01 GHz.

4.2.2- Reflection Coefficient , Gain, Directivity , Current Distribution

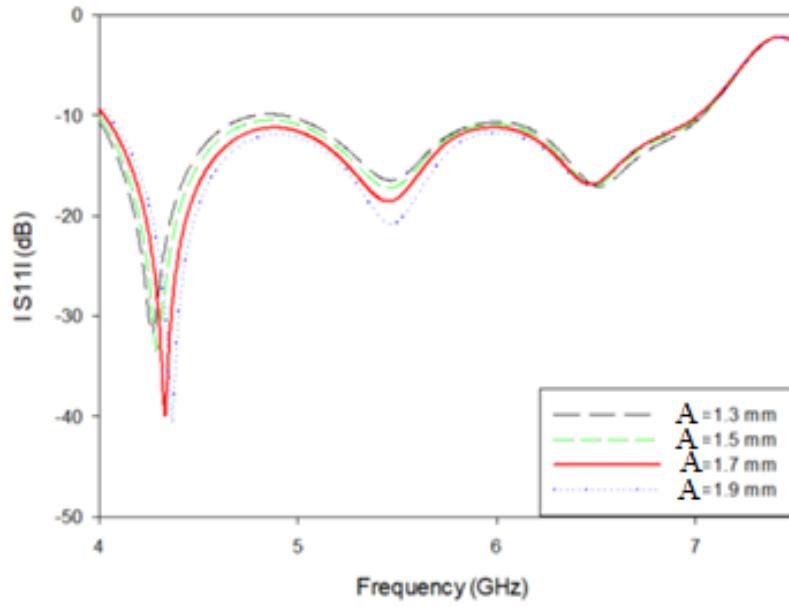
The proposed antennas are carefully designed, and their operating functionalities must be calculated accurately. The parametric study given here provides such a good example to understand the working mechanism of the proposed antenna and whose dimensions parameters impact the design performance.

4.2.2.1. Parametric Study

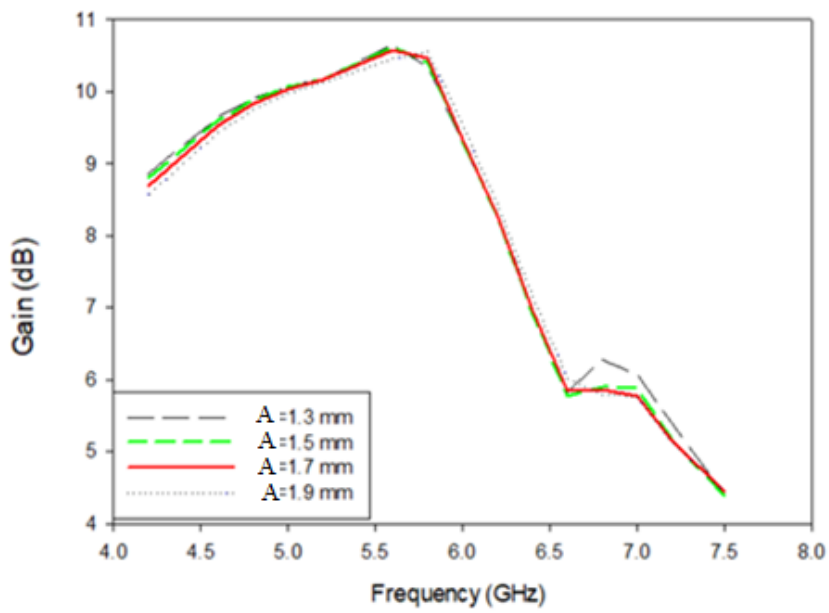
4.2.2.1.1- Impact of Gap Between Cell

In this section of the study try to reach the best results for each element, where beginning study with the capacitive effect of the gaps between cells and their effect on the gain and the bandwidth, and try to reach a value of the capacitive effect that is sufficient for the value of the inductive effect resulting from the slot in the conventional antenna, which will cancel it, making the antenna work at the best performance, Through the study, it was found that the best value in the two sides of the gain and the bandwidth is 1.7mm, which is specified in red.

While when the value of the gap between the cells of the metasurface layer is 1.3mm, the performance of the antenna is at the lowest possible in the bandwidth and this performance is shown in black color, but the same value of the gain is kept at 1.7mm. The value of the gap at 1.5 mm is slightly better, but the bandwidth the amount does not reach the performance obtained at 1.7mm.



(a)

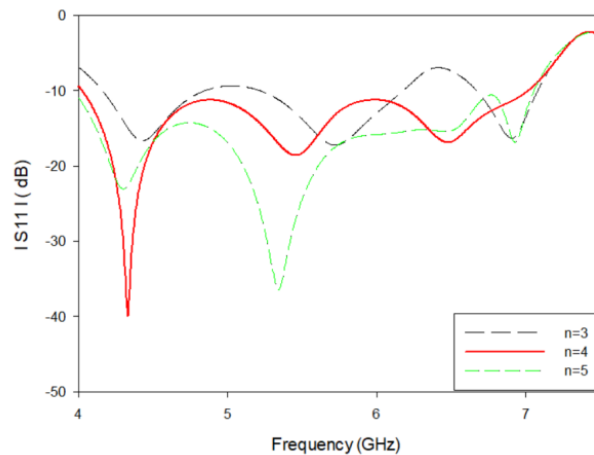


(b)

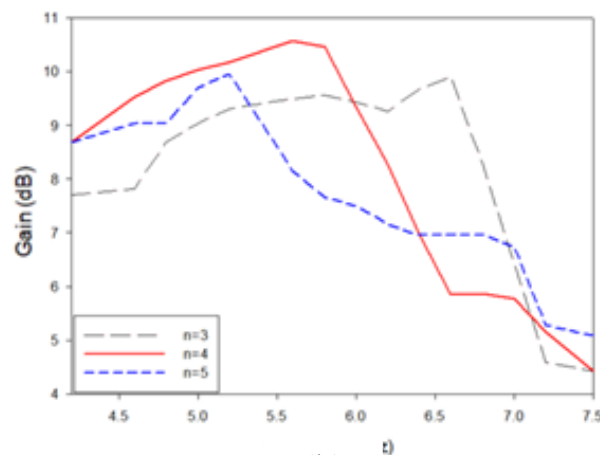
Fig.4.2: study (a) S11 and (b) Gain on gaps between unit cell start from 1.3mm to 1.9mm

4.2.2.1.2- Impact of Cell Number

In this part, the effect of the number of cells on both the gain and the bandwidth is studied, where conduct a study on the number of cells 3 x 3, 4 x 4 and 5 x 5 in an attempt to reach the best suitable capacitive effect between cells in addition to the effect of coupling between the metasurface layer and the conventional antenna, where all these factors effect focus on canceling the inductive effect of slot, as it was noticed that the best results were achieved in the number of cells 4 x 4 in the sides of the gain and the bandwidth.



(a)

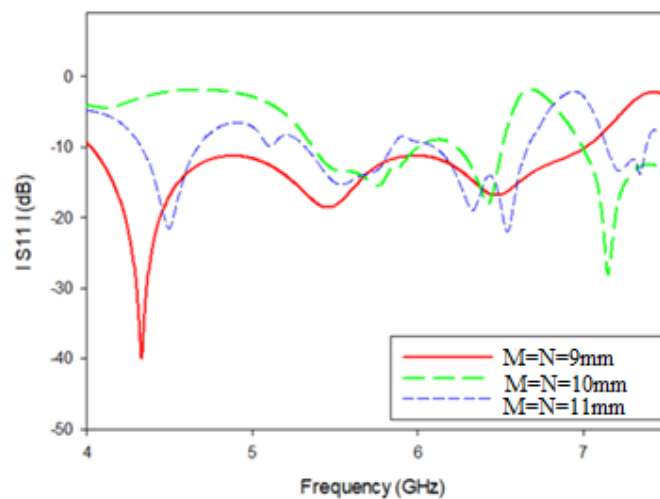


(b)

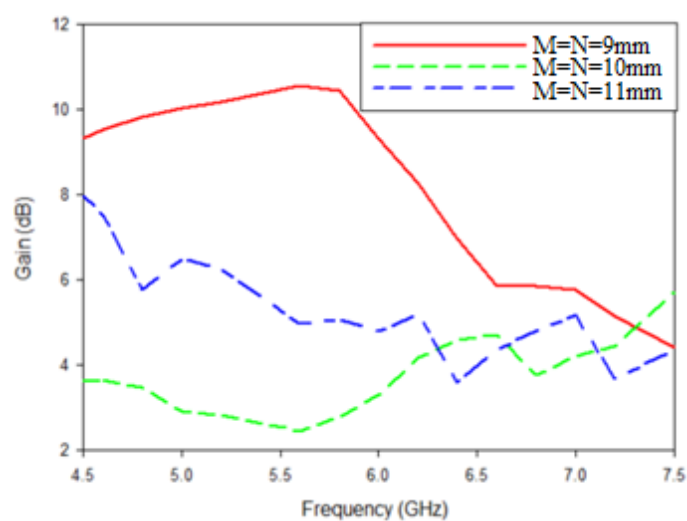
Fig.4.3: study effect of the number of the unit cells of the metasurface layer when $A=1.7\text{mm}$ on (a) S11 and (b) Gain on

4.2.2.1.3-Impact of Cell Size

The impact of various metallic patch unit cells sizes on gain and bandwidth performances are shown in Fig.4.4, M and N represent side length over each of x and y direction, respectively. Obtain the best result of both the gain and the range of bandwidth, and the reason is due to reaching the best size for the cell diameter at 9 mm that achieves the repeatability condition in the metasurface, which is smaller than a quarter of the wavelength.



(a)



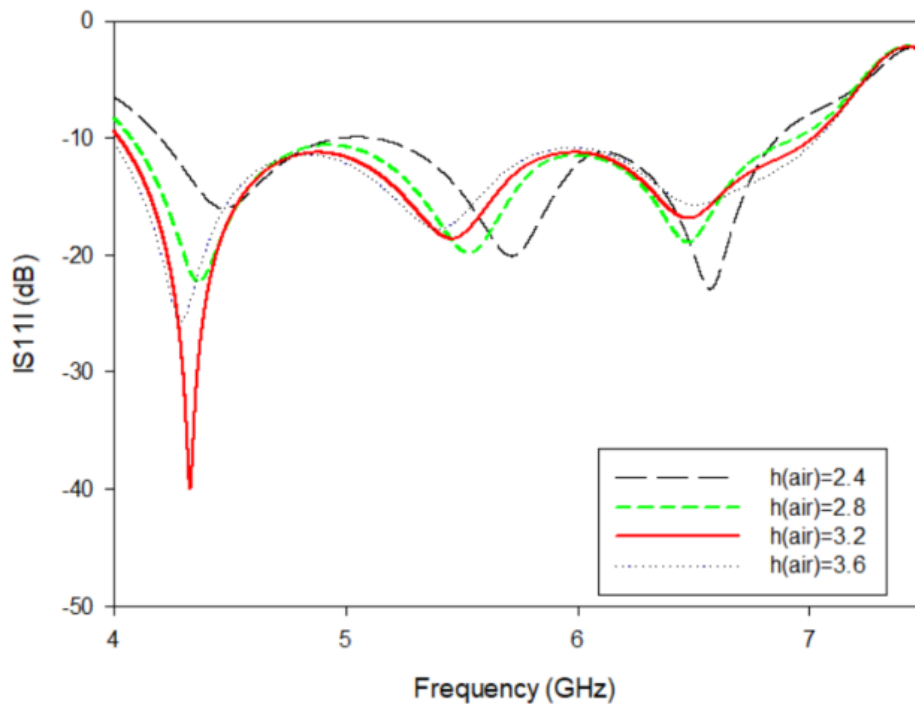
(b)

Fig 4.4: study the effect of the cell size on (a) S11 and (b) Gain from 9mm to 11mm

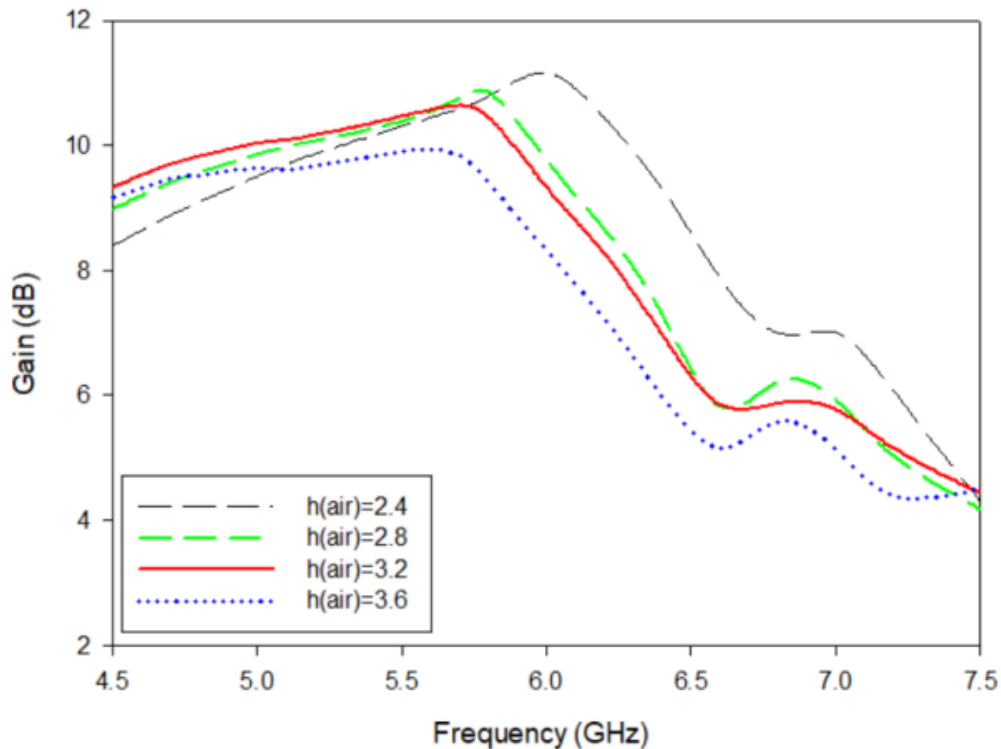
4.2.2.1.4- Influences of Air Cavity Height

It shows impacts of the air gap separating between the slot antenna and the metasurface layer on the bandwidth range and gain value of a proposed antenna, after several steps of optimization. To arrive at the best value for the height of the cavity, the constructive interference is achieved between the transmitted wave and the modulated phase wave after its reflection in the cavity. Accordingly, when the air gap is equal to 3.2 mm, the antenna offers a wide bandwidth. However, this air gap does not provide the highest gain, but it is acceptable if consider the bandwidth trading off.

In addition to another reason, which is to reach the best capacitive effect between the slot antenna and the metasurface layer, which in turn eliminates the inductive effect resulting from the slot in the slot antenna, thus achieving the best results for the designed antenna



(a)

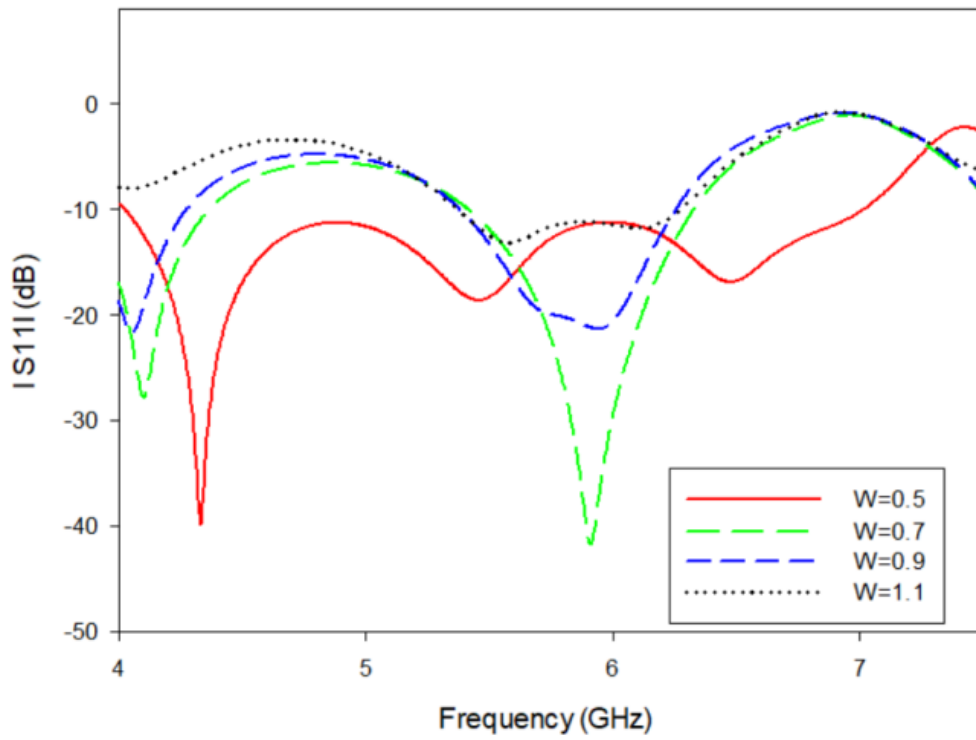


(b)

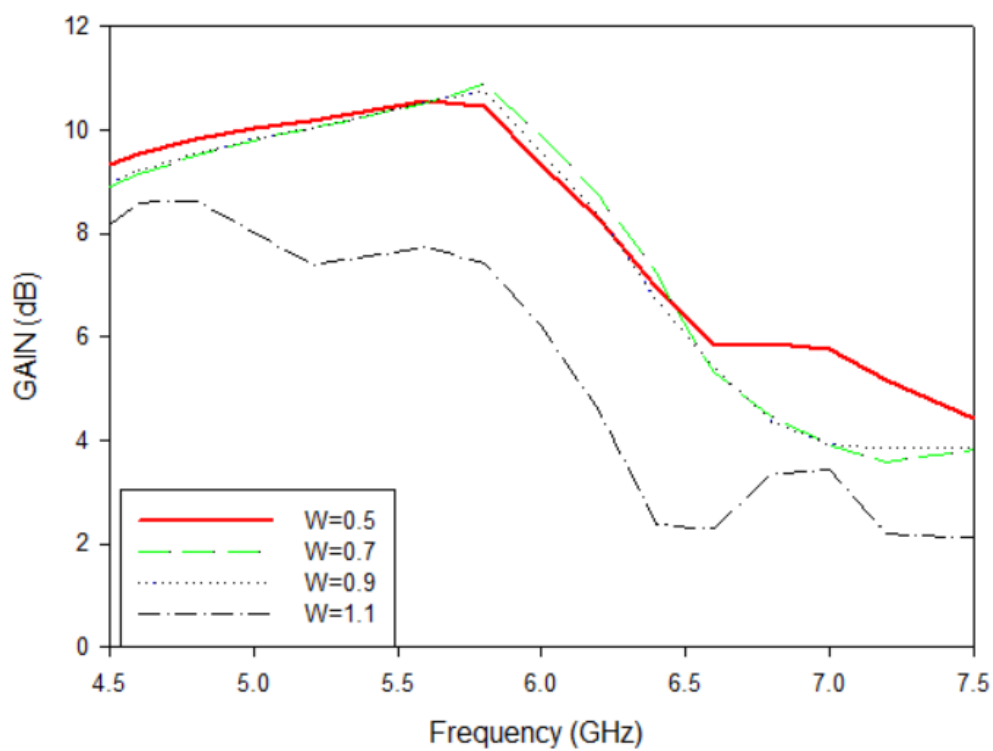
Fig 4.5: Study the effect of air cavity height on
(a) S11 and (b) Gain from 2.4mm to 3.6mm

4.2.2.1.5- The Effect of Feed Line Width

The influences of the feed line width on both gain and bandwidth are studied as shown in the Fig. 4.6. Can observe the increase in the width of the line lead to increases gain but with decrease in bandwidth. So the optimum value for the feed line width is $W=0.5\text{mm}$. It has got the best value for the feeding line and consequently obtaining the best antenna performance as a result of the flow of current through the feeding line, which contributes in correct feeding process for the slot etched on the ground plane.



(a)



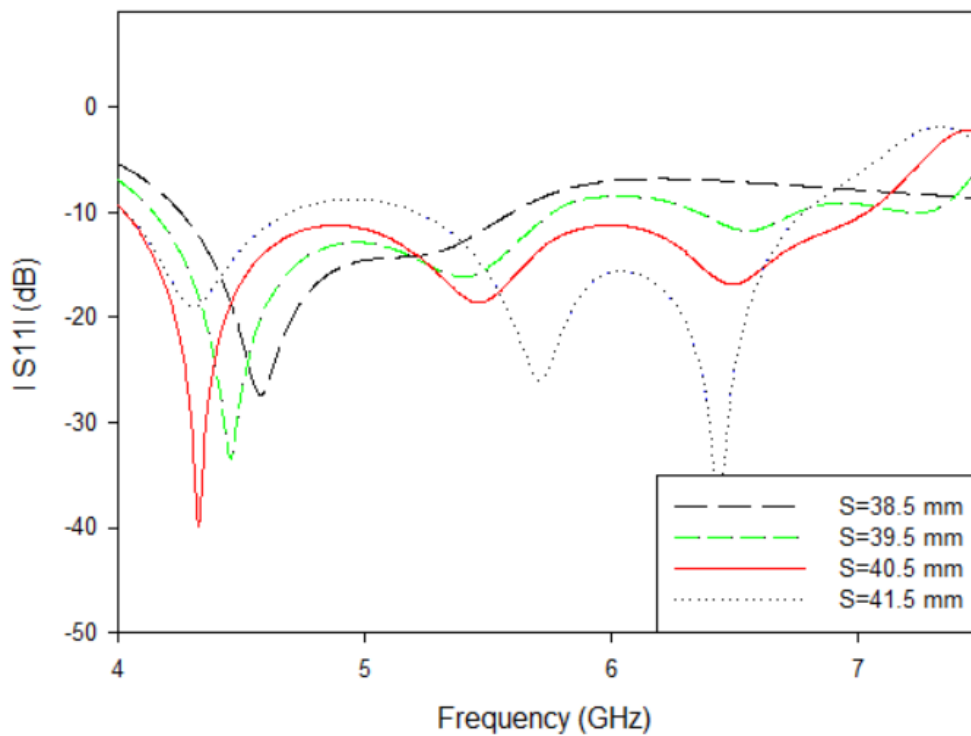
(b)

Fig 4.6: study the effect of feed line width on (a) S11 and (b) Gain from 0.5 mm to 1.1mm.

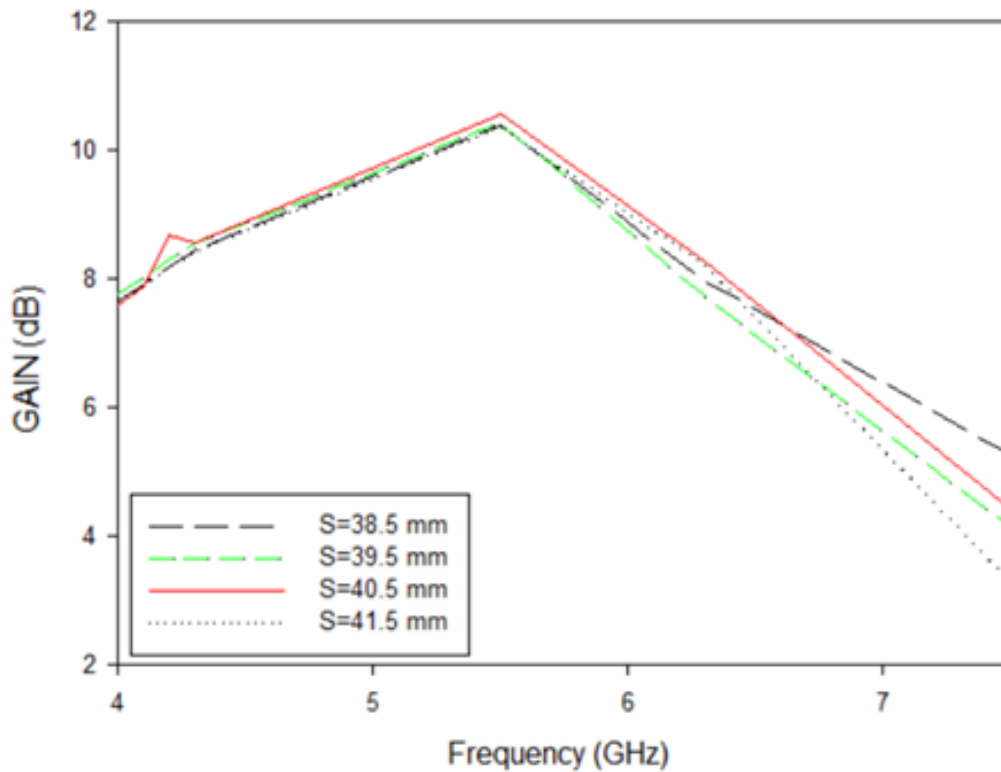
4.2.2.1.6- The Effect of Feed Line Length

The feed-line is 50Ω microstrip transmission line. In fact, it extends beyond the slot to reach the optimum matching. The distance beyond the slot should be around a quarter wavelength at a frequency which applies to effectively excite a slot. Since the microstrip transmission-line is open-ended, the current reaches its maximum value at the slot. This procedure aids to transfer energy from microstrip transmission-line to a slot. So the best optimum value for slot length is $S=40.5$ mm which provides good matching with the greater gain as shown in Fig.4.7 below.

The below curves perfectly illustrate the mechanism for reaching the appropriate length and improvement in resulting such as increasing the frequency range of the antenna by enhancing the amount of current reaching the slot in the slot antenna.



(a)

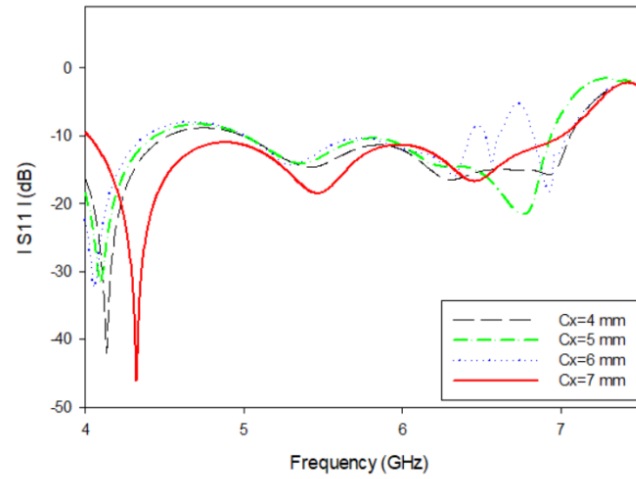


(a)

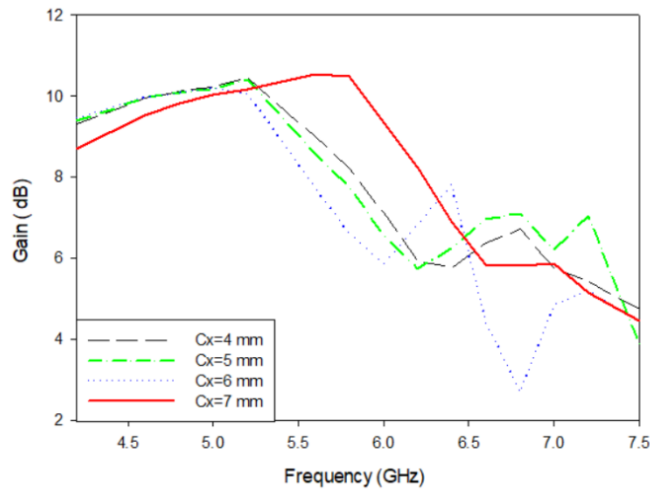
Fig 4.7: study the effect of feed line length on (a) S11 and (b) Gain from 38.5 mm to 41.5mm.

4.2.2.1.7- The Effect of Slot Length Inside Cell

Observed that by increasing the length of the slot inside the cell, the increase leads to a change in the resonance frequency to a higher frequency, On the other hand, notice an increase in the antenna bandwidth and also the gain as shown in Figure 4.8 below. The main reason for this phenomenon is due to the fact that the etched slot in the unit cell is a secondary source of radiation. The electromagnetic energy in each unit cell after the absorption process of the radioactive wave from the source. Consequently, the energy radiation from several secondary sources engraved on the unit cells lead to the best results at the length of the power slot 7mm.



(a)



(b)

Fig 4.8: study the effect of slot inside unit cells on (a) S11 and (b) Gain from 4mm to 7mm.

4.2.2.2. Reflection Coefficient, Gain, Directivity, and Current Distribution

Figure 4.9 compares between the result S11 of only slot antenna, and with a slot antenna loaded with metasurface layer. Can observe the enhancement in the reflection coefficient when metasurface loaded to the slot antenna. Slot antenna bandwidth extends from (6.25 GHz-7.007 GHz), being about 0.75 GHz, the reflection coefficient is less than -10 dBi. The bandwidth of slot antenna with metasurface extended from

(4.075 GHz to 7.01 GHz).Growing in an antenna bandwidth may make it a potential candidate for utilizing in wireless applications.

In absence of using metasurface layer. The gain of just slot antenna is about 4.19 dBi, whereas, with a metasurface layer, it can produce in growth the gain to 10.7 dBi as shown in Fig. 4.10. enhancing the gain value by 6.41 dBi has been obtained, However , the proposed antenna has gains values higher than a slot antenna gain values at all frequencies.

Through reflection coefficients S_{11} of the antennas, it can be seen that the resonant frequency of slot antenna is running at 6.7GHz, while resonance frequency of antenna with the presence metasurface is 4.33GHz, which is a lower frequency than slot antenna resonant frequency, and thus has achieved a reduction in the size of the antenna.

Raising of gain value by 6.41 dB is not an easy mission when utilizing small footprint single antenna.This requires utilizing the antenna array, and the structure will become very complicated. Here, a single antenna utilizing the exact same footprint is qualified for achieving this goal. The improvement of the bandwidth was done by adding a resonant frequency through each cell to the resonant frequency of the slot antenna. As for the increase of the gain, it is due to the concentration of the beam in a narrower area as a result of the negative refractive index that the metasurface possess , which makes it like a lens that focuses the radiation in a narrow beam. After carefully studying each element in the design and obtaining the best value from each element, the values are fixed in table 3.2 and based on it , the antenna was design, where the table considers the final result of the parametric sweep applied to each part of the antenna to reach the best values that improved the performance of the antenna.

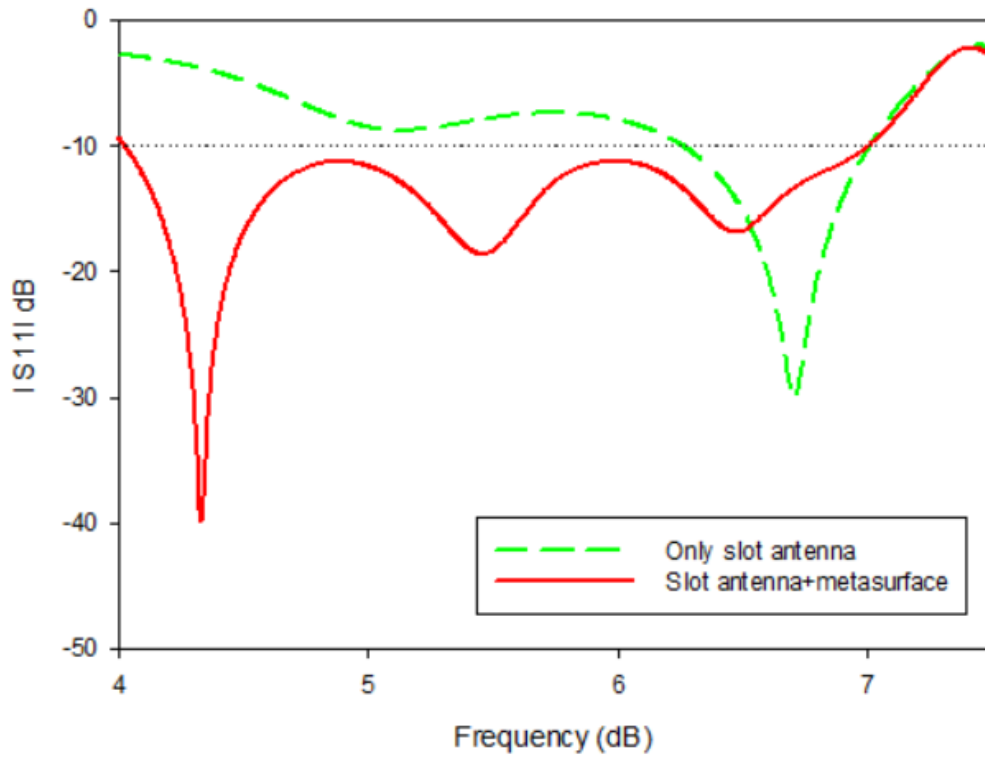


Fig 4.9: S_{11} of (Conventional slot antenna , Metasurface antenna).

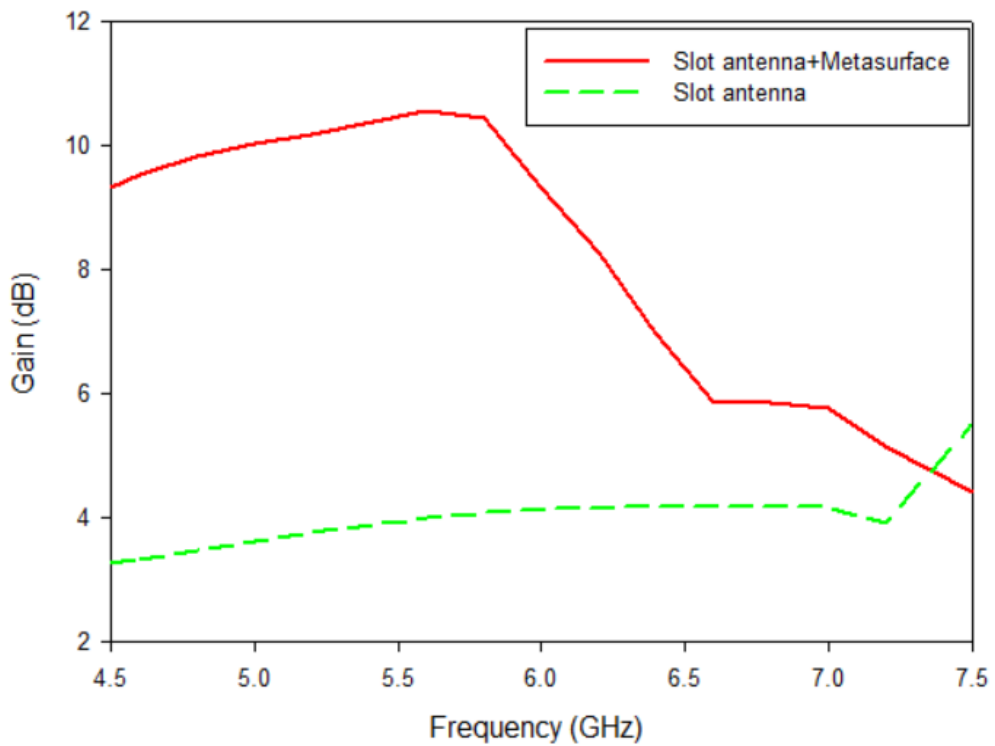
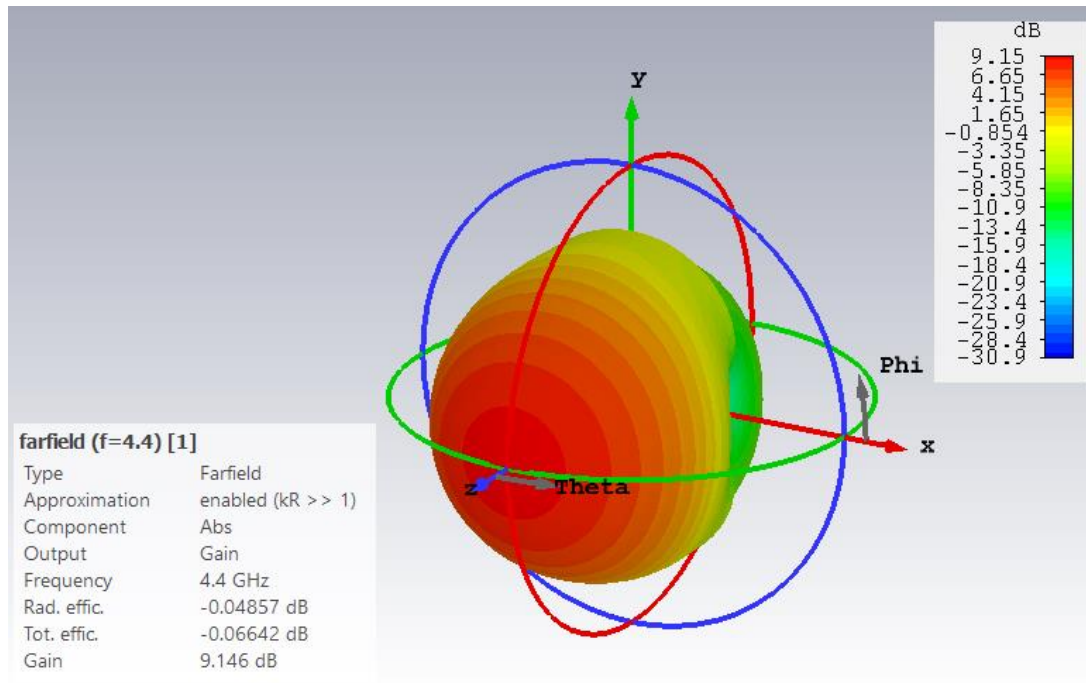
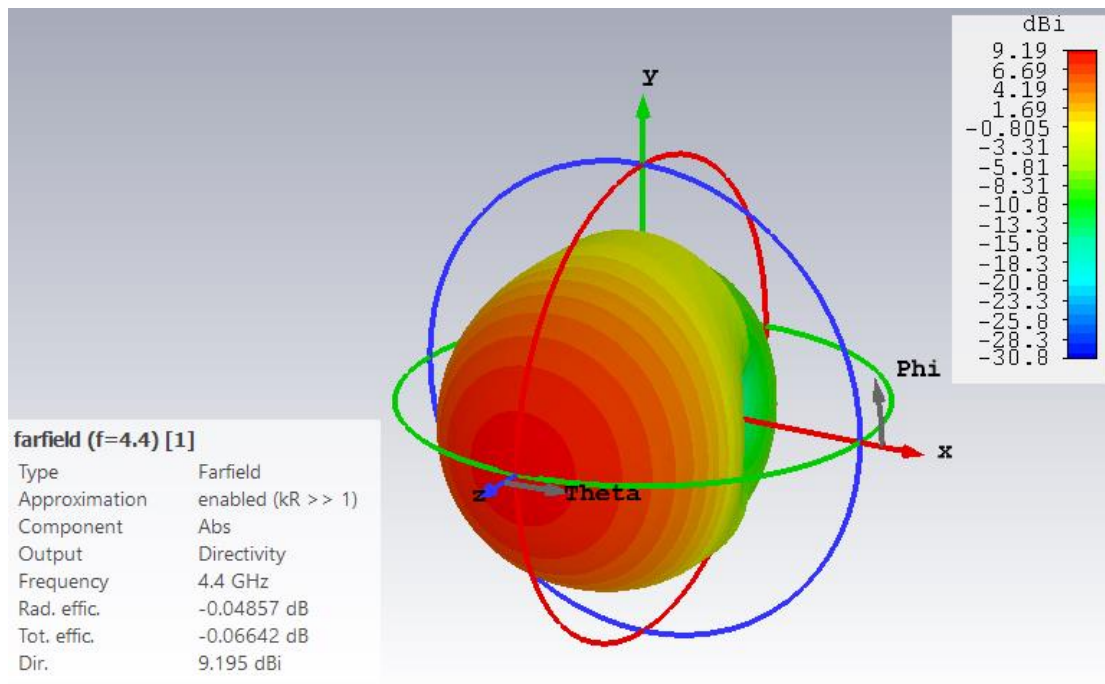


Fig 4.10: Gain of (Conventional slot antenna , Metasurface antenna).

The gain and directivity of the resonant frequency are shown below, where obtained a value of 9.14 dB gain and 9.19 dB directivity at the frequency 4.4GHz.



(a)



(b)

Fig 4.11: 3D Pattern for (a) Gain (b) Directivity at resonant frequency

The efficiency of the antenna reaches to an approximate value of 99 % depending on the equation that collects between directivity and gains to give the efficiency. Until get more insight into the electromagnetic characteristics of the metasurface antenna, generating the current distributions for the antenna at three different frequencies as shown in Fig 4.12 below.

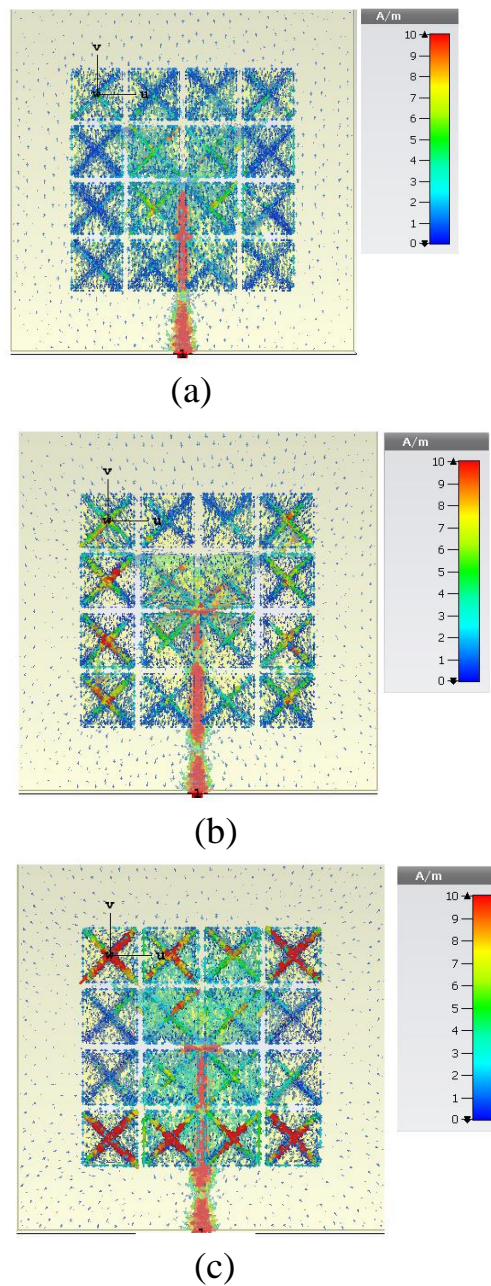


Fig 4.12: Current Distribution at (a) 4.33GHz (b) 5.5 GHz (c) 6.5 GHz

Figure 4.13 shows the polar metasurface plot with X slot in the centre of patch element. The value for the main lobe is (23) dB in the X-Y view ($\theta = 90^\circ$), whereas the main lobe direction has value (90°), and the last the angular width value is (88°). While the value for the main lobe is (37.7) dB in the Y-Z view ($\varphi = 90$), whereas the main lobe direction has value $=0^\circ$, and the last is the angular width is (64.4°). Finally, the X-Z view ($\varphi = 0$), the main lobe value is (33.7°)dB, whereas the main lobe direction is value $=0^\circ$, and finally the angular width value is (64.5°).

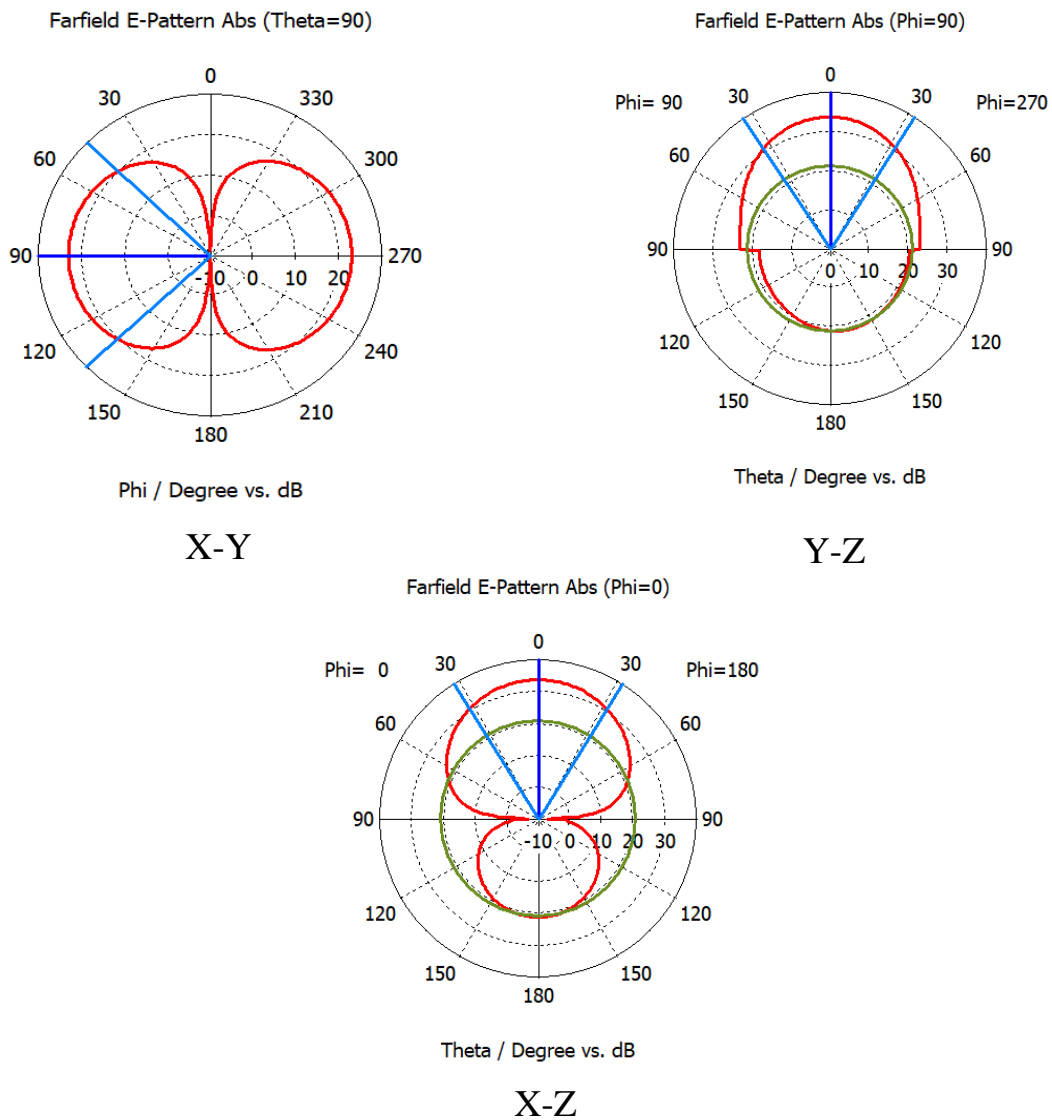


Fig 4.13: Radiation pattern (a) X-Y view (b) Y-Z view (c) X-Z view.

Introduces in tabel4.1 some of an antenna performance parameters

Table 4.1 : Results of The Proposed Antenna

No	Parameter Name	Only Slot	Metasurface
1	Resonant Frequency	6.7 GHz	4.33 GHz
2	Bandwidth	6.25 GHz- 7.01 GHz	4.01 GHz-7.01 GHz
3	Return Loss	-30 dBi	-40 dBi
4	Gain	4.19 dBi	10.7 dBi

In table above is a summary of all the previous discussions and clarifying the difference between the conventional antenna and the antenna loaded with metasurface in its construction, as the metasurface bandwidth antenna achieved a bandwidth of 3 GHz against only 500 MHz for the slot, as well as on the gain side, where antenna approved on metasurface achieved gain of 10.7 versus 4.19 only for the conventional antenna. While Table 4.2 introduces the comparison between our work and other recent works .

Table 4.2 :Performance Comparison.

No	Ref	Resonant Frequency	Max and Min frequency	Bandwidth	Return loss	Gain
1	[57]	5.06- 5.70 GHz	4.60-6.17 GHz	1.57 GHz	-40 dBi	9.8 dBi
2	[36]	5.2 GHz	4.26-5.75 GHz	1.49 GHz	-20 dBi	8.2 dBi
3	[58]	5.7 GHz	5.45-5.87 GHz	0.42 GHz	-22 dBi	7.88 dBi
4	[35]	6.1 GHz	5.89 - 6.6 GHz	0.71 GHz	-14 dBi	9.4 dBi
5	work	4.33 GHZ	4.01-7.01 GHz	3 GHz	-40 dBi	10.7 dBi

Table 4.2 is one of the most important tables mentioned in the first design, as it has an important role in highlighting the results reached and comparing them with the results of previous work and observe the improvements made to the results for a specific application where the reference of [57] has a bandwidth of 1.57 GHz and a gain of 9.8 dB, which is outperformed by the first design with a bandwidth of 1.43 GHz and gain of 0.9 dB. As for the reference of [36], it is surpassed by the first design with a bandwidth of 1.51GHz and a gain of 2.5 dB. 2.56 GHz as bandwidth and a 2.82 dB as gain.

This is what was obtained when compared with the antenna in the reference of [58]. As compare with reference of [35], the designed antenna is outperformed by 1.3 dB as gain and 2.29 GHz as bandwidth. This is a very excellent difference between the first design and the references when comparing in table 4.2.

It should be noted that the first design is the most adequate among the four designs mentioned in the thesis, due to its 3 GHz as bandwidth and 10.7 dB as gain, which was achieved as a result of the excellent optimization that was performed on the antenna in terms of studying each element in detail in both sides of the reflection coefficient, as well as the gain and when reaching the highest the performance of any element in which the best value that is reached and moving to other elements is fixed. It is mentioned that the number of elements for which optimization is done is seven each of the size and number of cells in addition to the length and width of the feeding line in addition to that slot inside the cell and finally the height of the gap and the gap between cells.

4.3 Characteristics of Metasurface with (Uniform Distribution and Gradient Distribution) (II).

4.3.1 Extraction Permittivity , Permeability ,and Refractive Index From S-Parameter.

By placing a single unit cell of design between two waveguide ports in order to extract permittivity, permeability and refractive index from the S-parameter and to ensure that the layer meets the metasurface requirements at a wanted frequency. which represents the frequency range from 6.3 GHz to 9 GHz. Fig.4.14 below shows the characteristics of the metasurface layer:

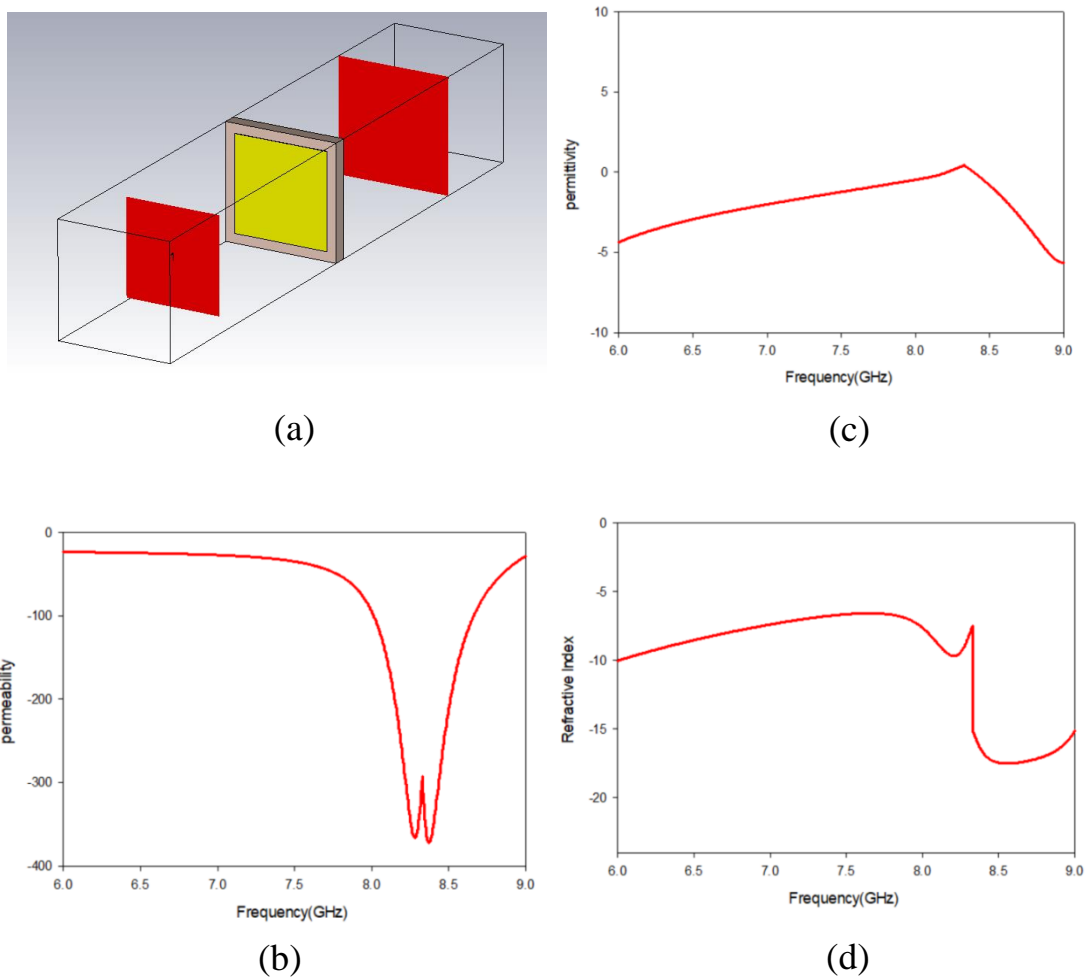


Fig 4.14:(a) The single unit cell of MS in CST,(b), Relative permeability of MS. (c), Relative permittivity of the MS. (d),

4.3.2 Reflection Coefficient, Gain , Directivity ,and Current Distribution

Figures below shows the results of S11 of only slot antenna, uniform and gradient distribution metasurfaces. One can see how much the reflection coefficient has enhanced when using the metasurface. The bandwidth of the only slot antenna extends from 6.2 GHz to 6.62GHz, being about 0.4 GHz as bandwidth, and S11 being less than -10dB. The bandwidth becomes 2.7 GHz for the antenna with uniform distribution metasurfaces, extending from 6.3 GHz to 9 GHz. Compared to the slot antenna, the bandwidth has enhanced by 2GHz. This increase in the antenna bandwidth may make the proposed antenna a potential candidate for imaging applications.

The slot antenna with a gradient distribution metasurface has less bandwidth which is about 2.4 GHz. Although the second proposed antenna has less bandwidth, it has higher gain which is one of our goals. In absence of the metasurface layer, the slot antenna gain is about 2.38 dBi, whereas in presence of the metasurface layer, it can result in increasing the gain to 8dBi for uniform distribution unit cells and to 9.75dBi for gradient unit cell metasurface layer as shown in Figures. Improving the gain by 7.12 dBi has been obtained.

The existing metasurface are all enhanced within the operating antenna bandwidth. As can be observed, the gain of slot antenna reaches its maximum value at 6.4GHz, whereas the antenna with gradient metasurfaces reaches its maximum value around 7.1GHz. This shift in the frequency is normal, because parasitic effects of metasurface can affect the antenna performance. However, the proposed antennas have gains higher than what the slot antenna has over all frequencies.

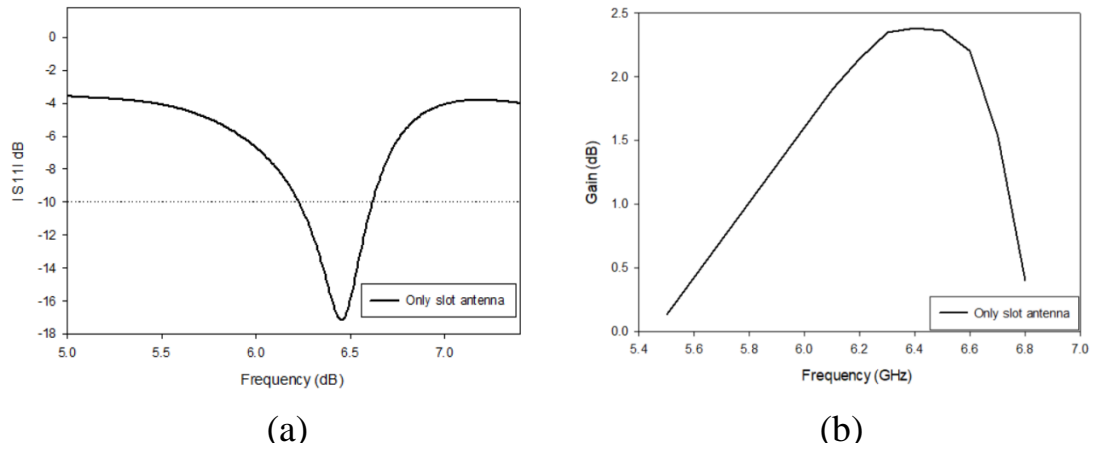


Fig 4.15 : (a) S11 of slot antenna (b) Gain of slot antenna

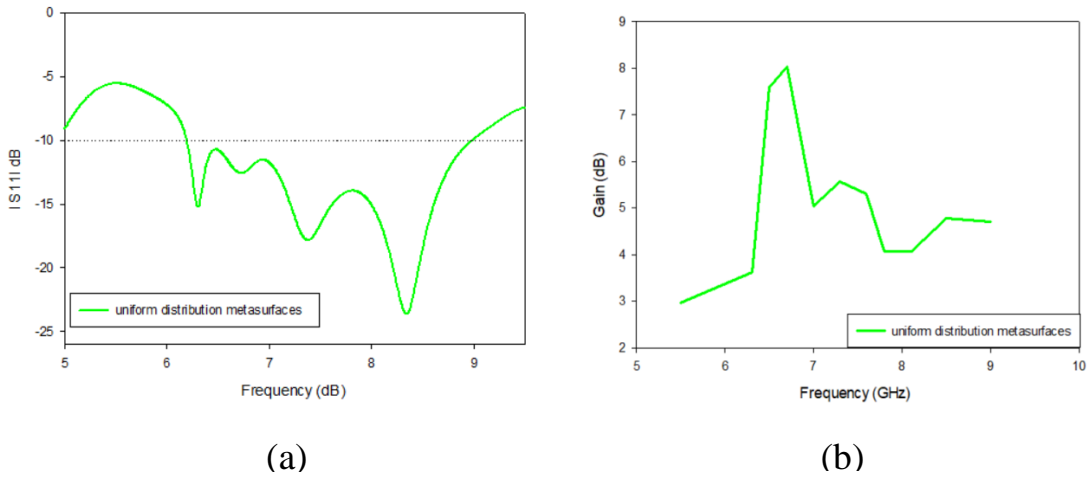


Fig 4.16 : (a) S11 of uniform distribution of metasurface (b) Gain of uniform distribution of metasurface

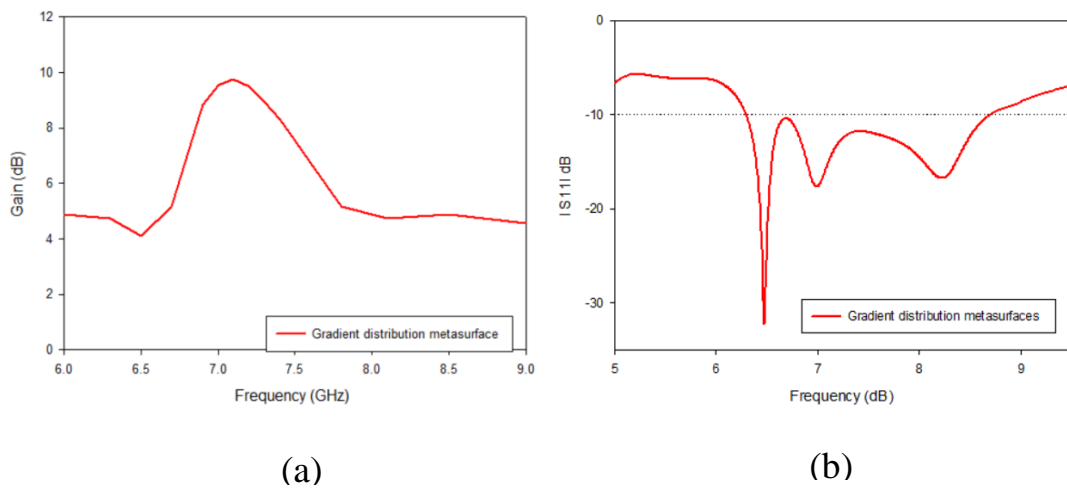


Fig 4.17 : (a) S11 of gradient distribution of metasurface (b) Gain of gradient distribution of metasurface

4.3.2.1-Parametric Study For Gradient Unit Cell Metasurface

The proposed antennas are carefully designed. The parametric study given here provides such a good example to understand the working mechanism of the proposed antenna whose dimensions parameters impact the design performance. The slot length L_s and the distance separating between the slot and the metasurface layer h_{air} are only chosen for this study for the sake of simplicity. These important parameters are set as variable in the CST software, whereas all other parameters are fixed in the design. These parameters, which have a deep impact on the coupling between metasurface and slot, have been varied. Fig. 4.18 shows the simulated return loss S_{11} of the proposed antenna for various slot lengths with fixed slot width $W_s=3$ mm. The L_s is varied from 13mm to 15 mm with a step of 0.5mm.

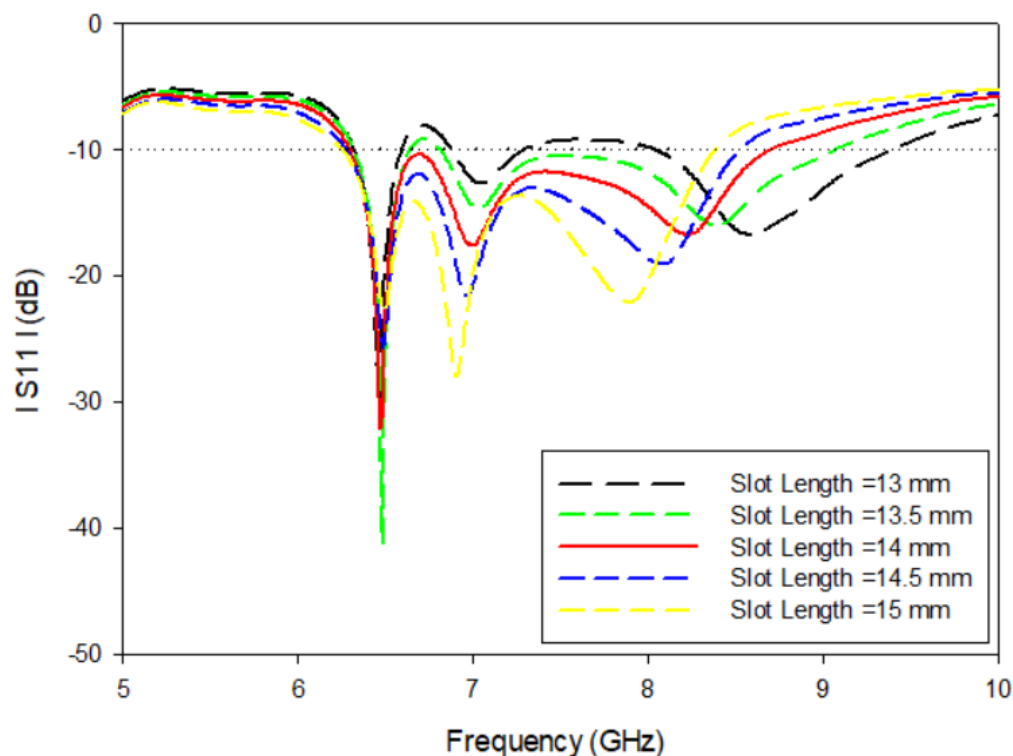


Fig.4.18: The return loss S_{11} of the proposed an antenna with various L_s when $W=3$ mm, and $h_{air}=5$ mm

All slot lengths have almost the same resonant frequency. L_s equal to 14 mm is the best choice because it offers wider bandwidth, see Fig. 4.18 with the red trace. Many reasons can be inferred from this result that the slot and the feeding line may interact effectively over all this frequency range. Also, when the slot length increases, surface current becomes denser along the slot, so the equivalent inductance becomes larger. The increase in the inductance cancels out the capacitance impact of the air gap separating between the slot and the metasurface layer.

Next, an influence of the parameter h_{air} on the S11 is also depicted in Fig. 4.19. h_{air} equal to 5mm is chosen. The bandwidth deteriorates as the air gap increases because the capacitance impact of the metasurface layer, which cancels out the inductance of the slot, decreases. After the parametric study, the return loss S11 and gain of the slot antenna with gradient distribution metasurfaces are given in Fig 4.20, when $L_s = 14$ mm and $h_{air}=5$ mm. The 3D radiation patterns for gain and directivity are depicted in Fig.4.21. The gains are very high in the broadside directions. The gain for conventional microstrip patch antennas are 2.38 dB, but our proposed design offers high gain with small footprints. Table 4.3 introduces some the antenna performance parameters. Table 4.4 compares the proposed an antenna with other recent designs.

After carefully studying each element in the design and obtaining the best value from each element, the values are fixed in Table 3.3 and Table 3.4 and based on it ,the antenna was design, where the table considers the final result of the parametric sweep applied to each part of the antenna to reach the best values that improved the performance of the antenna.

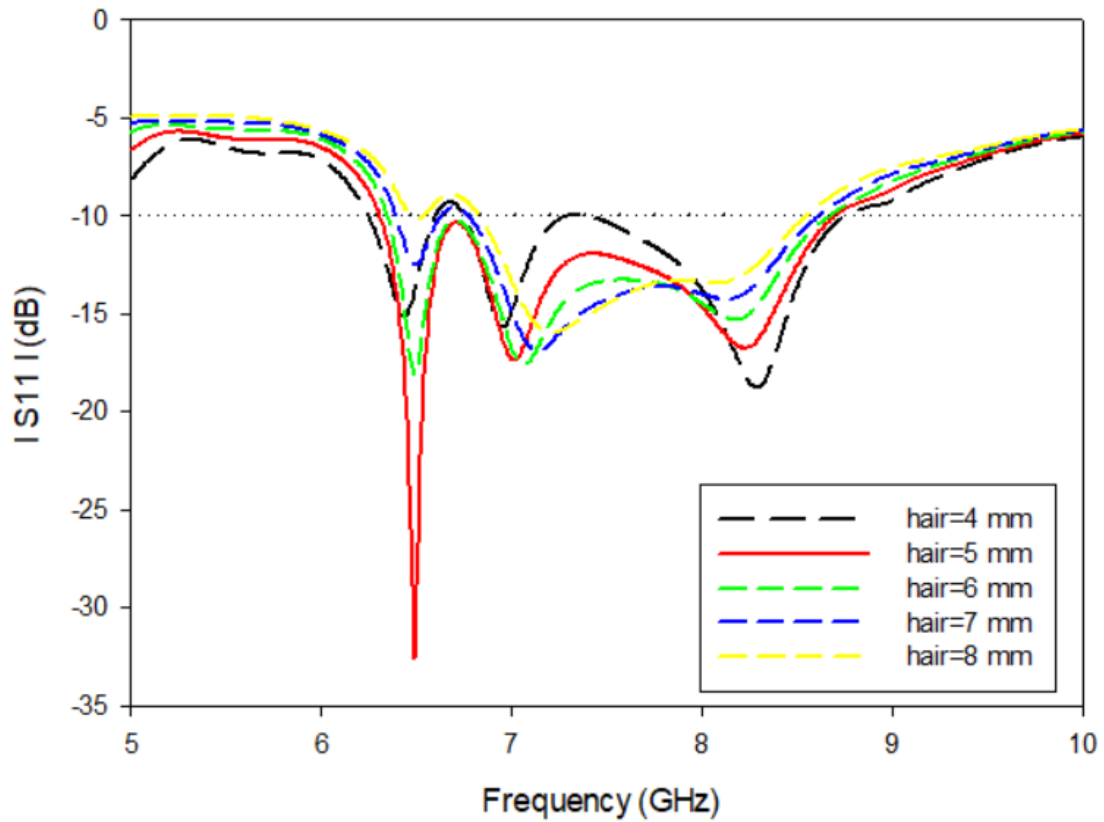
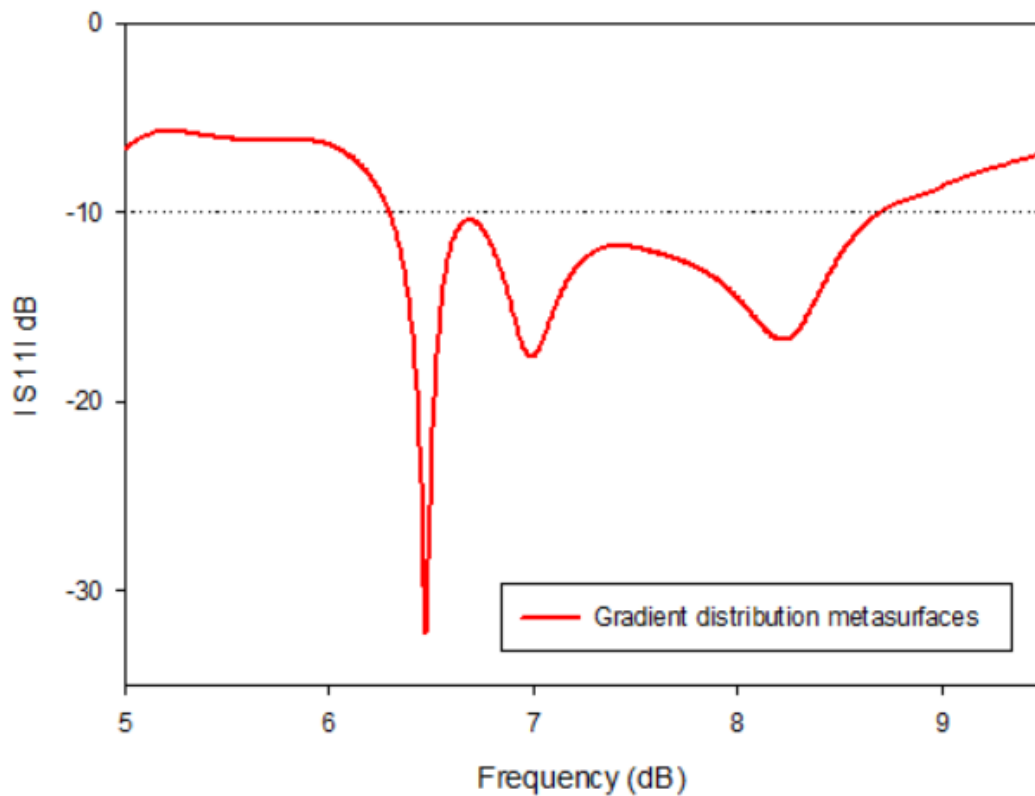
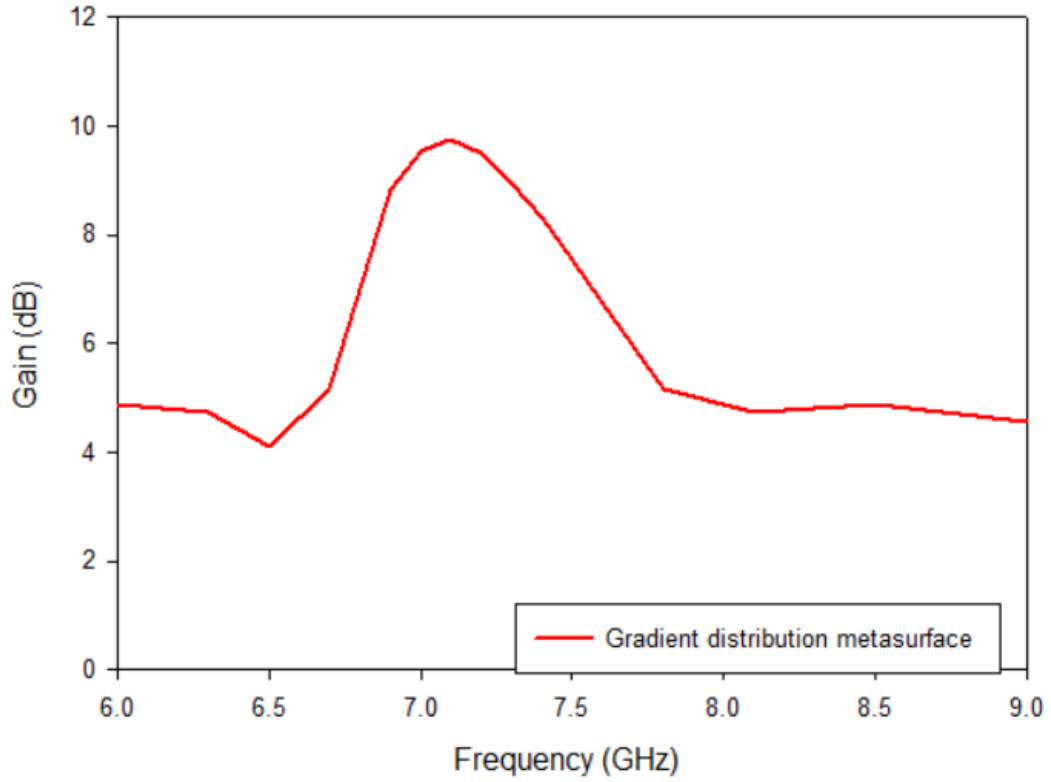


Fig 4.19: The simulated return loss S_{11} of the proposed antenna with various h_{air} when $W = 3$ mm, and $L_s = 14$ mm

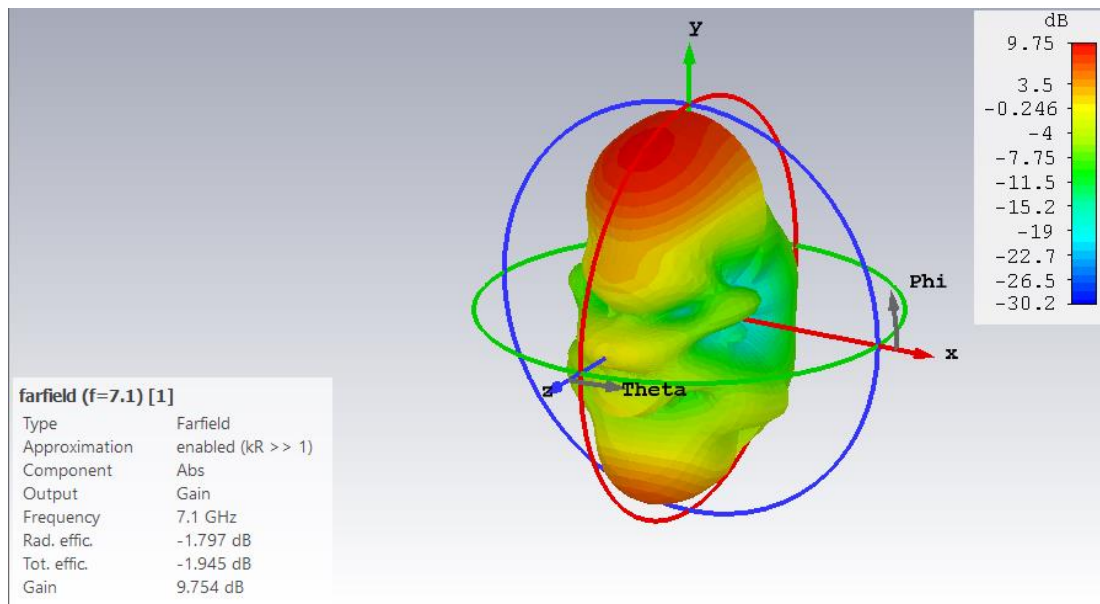


(a)

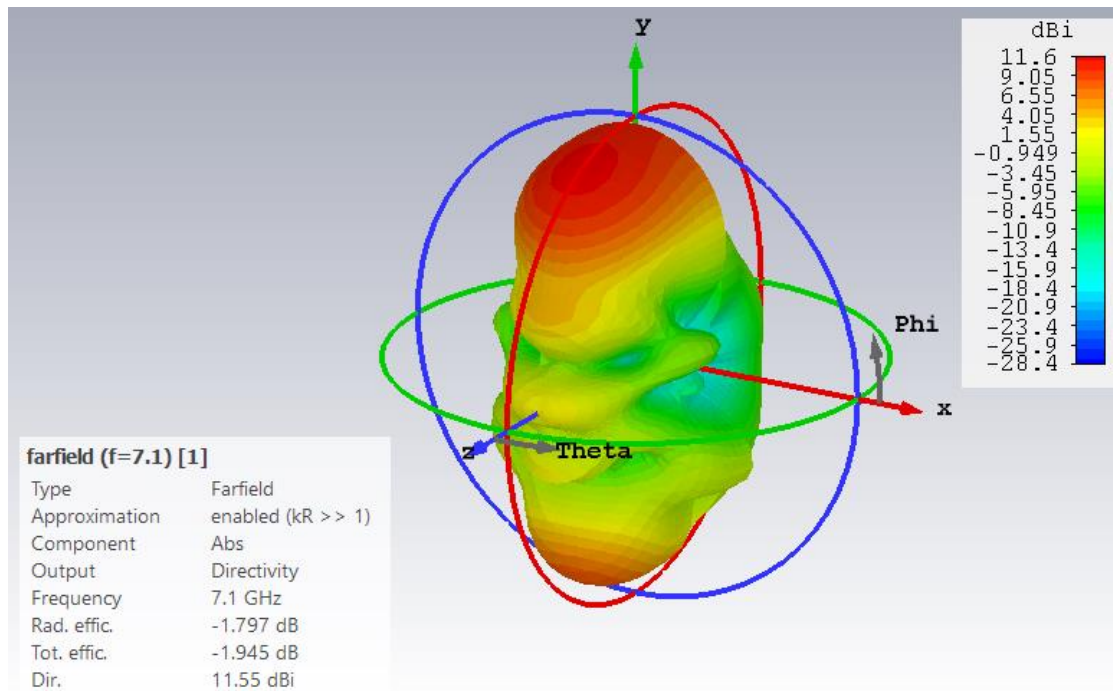


(b)

Fig 4.20: (a) S11 of Gradient distribution of metasurface (b) Gain of distribution of metasurface



(a)



(b)

Fig 4.21: 3D Pattern for (a) Gain (b) Directivity .

The gain and directivity of the resonant frequency are shown above, where obtained a value of 9.754 dB gain and 11.55 dB directivity at the frequency 7.1 GHz. The efficiency of the antenna reaches to an approximate value of 84 % depending on the equation that collects between directivity and gains to give the efficiency.

Table4.3: Results of The Gradient Metasurface Antenna:

No	Parameter name	Slot antenna	Uniform distribution of metasurface	Gradient distribution of metasurface
1	Resonant Frequency	6.3 GHz	8.3 GHz	6.5 GHz
2	Bandwidth	0.42 GHz	2.7 GHz	2.41 GHz
3	Return loss	-17 dBi	-24 dBi	-32.6 dBi
4	Gain	2.38 dBi	8 dBi	9.75 dBi

The Table 4.3 shown the best results in aspect of the bandwidth is in the uniform distribution antenna , while the best results in terms of gain are in the gradient distribution.

Table-4.4: A comparison between the proposed antenna with other

No	Ref	Resonant Frequency	Bandwidth	Return loss	Gain
1	[35]	6.1 GHz	710 MHz	-15dBi	9.4dBi
2	[38]	5.5 GHz	680MHz	-32dBi	9.2dBi
3	[37]	5.7 GHz	160MHz	-27dBi	5.8dBi.
4	[58]	5.7 GHz	420MHz	-20dBi	7.88dBi
5	work	6.5 GHz	2.41GHz	-32.6dBi	9.75dBi

Compared to other antennas, the gradient design showed good results, outperforming reference [35] by 1.43 GHz, 1.73 GHz for reference [38], 2.25 GHz for reference [37], and finally 1.99 GHz for reference [58]. Based on what occurs in the results, metasurface inclusion is a step in the right direction. Until get more insight into the electromagnetic characteristics of the metasurface antenna, generating the current distributions for the antenna at three different frequencies as shown in Fig 4.22 below:

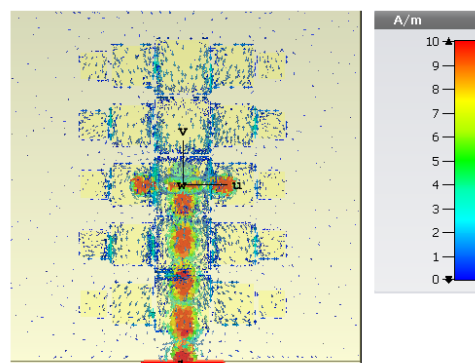


Fig 4.22: Current Distribution at 6.5 GHz.

The figure 4.23 shows the polar MS plot with gradient distribution of unit cell. The value for the main lobe is (18.8) dB in the X-Y view ($\theta = 90^\circ$), whereas the main lobe direction has value (89°), and the last the angular width value is (43.8°). While the value for the main lobe is (18.8)dB in the Y-Z view ($\varphi = 90^\circ$), whereas the main lobe direction has value $=71^\circ$, and the last is the angular width is (47.3°). Finally, the X-Z view ($\varphi = 0$), the main lobe value is (12.1)dB, whereas the main lobe direction is value $=41^\circ$, and finally the angular width value is (39.9°).

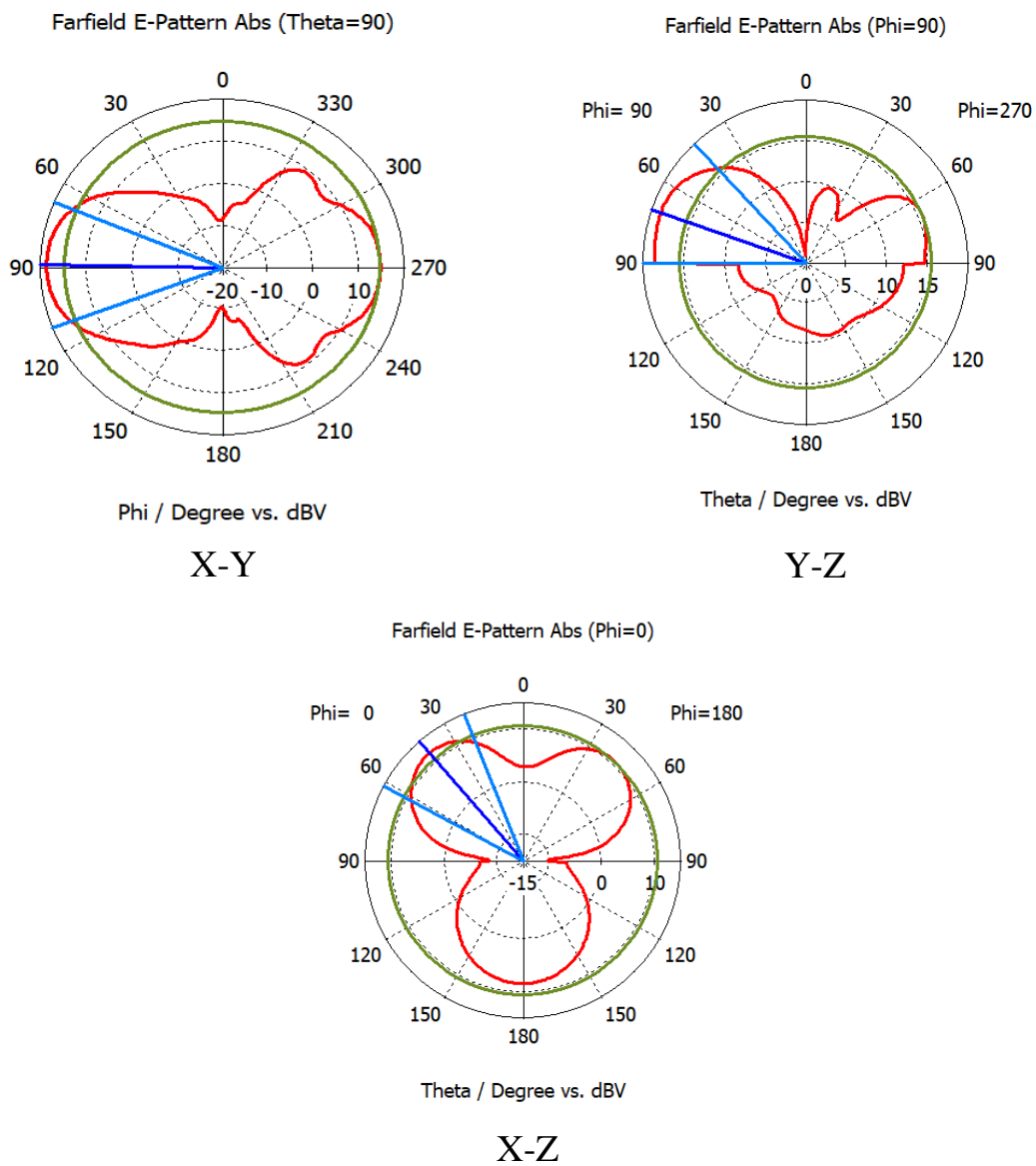


Fig 4.23: Radiation pattern (a) X-Y view (b) Y-Z view (c) X-Z view.

4.4 Characteristics of Metasurface with Different Cell (III):

4.4.1 Extraction Permittivity and Permeability from S-Parameter

By placing a single unit cell of design between two waveguide port in order to extract permittivity, permeability and refractive index from the S-parameter and to ensure that the layer meets the metasurface requirements at a wanted frequency, which represents the frequency range from 5.62 GHz to 8.43 GHz. Fig.4.22 shows the characteristics of the metasurface layer.

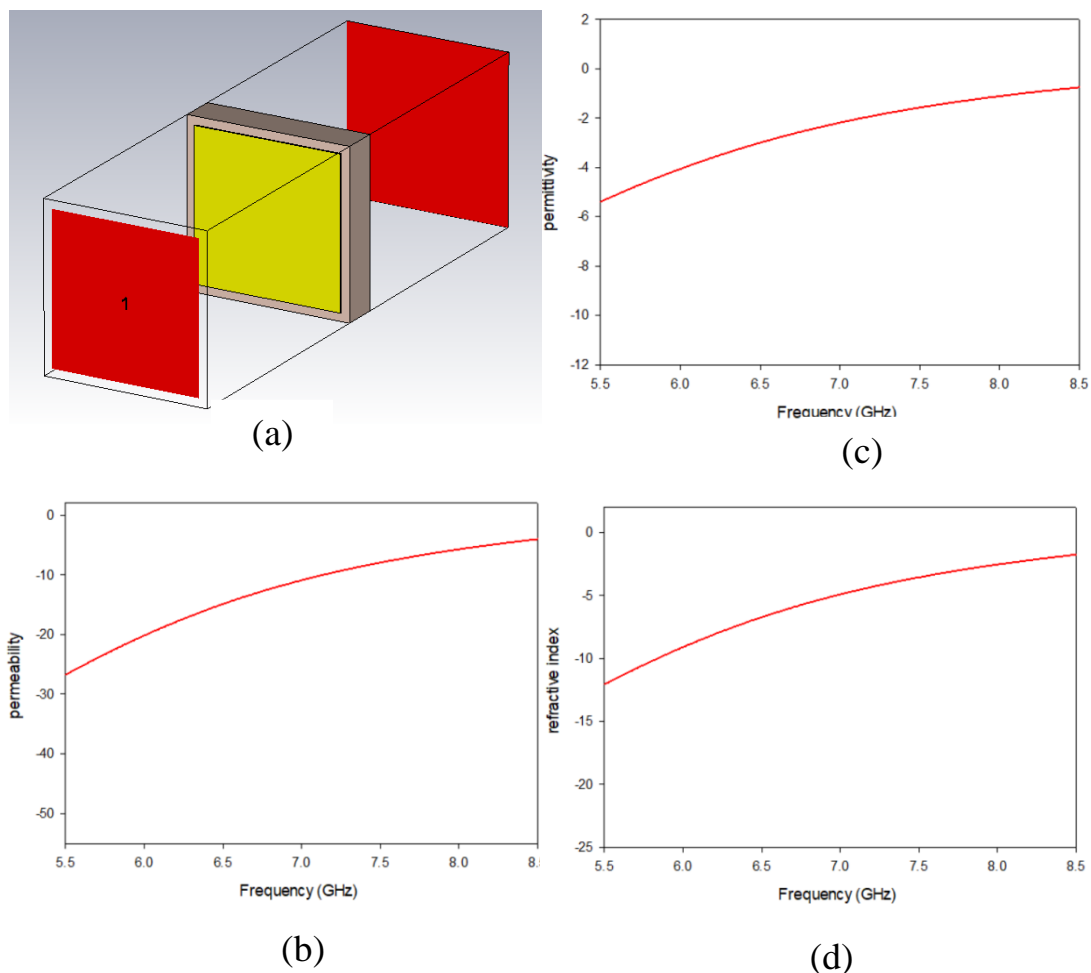


Fig 4.22 :(a) The single unit cell of MS in CST,(b), Relative permeability of MS. (c), Relative permittivity of the MS. (d), Refractive index of the MS.

4.4.2 Reflection Coefficient ,Gain , Directivity , Current Distribution

Figure 4.25 offers a comparison between results of only slot antenna and the slot integrated with metasurface layer. It is evidently observed how much bandwidth and gain have been attained when adding the metasurface layer. The bandwidth ranges from 6.15GHz to 6.52GHz for only slot antenna, being about 0.37 GHz. This narrowband behaviour is dramatically changed to very wideband about 2.81GHz, extending from 5.75 GHz to 8.67 GHz. Once the metasurface layer is added above the slot antenna. As pointed out earlier, this procedure aids to enhance matching for more frequencies, making the antenna very wideband. The improvement in the antenna bandwidth makes it a potential candidate for be utilized imaging applications.

In the absence of the MS layer, the gain of the slot antenna is about 5.6dB, while in the presence of the metasurface layer, it results in 8.76dB as a new gain as shown in Fig.4.26. The gain enhancement obtained by the proposed antenna is about 3.18 dB. Moreover, the proposed antenna possesses gain values greater than a slot antenna over all frequencies. Increasing a gain value by 3.18 dB is not an easy task especially when utilizing small footprint single antennas where antenna designers know that. To do the same job using conventional ways, more than one antenna should be closely placed, called an antenna array with many disadvantages such as big footprints, matching complicated circuits, feeding network re-equipment's, etc.

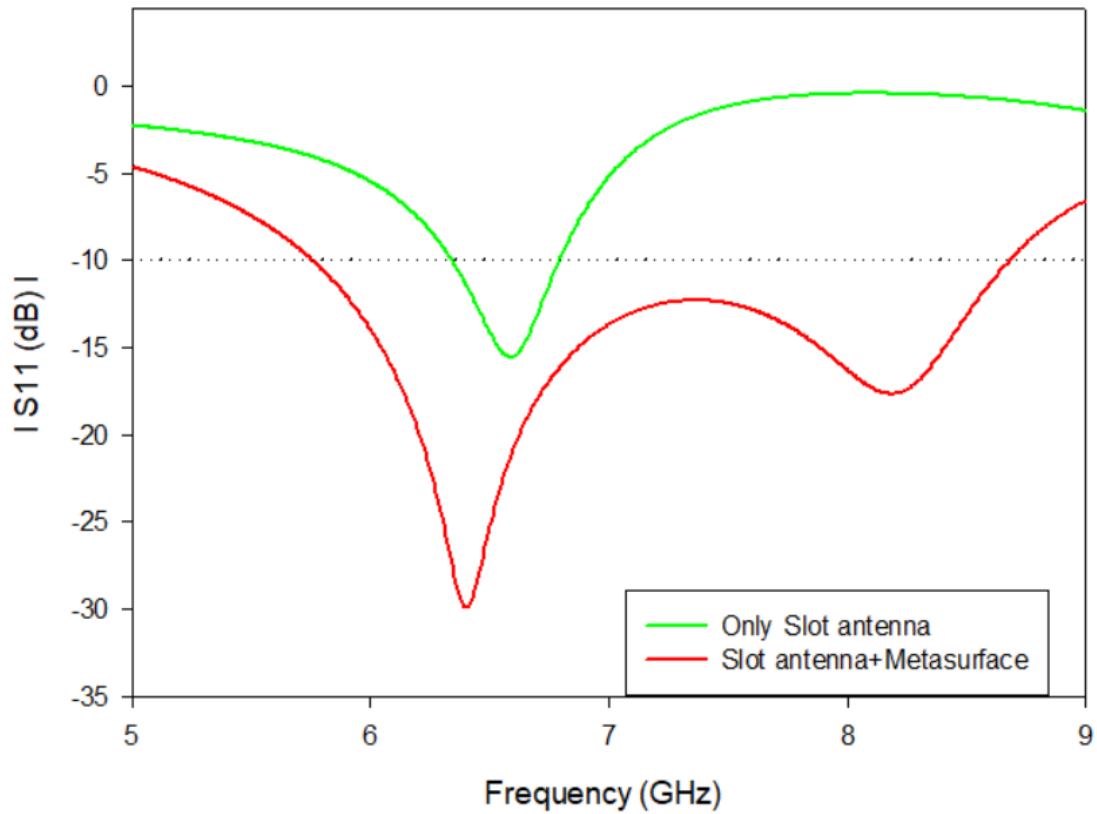


Fig 4.25 : S11 of (only slot , slot antenna+metasurface)

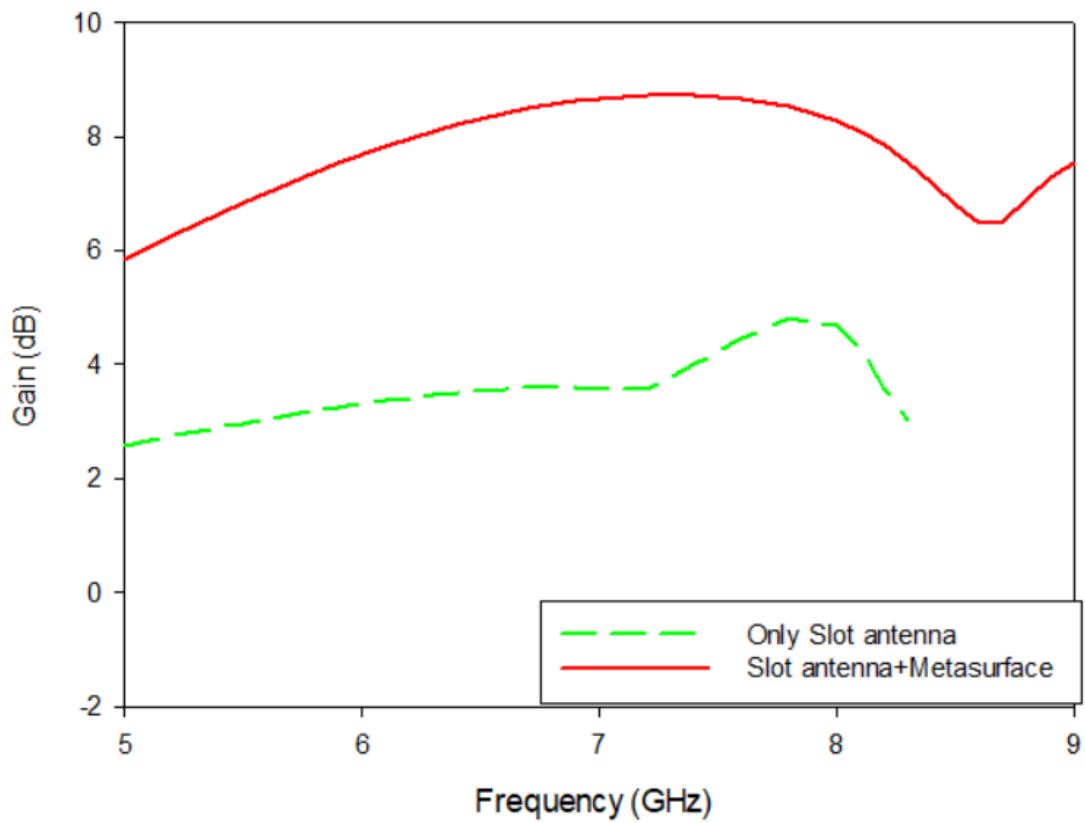


Fig 4.26: Gain of (only slot , slot antenna+metasurface).

Next, after showing the gain and the bandwidth of the proposed antennas, it becomes imperative to show impacts of the air gap separating between the slot antenna and the metasurface layer on the bandwidth range and gain value of the proposed antenna, after several steps of optimization. Fig.4.27 and 4.28 display the reflection coefficient S_{11} bandwidth and the antenna gain. Thus, when the air gap is equal to 3mm, the antenna offers the widest bandwidth compared to other distances.

However, this air gap does not provide the highest gain, it is acceptable if consider the bandwidth trading off. The one thing that should be mentioned here as the air gap distance increases, the antenna bandwidth deteriorates, belonging to capacitance impacts of the cavity, created by the substrate hosting the slot antenna and the metasurface layer. See the results when the air gap is equal to 3.5 mm and 4 mm. As known the slot antenna has inductance characteristics, the capacitance provided by the cavity decreases for larger distances, thereby reducing the cancellation out of the slot antenna inductance. Thus, air gap with 3mm is chosen.

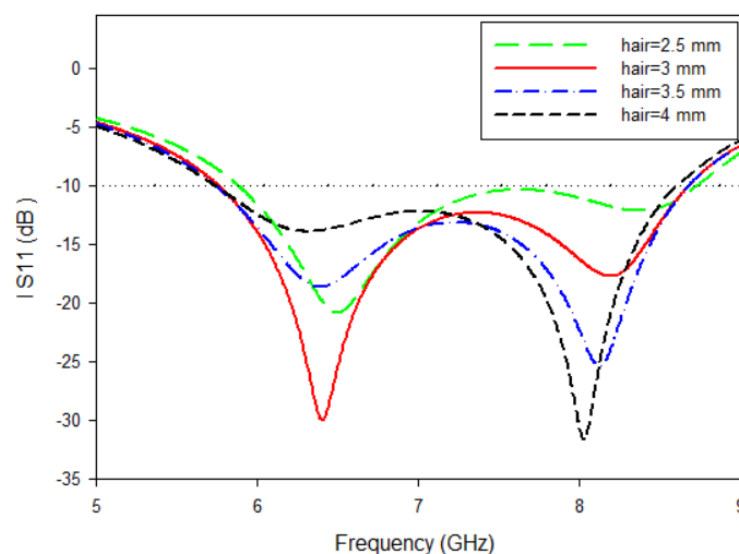


Fig 4.27: The simulated return loss S_{11} of the proposed antenna with various h_{air} from 2.5mm to 4mm.

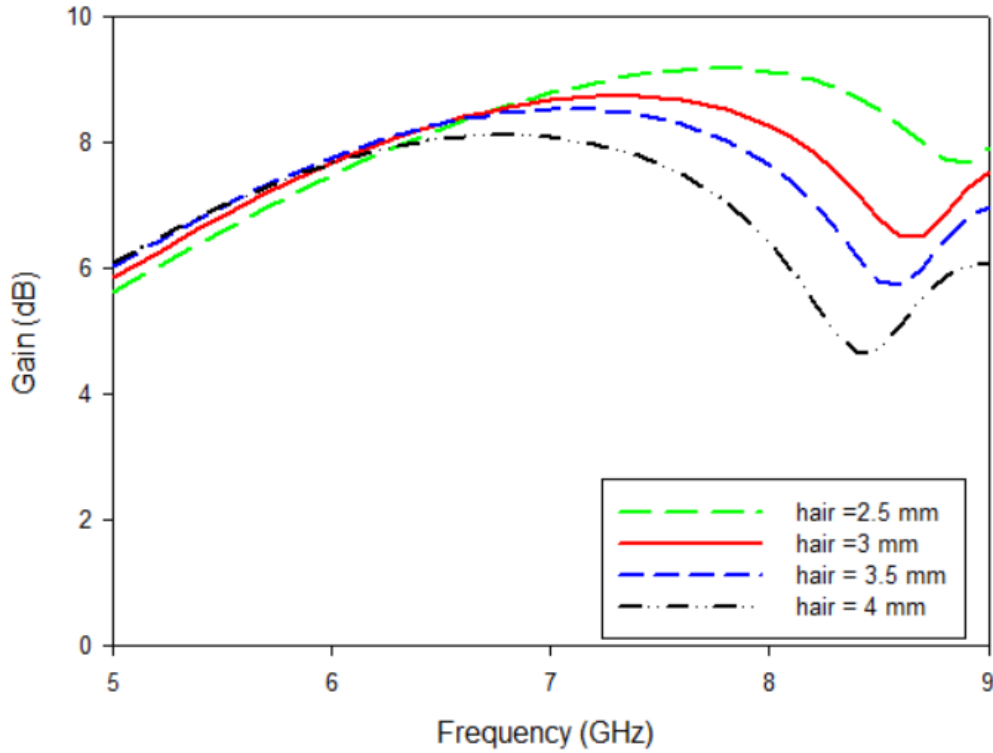
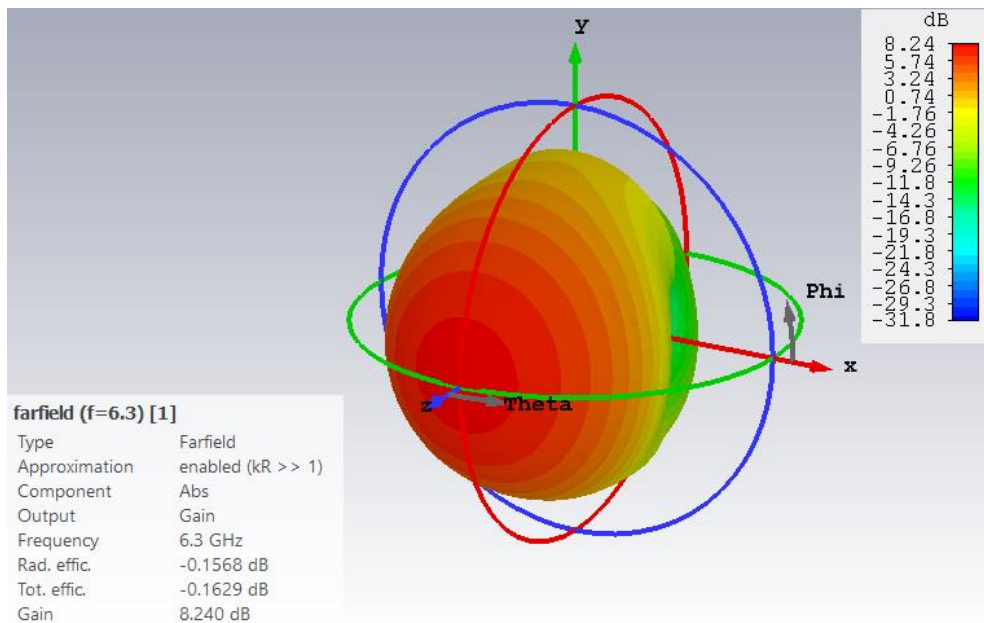
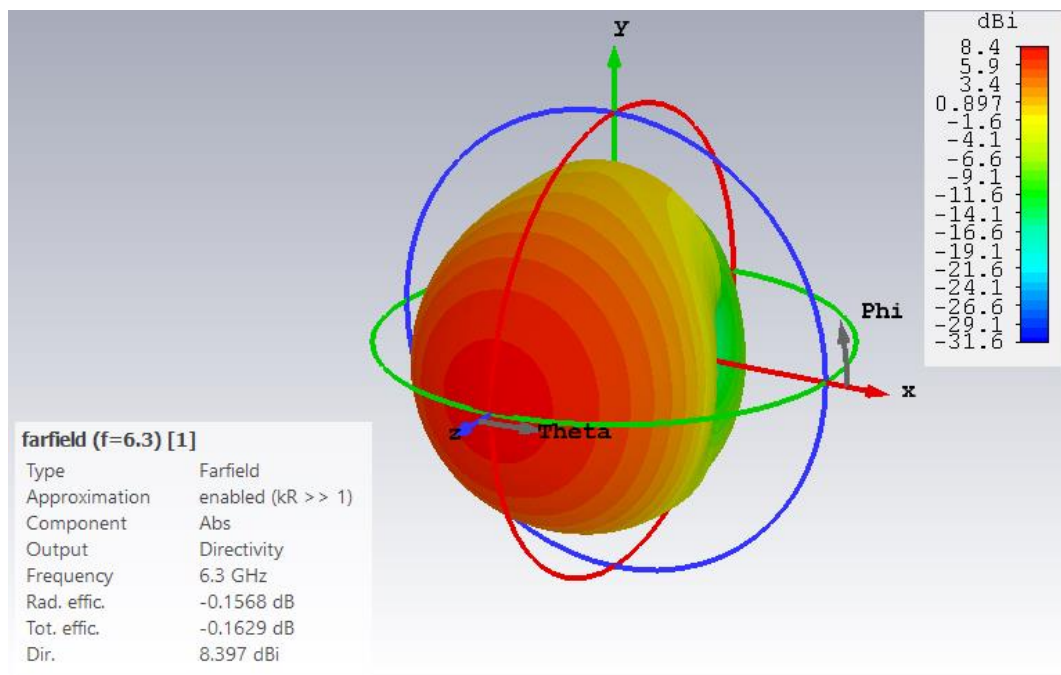


Fig 4.28: The simulated gain of the proposed antenna with various h_{air} from 2.5mm to 4mm.

The gain and directivity of the resonant frequency are shown below, where obtained a value of 8.2 dB gain and 8.39 dB directivity at the frequency 6.3 GHz.



(a)



(b)

Fig 4.29: 3D Pattern for (a) Gain (b) Directivity

The efficiency of the antenna reaches to an approximate value of 98 % depending on the equation that collects between directivity and gains to give the efficiency .

Table 4.5 introduces the results obtained for the slot antenna integrated with a metasurface layer, relying on the waveguide port applied on single unit cells of metasurfaces. This method provides whole information that the metasurface layer has negative permittivity, negative permeability, and negative refractive index using the S-parameters algorithm. The CST software was used in all analyses.

Table 4.6 is very important because it shows the strength of our contribution through the exceptional increase in the bandwidth, gain, and matching level compared to other related work. The value of bandwidth is 2.81GHz. This value is very excellent as compared to other reference,

where work in [37] has value 160MHz, 420MHz for [58], 1.49GHz for [36], 630 MHz for [39] and 2 GHz for [59]. also have increased the gain in the proposed antenna.

Table 4.5 : Proposed antenna result (only slot antenna, Slot antenna with MS) metasurface) and (slot antenna+metasurface layer)

No	Parameter	Only slot antenna	Slot antenna+metasurface
1	Resonant Frequency	6.35 GHz	6.22 GHz
2	Bandwidth	6.15 GHz - 6.52 GHz	5.62 GHz -8.43 GHz
3	Return loss	-14 dB	-36 dBi
4	Max Gain	5.6 dB	8.78 dBi
5	Max Directivity	7.88	8.94 dBi

Table-4.6 : Comparing with other antennas.

N o	Wor k	Resonant Frequency	Bandwidth	Bandwidt h	Return loss	Gain
2	[37]	5.7 GHz	5.64–5.8 GHz	160 MHz	-27 dBi	5.8 dBi.
3	[58]	5.7 GHz	5.45-5.87 GHz	420MHz	-17 dBi	7.88 dBi
4	[36]	5.2 GHz	4.26-5.75 GHz	1.49GHz	-21 dBi	8.2 dBi
5	[39]	2.3 GHz	2 – 2.63 GHz	630MHz	-22 dBi	1 dBi
6	[59]	7.6 GHz	7-9 GHz	2GHz	-32 dBi	5.53dB i
7	work	6.22 GHz	5.75-8.67 GHz	2.81GHz	-36 dBi	8.78 dBi

Until we get more insight into the electromagnetic characteristics of the metasurface antenna, generating the current distributions for the antenna at resonant frequency as shown in Fig 4.30 below:

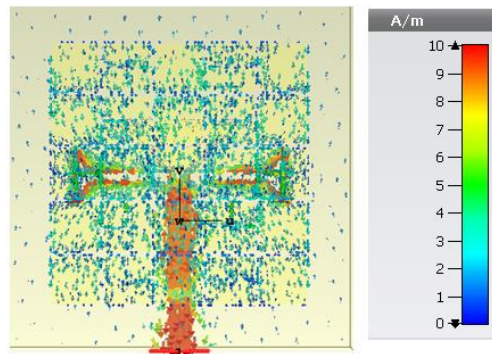


Fig 4.30: Current Distribution at 6.3GHz.

After carefully studying each element in the design and obtaining the best value from each element, the values are fixed in table 3.5 and based on it ,the antenna was design, where the table considers the final result of the parametric sweep applied to each part of the antenna to reach the best values that improved the performance of the antenna.

Figure 4.31 shows the polar metasurface plot with different cell size .Where the value for the main lobe is (14.6) dB in the X-Y view ($\theta = 90^\circ$), whereas the main lobe direction has value (90°), and the last the angular width value is (74.8°).

While the value for the main lobe is (23)dB in the Y-Z view ($\varphi = 90^\circ$), whereas the main lobe direction has value $=2^\circ$, and the last is the angular width is (71.4°).Finally, the X-Z view ($\varphi = 0^\circ$), the main lobe value is (23)dB, whereas the main lobe direction is value $=0^\circ$, and finally the angular width value is (66.7°).

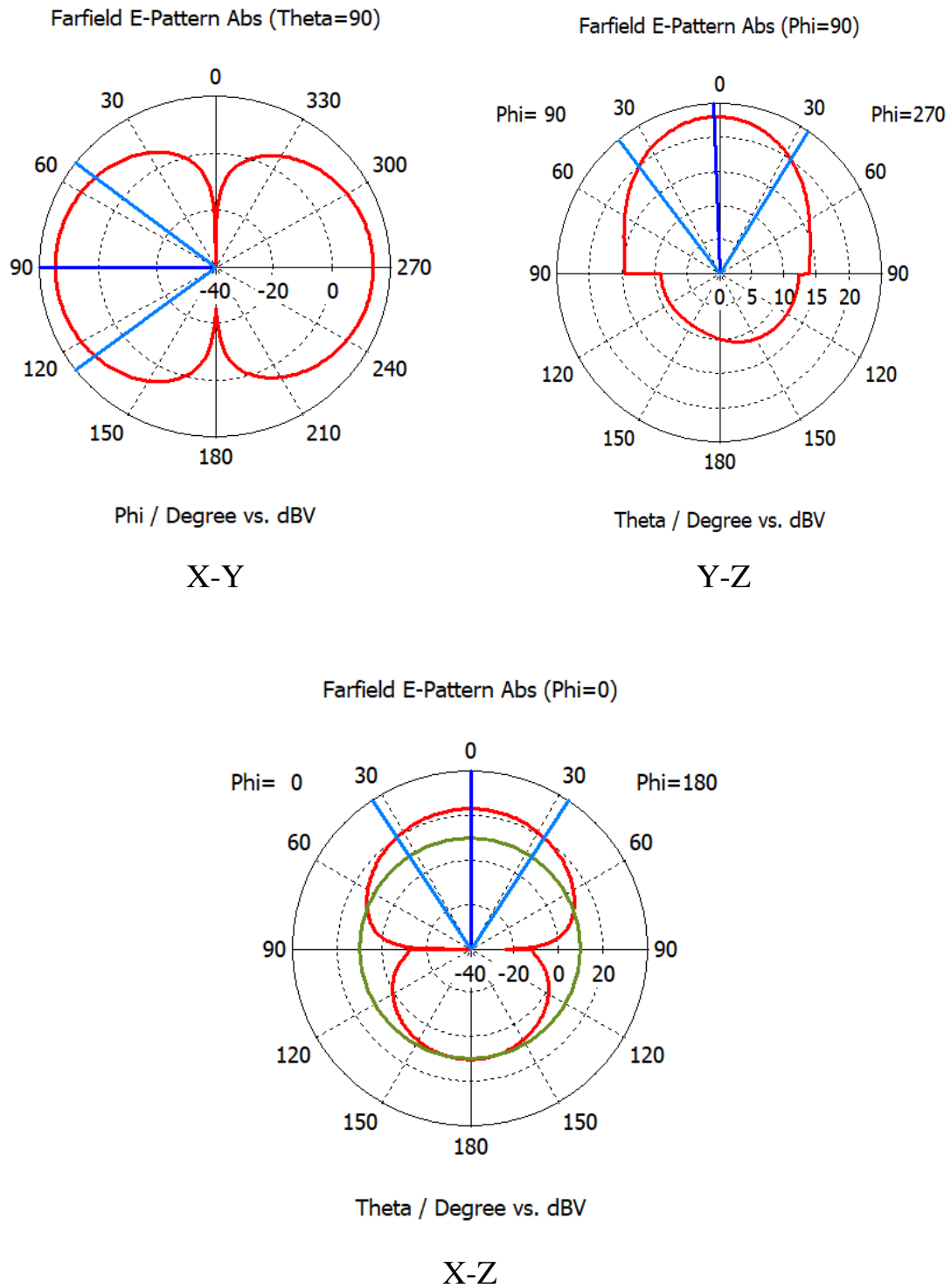


Fig 4.31: Radiation pattern (a) X-Y view (b) Y-Z view (c) X-Z view

4.5 The Characteristic of Metasurface with Hash Cell (IIV).

4.5.1 Extraction Permittivity and Permeability for S-Parameter

By placing a single unit cell of design between two waveguide port in order to extract permittivity, permeability and refractive index from the S-parameter and to ensure that the layer meets the metasurface requirements at a wanted frequency ,which represents the frequency range from 4.71 GHz to 6.89 GHz. Fig.4.30 below shows the characteristics of the MS layer.

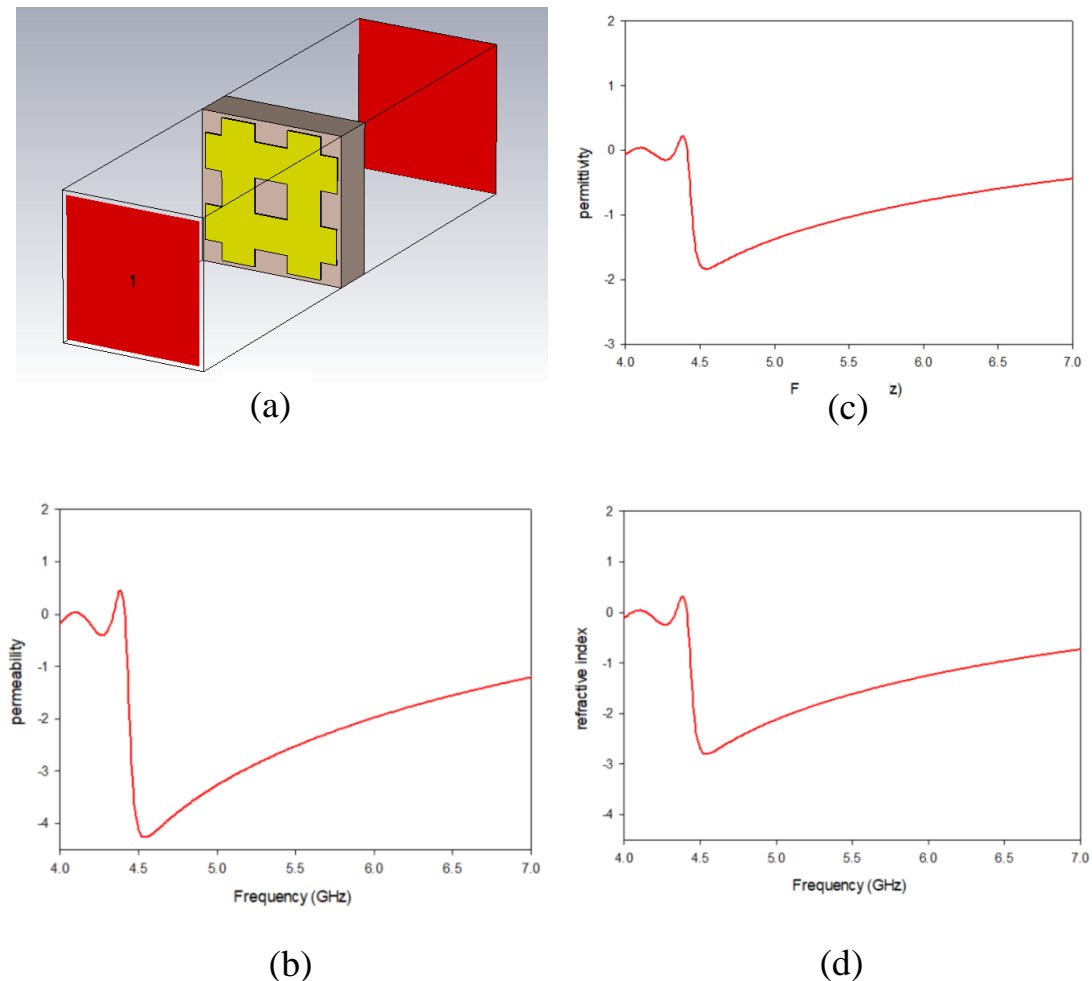


Fig4.32 :(a) The single unit cell of MS in CST,(b), Relative permeability of MS. (c), Relative permittivity of the MS. (d), Refractive index of the MS.

4.5.2 Reflection Coefficient, Gain, Directivity ,Current Distribution

Figure 4.33 offers a comparison between results of only slot antenna and the slot integrated with metasurface layer. It is evidently observed how much bandwidth and gain have been attained when adding the metasurface layer. The bandwidth ranges from 6.84 GHz to 7.23 GHz for only slot antenna. This narrowband behaviour is dramatically changed to very wideband about 2.18 GHz, extending from 4.71GHz to 6.89 GHz once the metasurface layer is added above the slot antenna. As pointed out earlier, this procedure aids to enhance matching for more frequencies, making the antenna very wideband. The improvement in the antenna bandwidth makes it a potential candidate for be utilized in some commercial wireless applications.

In the absence of the MS layer, the gain of the slot antenna is about 4.28 dB, while in the presence of the metasurface layer, it results in 7.43 dB as a new gain as shown in Fig.4.34. The gain enhancement obtained by the proposed antenna is about 3.15 dB. Moreover, the proposed antenna possesses gain values greater than a slot antenna over all frequencies.

After carefully studying each element in the design and obtaining the best value from each element, the values are fixed in Table 3.6 and based on it ,the antenna was design, where the table considers the final result of the parametric sweep applied to each part of the antenna to reach the best values that improved the performance of the antenna.

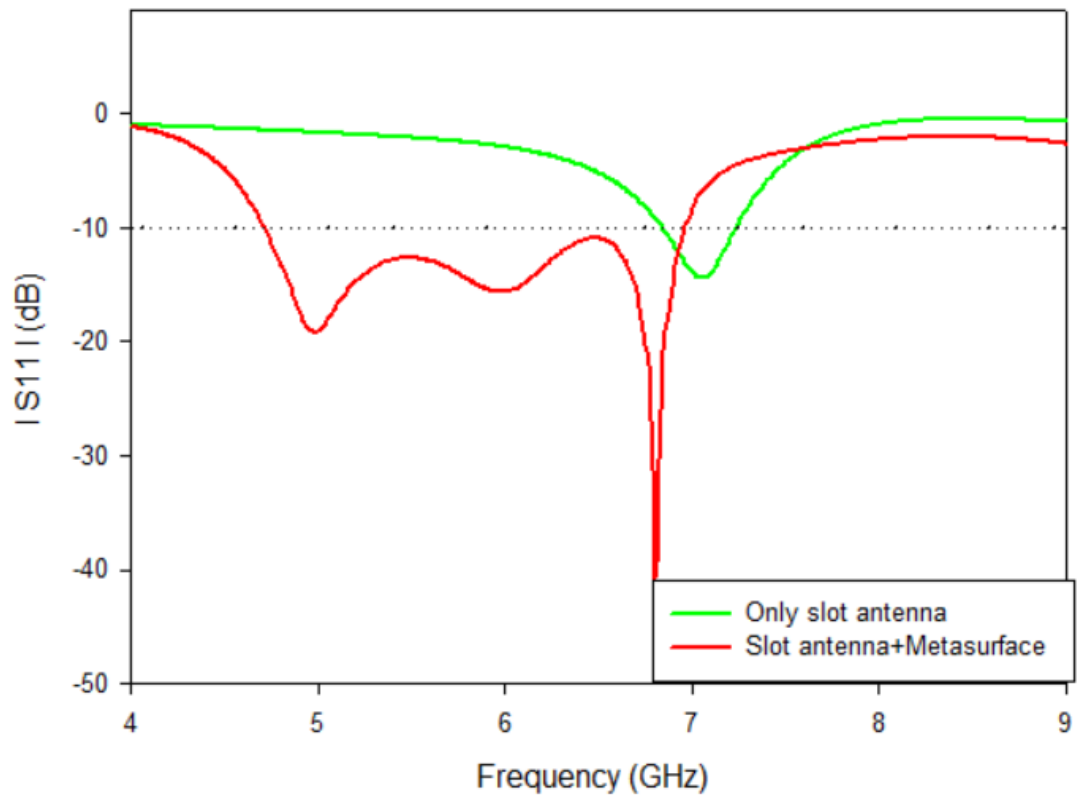


Fig 4.33: S_{11} of (only slot , slot antenna+metasurface).

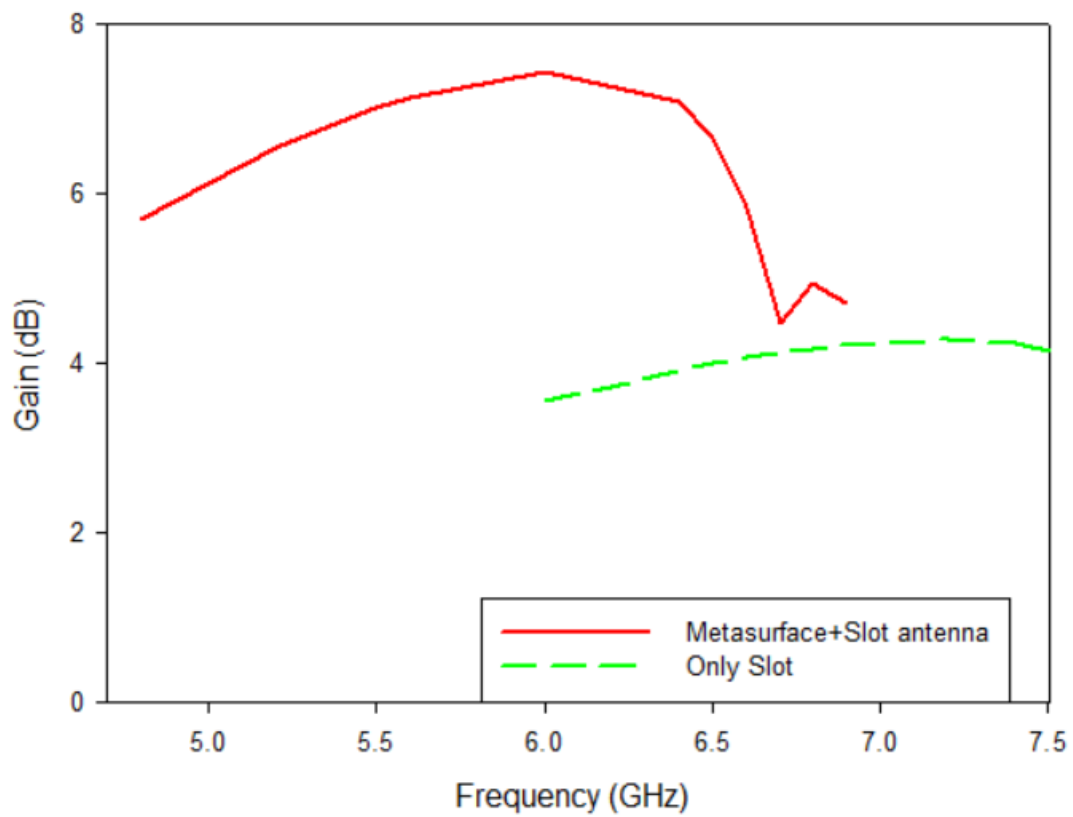


Fig 4.34: Gain of (only slot , slot antenna+metasurface).

4.5.2.1 Parametric Study for Hash Unit Cell Antenna

The proposed antennas are carefully designed, and their operating functionalities must be calculated accurately. The parametric study given here provides such a good example to understand the working mechanism of the proposed antenna and which dimensions parameters impact the design performance. The slot length L_s , the distance separating between the slot and the metasurface layer h_{air} , Feeding length and width are chosen for this study for the sake of simplicity. These many important parameters are set as a variable in the CST software, whereas all other parameters are fixed in the design. These parameters, which have a deep impact on the coupling between metasurface and slot, additional to the appropriate power supply to the antenna, have been varied. Fig4.35 shows the simulated return loss S11 of the proposed antenna for various slot lengths with fixed slot width $W_s=0.2$ mm. The L_s is varied from 6 mm to 11 mm with a step of 1mm. All slot lengths have

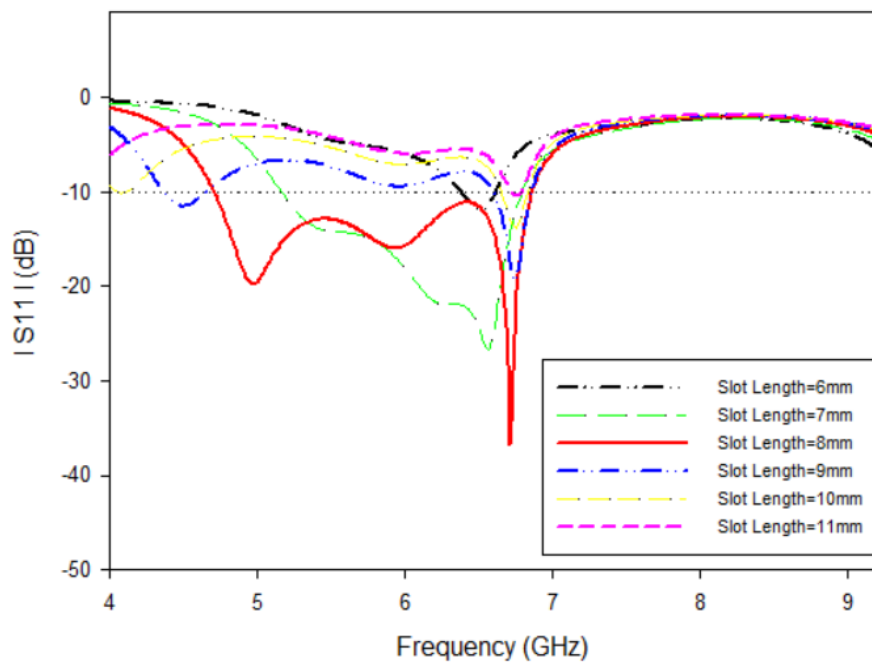


Fig 4.35: The simulated return loss S11 of the proposed antenna with various slot length from 6mm to 11mm.

almost the same resonant frequency. L_s equal to 8 mm is the best choice because it offers wider bandwidth, see Fig 4.35 with the red trace. Many reasons can be inferred from this result that the slot and the feeding line may interact effectively over all this frequency range. Also, when the slot length increases, surface current becomes denser along the slot, so the equivalent inductance becomes larger. The increase in the inductance cancels out the capacitance impact of the air gap separating between the slot and the metasurface layer.

Next, an influence of the parameter h_{air} on the S11 is also depicted in Fig. 4.36. h_{air} equal to 1mm is chosen. The bandwidth deteriorates as the air gap increases because the capacitance impact of the metasurface layer, which cancels out the inductance of the slot. Fig. 4.37 illustrates the change in values of both the length of the feed line and width to obtain the best specifications for the transmission line by reaching the appropriate length for the upper part of the slot location in the antenna. After the parametric study, the return loss S11 and gain of the slot antenna with hash distribution metasurfaces are given in Fig.4.36, when $L_s = 8$ mm and $h_{air}=1$ mm. The 3D radiation patterns for gain and directivity are depicted in Fig.4.39. Table 4.7 introduces some of the antenna performance parameters. Table 4.8 compares the proposed antenna with other recent designs.

The above-mentioned figures and tables will be discussed in detail to obtain the best results for the designed antenna by tracking the values of each element that is studied and in the end, the most important and influential element on the performance is explained, and it is possible to recommend the use of certain techniques in its design to reach better results and these points will be mentioned in chapter five

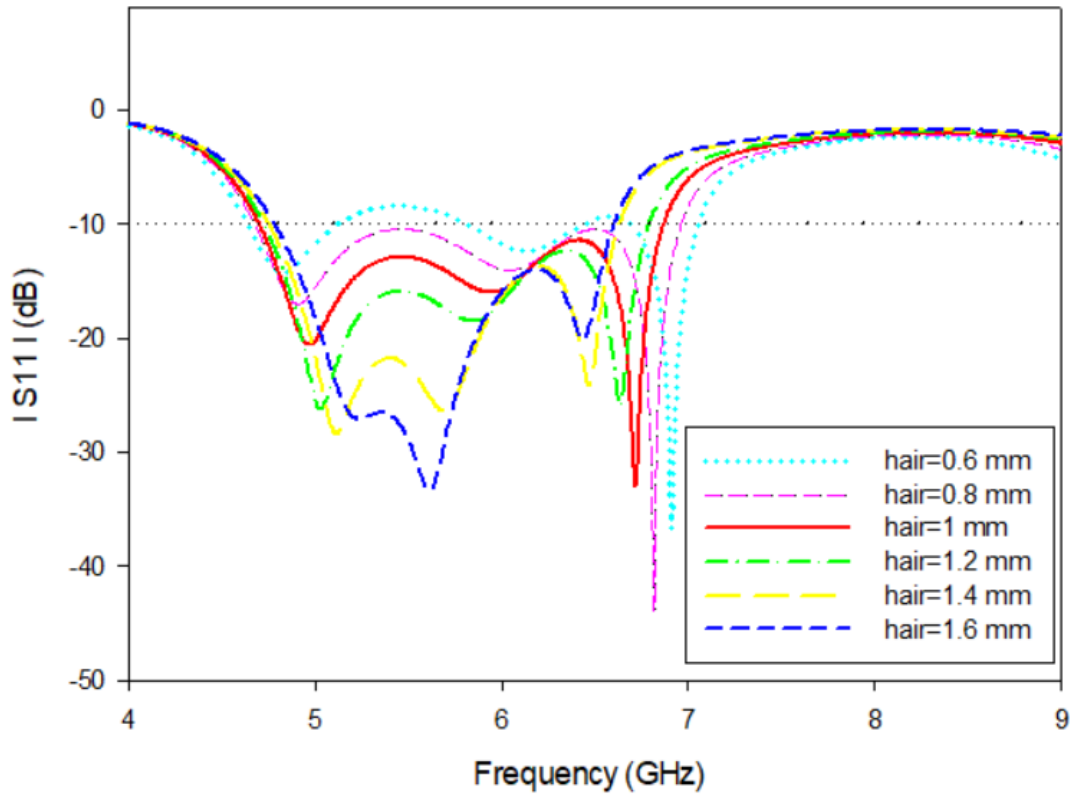
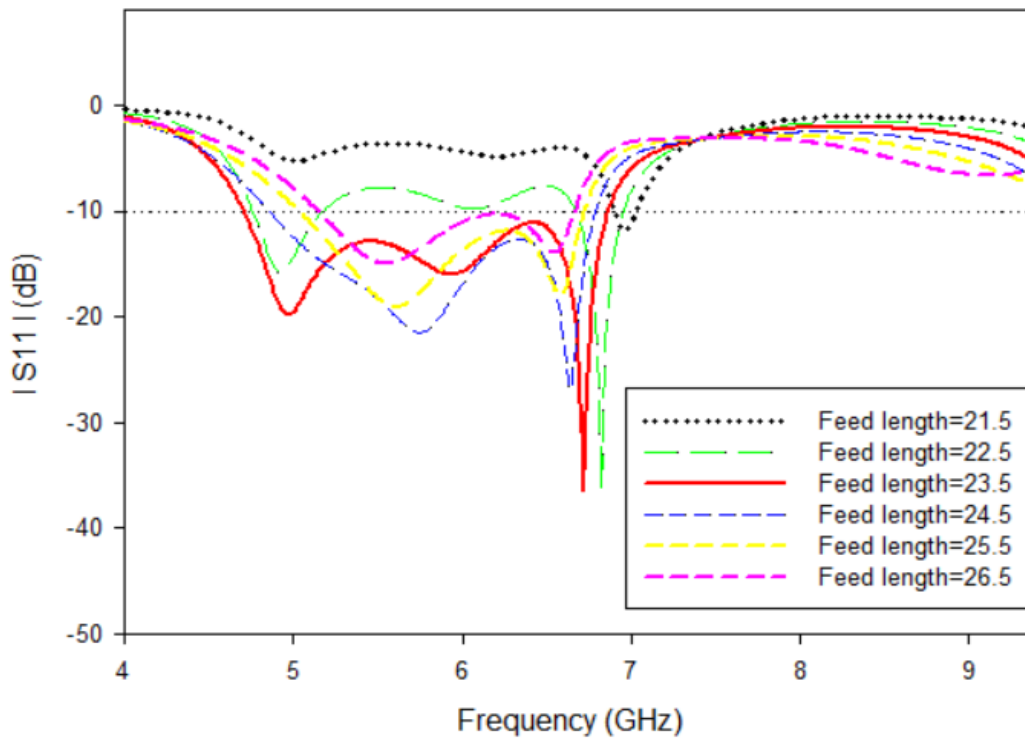
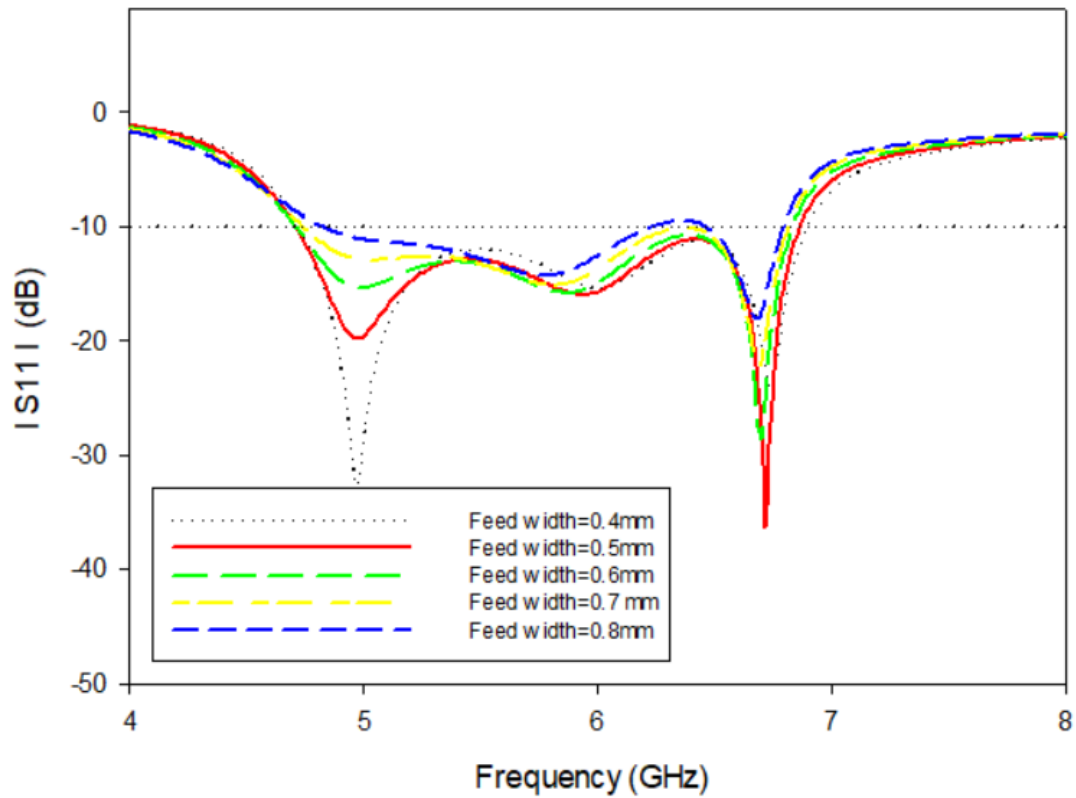


Fig 4.36: The simulated return loss S11 of the proposed antenna with various h_{air} from 0.6 mm to 1.6mm.

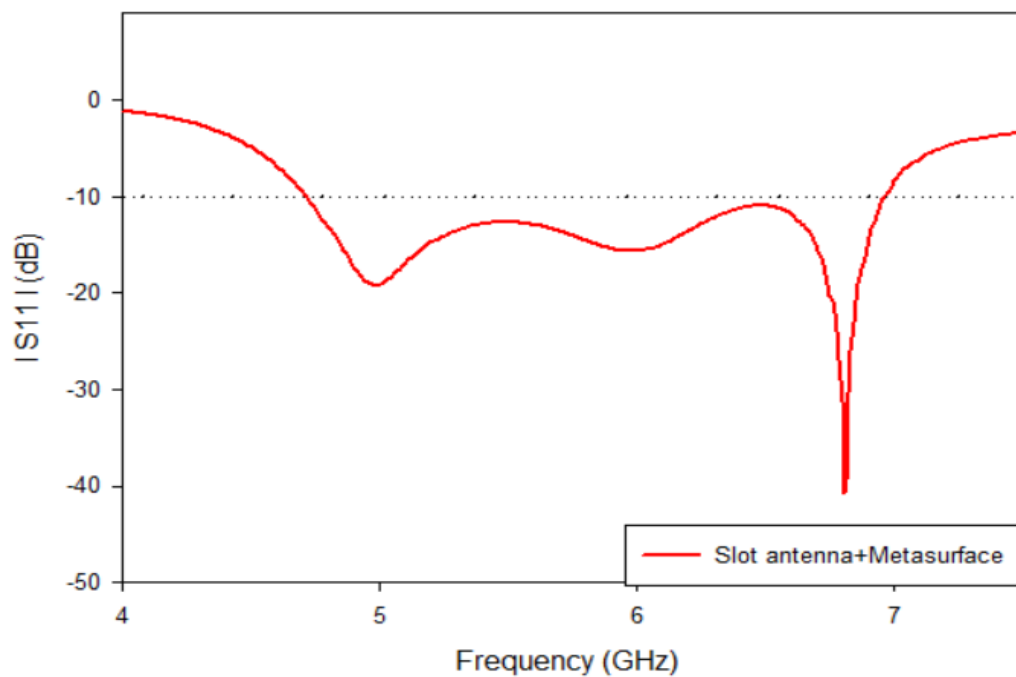


(a)

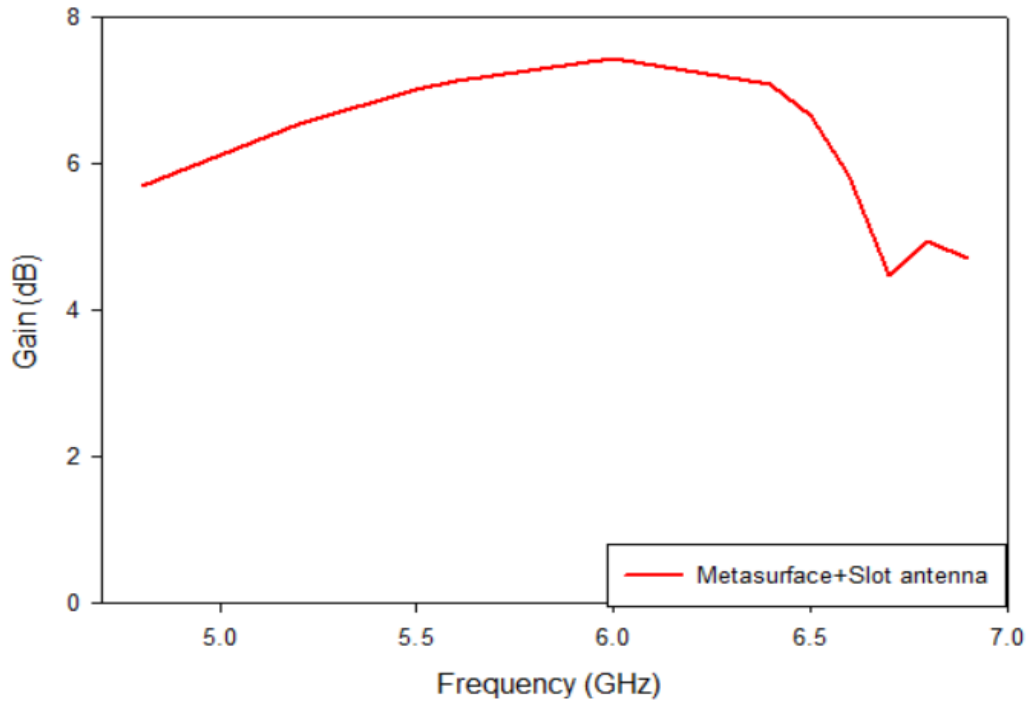


(b)

Fig 4.37:(a) Feed line length varies from 21.5mm to 26.5mm
(b) Feed line width varies from 0.4mm to 0.8 .

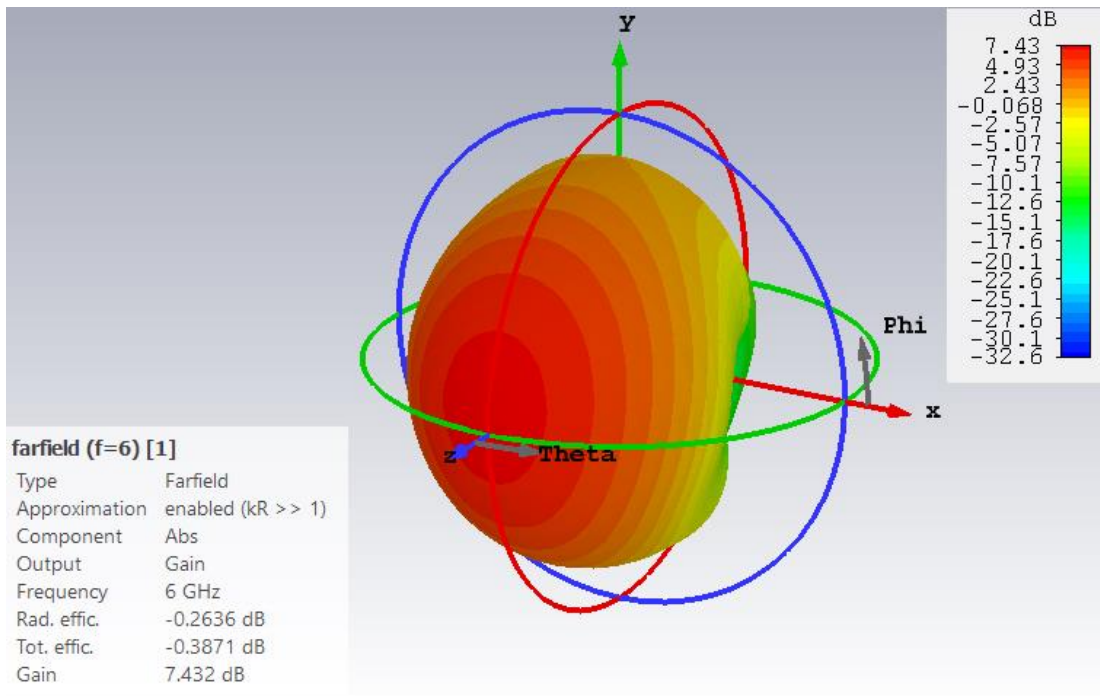


(a)

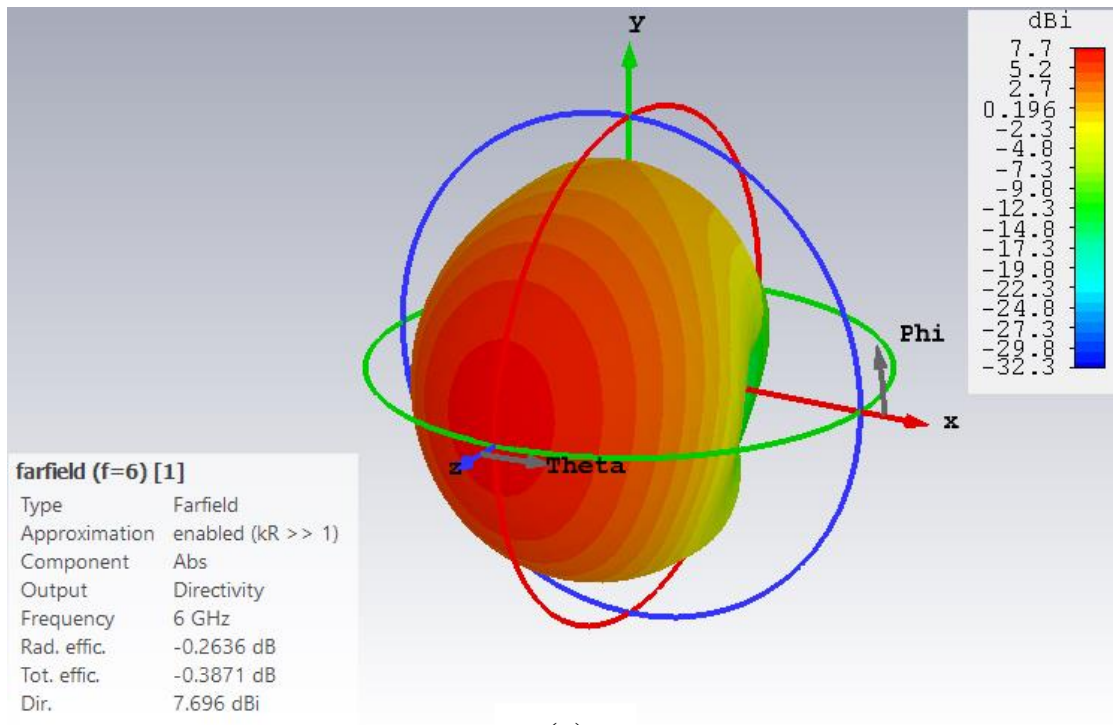


(b)

Fig 4.38: (a) S11 for slot antenna with metasurface (b) Gain of Metasurface antenna.



(a)



(a)

Fig 4.39: 3D Pattern for (a) Gain (b) Directivity.

The gain and directivity of the resonant frequency are shown above, where obtained a value of 7.43 dB as gain and 7.69 dB directivity at the frequency 6 GHz. The efficiency of the antenna reaches to an approximate value of 96 % depending on the equation that collects between directivity and gains to give the efficiency.

Table 4.7 antenna performance parameters:

No	Parameter name	Only Slot	Metasurface
1	Resonant Frequency	7.1 GHz	6.75 GHz
2	Bandwidth	0.39 GHz	2.18 GHz
3	Return loss	-12 dBi	-33.4 dBi
4	Gain	4.28 dBi	7.43 dBi

Table 4.7 shown the difference between slot antenna and slot antenna loaded with metasurface layer in bandwidth and gain ,where metasurface

antenna exceed slot antenna by 1.79 GHz as bandwidth and 3.15 dB as gain .

Table 4.8 antenna performance parameters.

No	Work	Resonant Frequency	Max and Min frequency	Bandwidth	Return loss	Gain
1	[37]	5.7 GHz	5.64–5.8 GHz	160 MHz	-27 dBi	5.8 dBi.
2	[39]	2.3 GHz	2 – 2.63 GHz	630MHz	-22 dBi	1 dBi
3	[59]	7.6 GHz	7-9 GHz	2GHz	-32 dBi	5.53dBi
4	work	6.75 GHz	GHz to 4.71 6.89	2.18 GHz	-33.4 dBi	7.43 dBi

Table 4.8 is very important because it shows the strength of our contribution through the exceptional increase in the bandwidth, gain, and matching level compared to other related work. The value of bandwidth is 2.18GHz. This value is very excellent as compared to other reference, where work in [37] has value 160MHz, 630MHz for [39], 2GHz for [59]. also have increased the gain in the proposed antenna. Until we get more insight into the electromagnetic characteristics of the metasurface antenna, generating the current distributions for the antenna at resonant frequency as shown in Figure below.

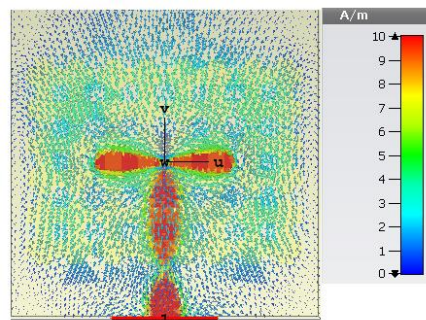


Fig 4.40: Current Distribution at 6.75GHz.

The figure shows the polar metasurface plot with hash shape of the unit cell. Where the value for the main lobe is (6.93) dB in the X-Y view ($\theta = 90^\circ$), whereas the main lobe direction has value (38°), and the last the angular width value is (52.2°). While the value for the main lobe is (18.9) dB in the Y-Z view ($\varphi = 90$), whereas the main lobe direction has value $=1^\circ$, and the last is the angular width is (61.9°). Finally, the X-Z view ($\varphi = 0^\circ$), the main lobe value is (19.2) dB, whereas the main lobe direction is value $=49^\circ$, and finally the angular width value is (138.7°).

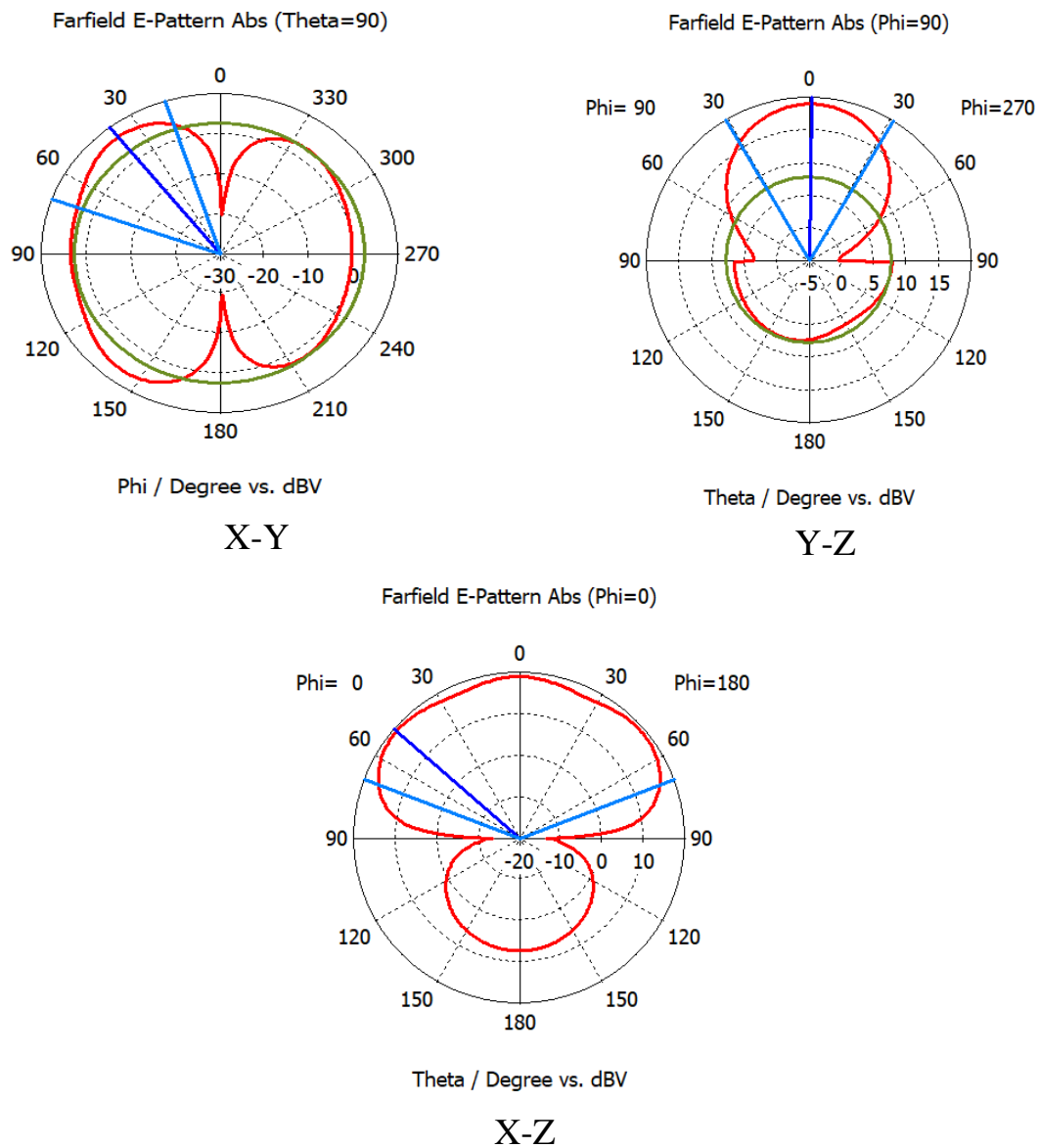


Fig 4.41: Radiation pattern(a) X-Y view (b) Y-Z view(c) X-Z view

Table 4.9 Comparison Between The Four Proposed Metasurface Antennas

Name	S11 (dB)	Frequency (GHz)	Gain(dB)	Bandwidth (GHz)	Efficiency
Slot antenna	-28	6.7	4.19	6.25-7.007	-
First Design (Metasurface layer with X slot in center)	-40	4.33	10.7	4.01-7.01	99%
Slot antenna	-16	6.4	2.38	6.2-6.62	-
Second Design (uniform Distribution)	-28	8.3	8	6.3-9	74%
Second Design (Gradient Distribution)	-32	6.4	9.75	6.3-8.7	84%
Slot antenna	-15	6.35	5.6	6.15-6.52	-
Third Design (Different cell size)	-30	6.22	8.78	5.75-8.43	98%
Slot antenna	-12	7	4.28	6.84-7.23	-
Fourth Design (Hash unit cell)	-40	6.8	7.43	4.71-6.89	96%

Table 4.9 is considered one of the most important tables mentioned in Chapter Four, because of its focus mainly on the results of each antenna, whether the original antenna, which is the slot antenna or the slot antenna loaded with the metasurface layer. The excellent result in the gain and bandwidth are realized in first antenna .Where it achieved a bandwidth value of 3 GHz and a gain of 10.7. As for the other antennas, the second antenna achieved a bandwidth of 2.41GHz and a gain of 9.75 dB, while the third antenna achieved a bandwidth of 2.81GHz and a gain of 8.78dB ,Finally antenna realized bandwidth of 2.18 GHz and gain of 7.43 dB .

In order for the applications to be identified correctly and not randomly, need a reliable group of reference through which correctly determine the frequency range for each application. Therefore, Table 4.10 shown below contains references for imaging and wireless applications and comparing them with the frequencies of the antennas used in the thesis. Finally, two antennas were identified for imaging applications and two antennas for wireless applications.

Table 10 : Application of Each Antenna.

Antenna name	Frequency range	application	Reference	Frequency range	application
First Design	4.01-7 GHz	Wireless-local area network	[61]	3.91-6.14 GHz	Wireless-local area network
Second Design	6.3-8.7 GHz	Imaging application in synthetic aperture radar (SAR)	[59]	7-9.2 GHz	Imaging application in synthetic aperture radar (SAR)
Third Design	5.62-8.43 GHz		[38]	5.14-5.82 GHz	Imaging application in synthetic aperture radar (SAR)
Four Design	4.71-6.89 GHz	A potential candidate for wireless communication system Wi-Fi	[37]	5.64-5.8 GHz	Wireless application Wi-Fi
			[58]	5.45-5.87 GHz	Wireless application Wi-Fi
			[57]	4.85-6.28 GHz	Wireless application system
			[62]	4.65-6.34 GHz	Wireless application system
			[41]	4.79-4.99 GHz	Wireless application system

Chapter Five

Conclusion and

Future Work

CHAPTER FIVE

CONCLUSION AND FUTURE WORK

5.1 Introduction

Will be mentioned the most important goals of this work, also the conclusion that is drawn from each design. After that highlight the recommendations that are most relevant.

5.2 Conclusion

1-In this section, related comments are provided on the four design methodologies for metasurface antennas. These four metasurface antennas are proposed with various geometrical shapes in the metasurface layer in order to demonstrate the effect of the different distribution of the metasurface layer on the antenna performance. Like bandwidth, gain, directivity, reflection coefficient S_{11} , current distribution and efficiency.

2- The first metasurface antenna design takes a uniform distribution of the unit cell with X slot in the centre. This antenna gives a range of the bandwidth from 4.075 GHz to 7.01 GHz with peak gain 10.7 dB.

3-The second metasurface antenna composes of two designs, uniform and gradient distribution metasurfaces. The uniform distribution metasurfaces have bandwidth range from 6.3 GHz to 9 GHz with peak gain 8 dB. While gradient distribution metasurfaces bandwidth begin from 6.29 GHz to 8.69 GHz with peak gain 9.75dB.

4-The third metasurface antenna design composes of the metasurface layer used in the proposed structure where unit cells have two different sizes. Every four patches within the small size unit cells are equal to one

size of the big unit cell. Thus, the bandwidth of the antenna starts from 5.62GHz to 8.43GHz with a peak gain of 8.78 dB.

5-The fourth antenna design takes form hash with antenna bandwidth start from 6.84 GHz to 7.23 GHz with peak gain value 7.43 dB.

6- A detailed comparison is made between the slot antenna and the slot antenna with the metasurface layer. The biggest difference has been observed in the gain and bandwidth of the proposed antennas. Thus the main benefit of adding the metasurface layer to the microstrip antennas in this thesis ,is to improve the performance of the antenna on both sides of the gain and bandwidth and very significantly compared to the original values of the microstrip antenna.

7- The best antenna in terms of results among the four antennas is the first antenna. The first design of the metasurface layer with an X slot in the middle of the unit cell, which achieved the gain values of 10.7 dB and bandwidth 3 GHz, overcomes all antennas that designed based on metasurface.

8- The technique used to improve the performance of the antenna is the Fabry Pérot technique , which depends on the constructive interference between the transmitted waves and the reflections waves.

9- In order to obtain the best performance, an analysis was carried out on each component in the design of the antennas and used the parametric sweep tool in the CST in this regard.

10- The applications of the four antennas are divided into two parts: use in imaging applications and use in wireless applications, and this division is mentioned in detail .

5.3 Recommendations for future work

Depending on the results getting from this thesis, the following points are recommended to work them in future :

1-Designing different shapes of the metasurface unit cell and getting their characteristics in order to improve bandwidth and gain.

2-Using another shape of the patch and feeding technique, then comparing them with the results of present in this work.

3- The use of optimization in calculating all the antenna elements, depending on that one of the sides of the Golden Triangle genetic, fuzzy and neural.

4-Trying to make designs based on the other type of metasurface which is the metascreen.

5- Improving the work of the Fabry-Perot technique by adopting designs that include bias circuits.

6- Using metasurface in circular polarization and beam steering , as well as improving the performance of the Fabry Pérot cavity by using active elements.

List of Publications	
1	Qahtan Mutar Gatea ,Faris Mohammed Ali, Nasr Al-Kafahji, Abdulkadhum Jaafar Alyasiri. Design Low Profile and Wide-band Antenna Based on Meta-surface. Al-Furat Journal of Innovation in Electronic and Computer Engineering, 2020, 1.02.
2	Qahtan Mutar Gatea ,Faris Mohammed Ali, Nasr Al-Kafahji, Abdulkadhum Jaafar Alyasiri "Gradient Distribution of Metasurface Based Antenna Performance Enhancement" .The accept manuscripts will be published in AIP.
3	Qahtan Mutar Gatea ,Faris Mohammed Ali, Nasr Al-Kafahji, Abdulkadhum Jaafar Alyasiri "Hash Unit Cell Shape Used To Enhancement Gain and Bandwidth of Metasurface Antenna" . The accept manuscripts will be published in IOP.
4	Qahtan Mutar Gatea ,Faris Mohammed Ali, Nasr Al-Kafahji, Abdulkadhum Jaafar Alyasiri " Design Dual-Layer Metasurfaces Antenna for Wireless Application" .

REFERENCE

- [1] A John Wiley & sons "ANTENNA THEORY ANALYSIS AND DESIGN", third edition,0-471-66782-X,2005.
- [2] Engheta, Nader, and Richard W. Ziolkowski "Metamaterials: physics and engineering explorations",13 978-0-471-76102-0,2006.
- [3] SIHVOLA, Ari. "Metamaterials in electromagnetics". Metamaterials, 2007, 2-11.
- [4] Veselago, Victor Georgievich "The Electrodynamics of Substances with Simultaneously Negative Values of ϵ and μ ", Physics-Uspekhi,10.,4,1968.
- [5] D. R. Smith,* Willie J. Padilla, D. C. Vier, S. C. Nemat-Nasser, and S. Schultz" Composite Medium with Simultaneously Negative Permeability and Permittivity", Physical review letters,84.,18,2000.
- [6] Shelby, R. A., Smith, D. R., & Schultz, S. "Experimental verification of a negative index of refraction". science, 292.,5514), 2001.
- [7] Christopher L. Holloway, Edward F. Kuester, Joshua A. Gordon, John O'Hara, Jim Booth, and David R. Smith "An overview of the theory and applications of metasurfaces: The two-dimensional equivalents of metamaterials",54.,2,2012.
- [8] Cihan Kurter,, a John Abrahams, and Steven M. Anlage "Miniaturized superconducting metamaterials for radio frequencies", Applied Physics Letters, 96.,25,2010.
- [9] M. Gokkavas,K. Guven,I. Bulu, K. Aydin, R. S. Penciu, M. Kafesaki, C. M. Soukoulis, and E. Ozbay"Experimental demonstration of a left-handed metamaterial operating at 100 GHz", Physical Review,73.,193103,2006.
- [10] Yen, Ta-Jen, et al. "Terahertz magnetic response from artificial materials." Science 303.5663,2004.
- [11] Dolling, Gunnar, et al. "Negative-index metamaterial at 780 nm wavelength" ,Optics letters 32.1,2007.

- [12] Bilotti, F., Tricarico, S., & Vegni, L. "Plasmonic metamaterial cloaking at optical frequencies". *IEEE Transactions on Nanotechnology*, 9.1, 2009.
- [13] Pendry, John Brian. "Negative refraction makes a perfect lens." *Physical review letters* 85.18 ,2000.
- [14] Ramahi, Omar M., et al. "Metamaterial particles for electromagnetic energy harvesting." *Applied Physics Letters* 101.17,(2012): 173903.
- [15] Ziolkowski, Richard W, and Aycan Erentok, "Metamaterial-based efficient electrically small antennas." *IEEE Transactions on antennas and propagation* 54.7 (2006): 2113-2130.
- [16] Kuester, Edward F., et al. "Averaged transition conditions for electromagnetic fields at a metafilm." *IEEE Transactions on Antennas and Propagation* 51.10 (2003): 2641-2651.
- [17] Lapine, M., and S. Tretyakov. "Contemporary notes on metamaterials." *IET microwaves, antennas & propagation* 1.1 (2007): 3-11.
- [18] Achouri, Karim, Mohamed A. Salem, and Christophe Caloz. "General metasurface synthesis based on susceptibility tensors." *IEEE Transactions on Antennas and Propagation* 63.7 (2015): 2977-2991.
- [19] El Badawe, M. "Metasurfaces for Antennas, Energy Harvesting and Imaging", *Electrical and Computer Engineering, University of Waterloo, Ontario, Canada, 2018.*
- [20] Landy, N. I., Sajuyigbe, S., Mock, J. J., Smith, D. R., & Padilla, W. J. "Perfect metamaterial absorber. *Physical review letters*", 100(20), 2008,207402.
- [21] Huang, L., Zhang, S., & Zentgraf, T. "Metasurface holography: from fundamentals to applications". *Nanophotonics*, 7(6),2018, 1169-1190.
- [22] Almoneef, Thamer S., and Omar M. Ramahi. "Metamaterial electromagnetic energy harvester with near-unity efficiency." *Applied Physics Letters* 106.15 (2015): 153902.
- [23] Gordon, J. A., Holloway, C. L., Booth, J., Kim, S., Wang, Y., Baker-Jarvis, J., & Novotny, D. R. "Fluid interactions with

metafilms/metasurfaces for tuning, sensing, and microwave-assisted chemical processes." *Physical Review B*, 83(20),2011, 205130.

[24] Vijitsulakkana, Pawares, et al. "UHF RFID reader using slanted slot patch metasurface on microstrip patch antenna." 2015 IEEE Conference on Antenna Measurements & Applications (CAMA). IEEE, 2015.

[25] TA, Son Xuat, et al. Single-feed, compact, GPS patch antenna using metasurface. In: 2017 International Conference on Advanced Technologies for Communications (ATC). IEEE, 2017. p. 60-63.

[26] Huang, Y., Li, J., & Wen, G. Wideband low-profile circular polarization slot antenna based on metasurface. In 2017 IEEE International Symposium on Antennas and Propagation & USNC/URSI National Radio Science Meeting (pp. 471-472). IEEE.2017.

[27] da Silva Paiva, José Lucas, et al. "Using metasurface structures as signal polarisers in microstrip antennas." *IET Microwaves, Antennas & Propagation* 13.1 (2018): 23-27.

[28] MARTINEZ, Idellyse; WERNER, Douglas H. Reconfigurable beam steering metasurface absorbers. In: 2014 IEEE Antennas and Propagation Society International Symposium (APSURSI). IEEE, 2014. p. 1674-1675.

[29] Xie, Peng, et al. "Novel fabry-pérot cavity antenna with enhanced beam steering property using reconfigurable meta-surface." *Applied Physics A* 123.7 (2017): 462.

[30] LIU, Wei; CHEN, Zhi Ning; QING, Xianming. Miniaturized broadband metasurface antenna using stepped impedance resonators. In: 2016 IEEE 5th Asia-Pacific Conference on Antennas and Propagation (APCAP). IEEE, 2016. p. 365-366.

[31] Liu, Wei EI, et al. "Miniaturized wideband metasurface antennas." *IEEE Transactions on Antennas and Propagation* 65.12 (2017): 7345-7349.

[32] Li, Ximing, et al. "Design and Characterization of a Miniaturized Antenna Based on Palisade-Shaped Metasurface." *International Journal of Antennas and Propagation* 2018 (2018).

- [33] CHAIMOOL, Sarawuth; RAKLUEA, Chawalit; AKKARAEKTHALIN, Prayoot. Low-profile unidirectional microstrip-fed slot antenna using metasurface. In: 2011 International Symposium on Intelligent Signal Processing and Communications Systems (ISPACS). IEEE, 2011. p. 1-5.
- [34] Chen, Ke, et al. "Improving microwave antenna gain and bandwidth with phase compensation metasurface." *AIP Advances* 5.6 (2015): 067152.
- [35] Majumder, B., et al. "Wideband compact directive metasurface enabled pair of slot antennas." *Electronics Letters* 51.17 (2015): 1310-1312.
- [36] Pan, Y. M., et al. "A low-profile high-gain and wideband filtering antenna with metasurface." *IEEE Transactions on Antennas and Propagation* 64.5 (2016): 2010-2016.
- [37] Rajak, Neha, and Neela Chatteraj. "A bandwidth enhanced metasurface antenna for wireless applications." *Microwave and Optical Technology Letters* 59.10 (2017): 2575-2580.
- [38] Cai, Ming, et al. "Broadband compact CPW-fed metasurface antenna for SAR-based portable imaging system." *International Journal of RF and Microwave Computer-Aided Engineering* 28.2 (2018): e21175.
- [39] MUNIR, Achmad, et al. Metasurface-backed monopole printed antenna with enhanced bandwidth. In: 2017 International Symposium on Antennas and Propagation (ISAP). IEEE, 2017. p. 1-2.
- [40] HUSSAIN, Niamat, et al. A microstrip patch antenna sandwiched between a ground plane and a metasurface for WiMAX applications. In: 2018 Asia-Pacific Microwave Conference (APMC). IEEE, 2018. p. 1016-1018.
- [41] Iyampalam, Paulkani, and Indumathi Ganesan. "Low profile antenna based on a fractal shaped metasurface for public safety applications." *International Journal of RF and Microwave Computer-Aided Engineering* 30.2 (2020): e22048.

- [42] Liu, Guo, et al. "Wideband printed slot antenna using Koch fractal metasurface structure." *International Journal of RF and Microwave Computer-Aided Engineering* 30.3 (2020): e22058.
- [43] Caloz, Christophe; ITOH, Tatsuo. "Electromagnetic metamaterials: transmission line theory and microwave applications". John Wiley & Sons, 0-471-66985-7,2005.
- [44] Bukhari, Syed S., J. Yiannis Vardaxoglou, and William Whittow. "A metasurfaces review: Definitions and applications." *Applied Sciences* 9.13 (2019): 2727.
- [45] Konstantinidis, Konstantinos. . Multi-layer periodic surfaces and metasurfaces for high-gain antennas, College of Engineering and Physical Sciences, University of Birmingham.2015.
- [46] Sourabh Bisht et.al, "Study The Various Feeding Techniques of Microstrip Antenna Using Design and Simulation Using CST Microwave Studio," *International Journal of Emerging Technology and Advanced Engineering*, vol. 4, no. 9, 2008.
- [47] Zhang, Kai, et al. "Design and optimization of broadband single-layer reflectarray." *2013 Proceedings of the International Symposium on Antennas & Propagation. Vol. 2. IEEE*, 2013.
- [48] Zubir, Farid, et al. "Design and analysis of microstrip reflectarray antenna with minkowski shape radiating element." *Progress In Electromagnetics Research* 24 (2010): 317-331.
- [49] Numan, Ahmad B., and Mohammad S. Sharawi. "Extraction of material parameters for metamaterials using a full-wave simulator [education column]." *IEEE Antennas and Propagation Magazine* 55.5 (2013): 202-211.
- [50] Tamim, Ahmed Mahfuz, et al. "Split ring resonator loaded horizontally inverse double L-shaped metamaterial for C-, X-and Ku-Band Microwave applications." *Results in Physics* 12 (2019): 2112-2122.
- [51] Smith, D. R., et al. "Electromagnetic parameter retrieval from inhomogeneous metamaterials." *Physical review E* 71.3 (2005): 036617.
- [52] Simovski, Constantin R., Pavel A. Belov, and Sailing He. "Backward wave region and negative material parameters of a structure

formed by lattices of wires and split-ring resonators." *IEEE Transactions on Antennas and Propagation* 51.10 (2003): 2582-2591.

[53] Chen, Xudong, et al. "Robust method to retrieve the constitutive effective parameters of metamaterials." *Physical review E* 70.1 (2004): 016608.

[54] Zakariyya, Sikiru Olayinka. "Modeling of Miniaturized, Multiband and Ultra-Wideband Fractal antenna". Master's Thesis. Eastern Mediterranean University (EMU)-Doğu Akdeniz Üniversitesi (DAÜ).2015.

[55] Anusha, N., et al. Design and investigation of terahertz antenna using different configurations. In: 2017 International conference of Electronics, Communication and Aerospace Technology (ICECA). IEEE, 2017. p. 529-532.

[56] Bai, Hao, Guang-Ming Wang, and Ting Wu. "High-Gain Wideband Metasurface Antenna With Low Profile." *IEEE Access* 7 (2019): 177266-177273.

[57] Liu, Wei, Zhi Ning Chen, and Xianming Qing. "Metamaterial-based low-profile broadband aperture-coupled grid-slotted patch antenna." *IEEE Transactions on Antennas and Propagation* 63.7 (2015): 3325-3329.

[58] Rajak, Neha, Neela Chatteraj, and Raghvendra Kumar. "A gain and bandwidth enhanced metamaterial based surface antenna for wireless communication." *parameters* 50 (2019): 11.

[59] RAJESH, Galaba Sai; KUMAR, Vijay. Designing multiband metamaterial loaded microstrip patch antenna for SAR applications. In: 2015 International Conference on Microwave and Photonics (ICMAP). IEEE, 2015. p. 1-2.

[60] Yang, Zhen-Zhong, et al. "Metasurface-based wideband, low-profile, and high-gain antenna." *IET Microwaves, Antennas & Propagation* 13.4 (2019): 436-441.

[61] Zhou, Changfei, et al. "Bandwidth and gain improvement of a crossed slot antenna with metasurface." *Applied Physics Letters* 110.21 (2017): 211603.

[62] Liu, Wei, Zhi Ning Chen, and Xianming Qing. "Metamaterial-based low-profile broadband mushroom antenna." *IEEE Transactions on Antennas and Propagation* 62.3 (2014): 1165-1172.